DESIGN AND EVALUATION OF AN ATMOSPHERIC LASER COMMUNICATION LINK UTILIZING AN INFRARED EMITTING INJECTION LASER DIODE

A Thesis

Presented to

the Faculty of the Department of Electrical Engineering

University of Houston

In Partial Fulfillment

of the Requirements for the Degree

Master of Science

by

Kiran N. Mayur

July 1975

ACKNOWLEDGEMENTS

I am deeply indebted to my Thesis adviser and committee chairman, Dr. R. S. Simpson, for his valuable suggestions, stimulating discussions and able guidance throughout the course of this Thesis.

Thanks are also in order for Drs. K. Y. Wang and B. D. Cook for serving on my Thesis committee and supervising this work. I sincerely appreciate the cooperation and patience of Ms. Sandi White in diligently typing the manuscript.

Finally, I would like to express my profound gratitude to the members of my family and in particular my brother, Dan, without whose support and inspiration this thesis would not have been a reality.

DESIGN AND EVALUATION OF AN ATMOSPHERIC LASER COMMUNICATION LINK UTILIZING AN INFRARED EMITTING INJECTION LASER DIODE

An Abstract of a Thesis

Presented to

the Faculty of the Department of Electrical Engineering

University of Houston

In Partial Fulfillment

of the Requirements for the Degree

Master of Science

---

by

Kiran N. Mayur

July 1975

ABSTRACT

The design of a digital optical communication link operating over a short atmospheric path is presented. The system utilizes direct detection technique to detect the pulses transmitted by a Gallium Arsenide injection laser source emitting at 0.904 μm. The maximum bit rate is about 10 kbps. Theory and operating principles of the devices and the atmospheric effects in optical communication are described. Data on the performance of the link has been obtained and probability of error curves have been plotted for operation during different atmospheric conditions. The experimental study allows an evaluation of the injection laser as a device for transmitting digital information over short atmospheric paths.

TABLE OF CONTENTS

Chapter Page

Chapter Page

LIST OF TABLES

LIST OF FIGURES

Chapter 1

INTRODUCTION

1.1 A Brief Survey

Optical communication, or transmission of information with the help of light, has been in practice in various forms for years. The advent of lasers in 1960, however, has given a real stimulus to serious examination of the use of optical frequencies for communication purposes. Recognizing the potential of enormous bandwidth capacity and directionality of this newly discovered source of light, excited physicists speculated on how all the TV programs in the United States could be put on a single light beam or how one could talk to Mars. Indeed, some spectacular experiments in optical communication took place in the early sixties [1,2,3].

This initial flurry of activity soon subsided when the tough problems of transmitting information through atmospheric turbulence became evident. The problem of getting useful information through a turbulent atmosphere on an optical beam called for better optical devices, new techniques and better understanding of the atmospheric channel. In addition, the usefulness and practicality of a laser communication system seemed questionable because existing communications systems were adequate to handle current demands and thus there was no clear cut pressing

need for new communications systems. For a while, the researchers thought that practical optical communications systems lay still far ahead in the future.

However, a counterswing was already beginning in the late sixties, and several interesting developments occured during this period. There was a general movement toward the infrared, stimulated by the development of reliable laser sources; gallium arsenide at 0.9 μm, Nd:YAG at 1.06 μm and CO_2 at 10.6 μm. At the same time, sophisticated techniques in modulation, detection, pointing and tracking were developed. Predicted crowding of radio frequency channels and growing demands on available spectrum warranted a serious consideration for the alternate mode of communication in the future. Laser communication systems were recognized as a possible solution to meet the anticipated communication demands.

In view of all these developments and considerations, researchers have once again turned their attention to investigating the use of optical frequencies for the communication applications. Today, optical communication using laser devices has become an active research area in many universities and industries around the world.

1.1.1 Potential advantages of optical communication. The two highly publicized advantages of a laser communication system are its capacity and antenna gain. Large information carrying capacity of a laser channel results from a large

bandwidth attributed to the inherently high optical carrier frequency. Theoretically, the information carrying capacity of an electromagnetic channel is given by

$$C = B \log_2(1 + S/N) \tag{1.1}$$

where, C is the channel capacity in terms of the maximum rate at which the information can be transmitted, B is the bandwidth and S/N is the signal power to noise power ratio. The bandwidth of a single laser channel could be several thousand times greater than the total currently available spectrum at radio and microwave frequencies, resulting in an enormous capacity. However, this advantage cannot be fully realized at present due to the lack of adequate optical modulators and receivers to operate at such high frequencies.

It has been shown that for a given transmitting antenna size, the angular width of the transmitted beam is inversely proportional to the optical frequency and the spatial power density at the receiver is proportional to the square of the frequency [4]. The extremely narrow beam width of a laser light makes it highly directional. The directivity in turn allows the transmitted power to be concentrated on a given receiver area. Therefore, in a laser system, much less power needs to be transmitted to obtain the same power density as in a microwave system. For example, the spatial power density at the receiver is one million times larger for an optical system with a ten centimeter diameter antenna, compared to a microwave system

transmitting the same amount of power with a ten meter diameter antenna. It is evident that very high antenna gain is possible with the laser systems.

There are also several other advantages. Optical communication offers a very secure link between two points. The transmission secrecy is particularly desirable in military applications. The system is not susceptible to external electromagnetic interferences. Because of the narrow spectral widths of the laser sources, filtering from ambient light is simple and background noise can be easily minimized. Laser links can be quickly established without going through the problems and delays involved in obtaining a government license for wireless communication.

1.1.2 Applications of laser communication systems. In view of the above mentioned features several practical applications of laser communication systems have been envisioned. They are summarized in Figure 1-1. The high antenna gain resulting from the directivity of a laser beam can best be exploited in space applications such as the links between the earth and the moon, and between spaceships and satellite interconnections, where the antenna size must be minimized to meet the weight and space limitations. Lasers may well be the key to communication outside our solar system.

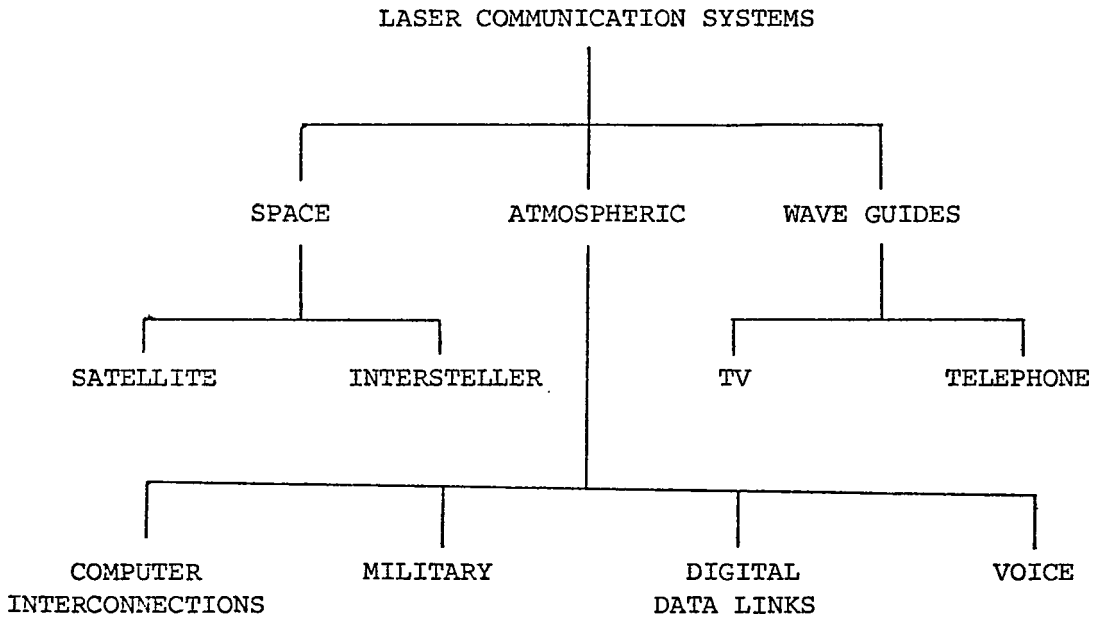

FIGURE 1-1

The directivity which is so desirable for the space applications might appear to be a handicap for the terrestrial applications because the communication is restricted to a line of sight path. However, the use of optical pipes and wave guides is being investigated to overcome this difficulty and take advantage of laser bandwidths to establish coast to coast television-telephone communications. Several applications are also possible over short distance, line of sight atmospheric paths. Here, the security and convenience of laser systems, along with their immunity from federal licensing problems appear attractive. For instance, the voice communication links could be used in large industrial complexes, aircraft or

ship to ship communications, or in tactical applications. Such links can also be easily installed across highways, rivers, mountains or difficult terrain. Optical links between computer circuits can decrease the transmission delays, thus breaking one of the bottlenecks of computer speeds. Digital data links could be established between computer terminals or business districts.

1.1.3 Sources for optical communication. For atmospheric laser communication systems only those transmission frequencies are useful which lie in an atmospheric window, so that the atmosphere is relatively transparant to them. He-Ne laser transmitting red light at 0.6328 μm, the CO_2 laser emitting infrared at 10.6 μm, the ND:YAG laser emitting at 1.06 μm, the gallium-arsenide (GaAs) injection laser emitting at 0.9 μm, as well as the light emitting diodes emitting over a wide spectrum are some of the sources at the disposal of the communication system engineer. The potential of the LED is, however, very limited due to its low output power and diverging beam.

Among the various laser sources available for optical communication, the infrared emitting GaAs semiconductor injection laser diodes seem very promising due to some of their outstanding characteristics. The most striking feature of the injection laser is the simplicity with which its electrons are "pumped", or excited into higher energy states. Figure 1-2 compares the pumping mechanism of the injection laser with that of the other lasers.

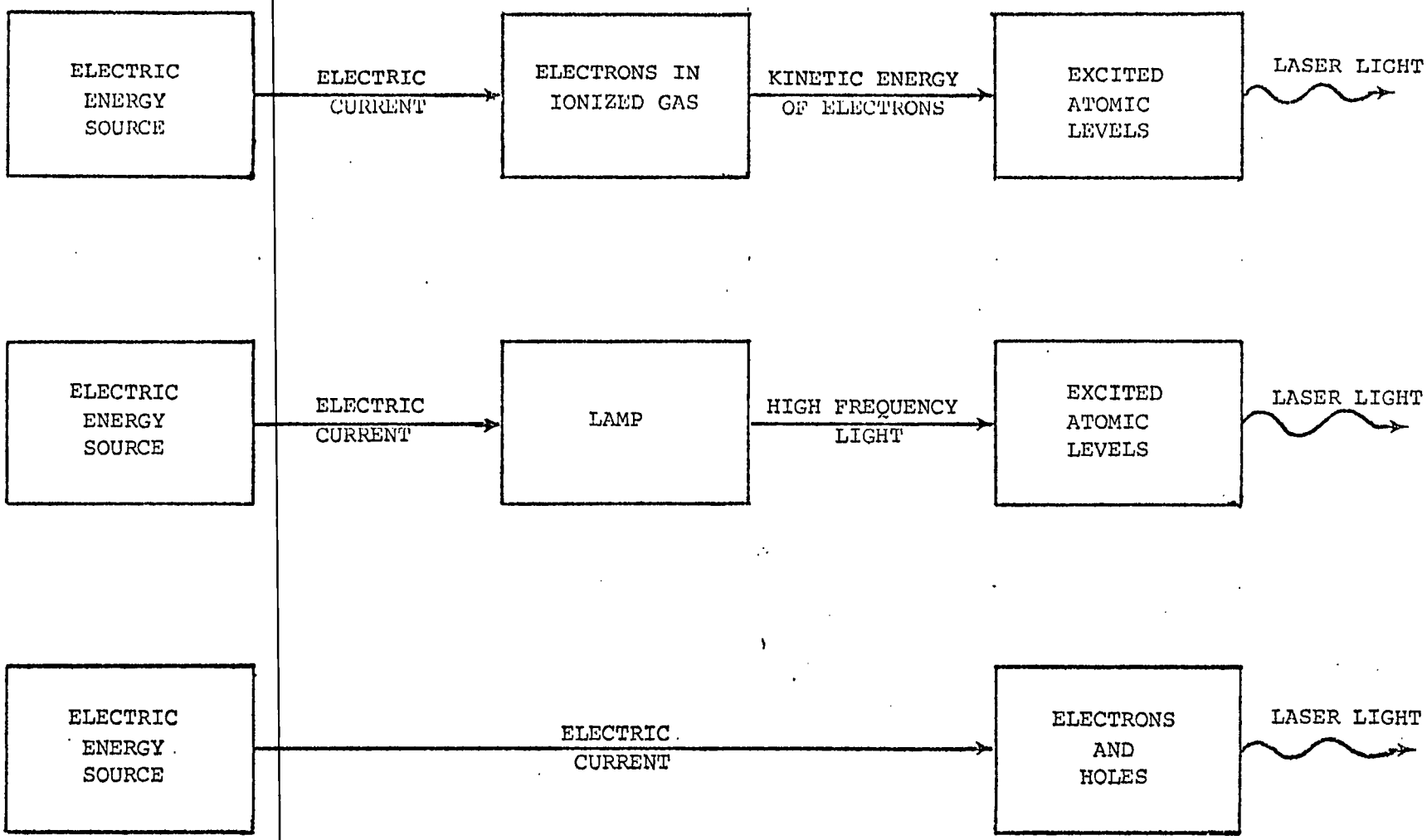

FIGURE 1-2

COMPARISON OF ENERGY TRANSFER MECHANISMS IN LASER SOURCES

In the case of some gas lasers, the electrical energy is first converted into the kinetic energy of electrons. The high energy electrons then excite the atoms of the gas by colliding with them. In some optically pumped lasers, the electric current flashes a lamp that emits radiation to excite the atoms of the solid state material. Injection lasers, however, use electrical energy directly, pumping the electrons to high energy states by injecting them across a p-n junction.

The elimination of the auxiliary pumping apparatus, which is often quite bulky and expensive, makes injection lasers an extremely compact, rugged and inexpensive source of laser radiation. The conversion of energy from one form to another as required in the other types of lasers is usually inefficient, but the direct energy transfer in the injection laser results in relatively high efficiencies. For example, even in the earlier homojunction injection lasers this conversion efficiency was typically 20%, compared to 1% in optically pumped lasers and 0.01% in gas lasers. Now with more sophisticated close confinement heterojunction structures (Chapter 2), the efficiencies of about 40% are possible. The fact that the injection lasers need simply a passage of current for activation is most interesting from the communication point of view. These lasers can be directly modulated just by modulating the current through them. In spite of their tiny size, the injection lasers are capable of emitting fairly high peak

powers. Laser diodes giving up to one-hundred watt output power in a room-temperature operation are available with the present day technology.

The small size, however, also imposes some limitations on the injection lasers. Due to the very high current densities involved in the excitation of these lasers, they suffer from a rather serious heating problem. In fact, the fullest utilization of the attractive features of the injection laser and its continuous operation is possible only at the cryogenic temperatures. Although efforts are being made to achieve continuous room-temperature operation, at present the room-temperature operation of injection lasers is possible only in a pulse mode and at very low duty cycles (0.1% typical[1]). In an injection laser, the lasing action takes place in a junction region only a few mils wide. This gives rise to further limitations. First, it limits the output power capability of the laser. For example, the injection laser cannot match the output of a solid state laser in which the laser action takes place throughout the volume of many cubic inches. Also the narrow emitting region causes the injection laser beam to diffract more, so that the emerging light is more divergent. The spectral width of a typical injection laser light is about 40 Å, with the result that the coherence length, $C/\Delta f$, of laser radiation is only a fraction of a millimeter.

---

[1] Recently developed large-optical-cavity (LOC) laser diodes [6] offer duty cycles up tc 5% at room-temperature operation.

Injection lasers, therefore, lack the excellent coherence and spectral purity of gas or solid state lasers.

Fortunately, these limitations are not serious disadvantages. The divergence of the beam can be corrected by a suitable lens assembly, although it somewhat negates the basic simplicity and compactness of the injection lasers. The lack of coherence is not a major consideration, as it is difficult to visualize many systems which could make full use of a coherent source. The coherence is very soon destroyed by the effects of atmospheric turbulence (Chapter 3). It can be safely concluded that the advantages of the injection laser easily outweigh its limitations and it remains a strong contender for optical communication applications.

1.2 Review and the State of the Art in Injection Laser Communication Research

After the emergence of lasers, early research in the field of optical communication was concentrated on gas and solid state laser systems. Injection laser communication systems did not look too promising, because of the unreliable nature of the devices resulting from metallurgical flaws in the junction and lack of adequate understanding of the material limitations. Nevertheless, some interesting experiments did take place. As early as 1962, a team of MIT scientists demonstrated TV transmission with a GaAs source in the laboratory [1] and soon thereafter with an elaborate setup and cryogenic operation of the

laser diode, they suceeded in transmitting the video signal as far as thirty miles. In 1964, RCA researchers demonstrated a GaAs laser voice communication system operational at room temperature. The system used pulse frequency modulation and had a six kilohertz wide voice channel [7].

The devices began to improve in the late sixties. Recognizing its potential in secure tactical communications, the military took active interest in the development of injection laser communication links. Schiel and co-workers demonstrated a link operating at liquid nitrogen temperature at an average rate of ten kilobits per second. They reported signal-to-noise ratio of seventy decibels over a one mile range [8]. Dworkin and co-workers at the U. S. Army Electronics Command proposed a link transmitting at a data rate of 98 kilohertz and anticipated an error rate of 10^{-6} over a three kilometer path [9]. Holobeam Inc. designed a compact PPM voice communication system for the Navy for ship to ship communication during refueling. Optics were mounted on the helmet with electronics and power supply fitted to the belt. With a defocused beam, the link could operate up to a 250' range [10]. Investigating the space applications of the injection laser, IBM conducted voice communication experiments on Gemini VII utilizing a PFM technique with an average pulse repetition rate of eight kilohertz [11]. Gammarino, et al. have presented a detailed design and theoretical performance of a high data rate injection laser link for space applications [12].

With the present day technology, injection laser communication systems have attained a good degree of sophistication. Although the systems are still mainly in a research and development stage, a few commercial voice and data links have recently started appearing in the market. American Laser Systems Inc. have designed a GaAs transmitter generating ten watt pulses at rates to ten kilohertz. Ninety-nine percent reliability is predicted in almost any weather for ranges up to three miles. OpCom Inc. markets a short distance PFM voice communication link using a five watt laser source and the pulse repetition rate is over one-hundred kilohertz. They have also produced a digital data link operating at data rates up to about thirty-eight kilobits per second, with a five watt GaAs laser. Error rate is specified as 10^{-8} for one mile range, in virtually all weather conditions.

1.3 Objective

This work is primarily concerned with the investigation of a GaAs injection laser diode as a source of optical frequency for the short distance atmospheric communication applications. To accomplish this, a pulsed communication link was established on the University campus. The index of the performance of such a communication system is considered to be the bit-error-rate. Based on this index, the performance of the link has been evaluated. It is intended that this experimental setup will serve as a groundwork for further research in related areas.

Chapter 2

SYSTEM ASSEMBLY: COMPONENT ANALYSIS

The technique of optical communication essentially consists of transmitting a suitably modulated and collimated light beam to the receiver and then demodulating it in order to retrive the information. The information signal varies some attributes such as intensity, frequency or polarization of the transmitted beam. Since the room-temperature operation of an injection laser is limited to the pulse mode, it is a very suitable source for transmitting digital information. In a PCM format, for example, the pulse can represent a "one" bit and no pulse can represent a "zero" bit of the binary code.

A block diagram of the physical model of an optical communication link utilizing an injection laser source is illustrated in Figure 2-1. The statistical model of the system is discussed in Chapter 3. The major components of the system and their operating characteristics are discussed in this chapter.

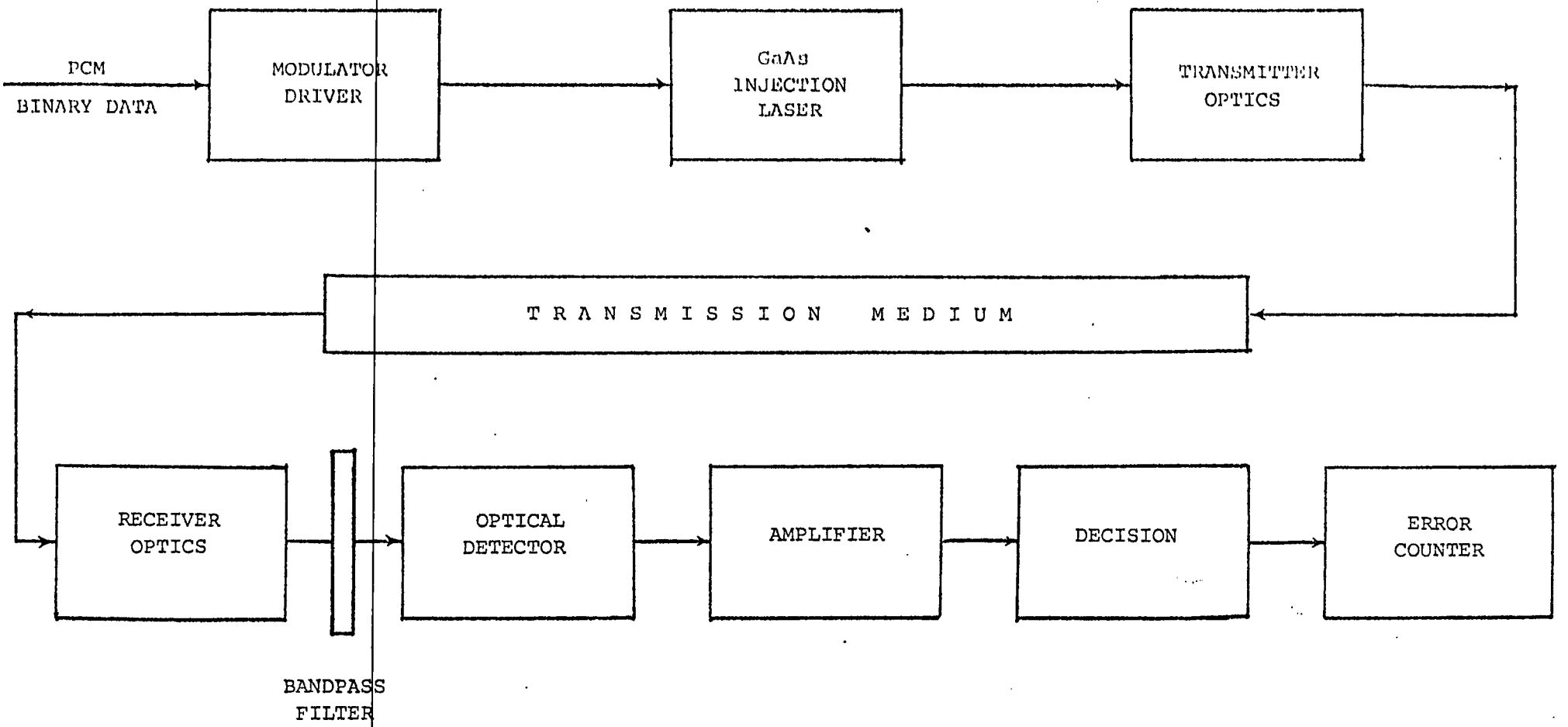

FIGURE 2-1

BLOCK DIAGRAM OF THE OPTICAL COMMUNICATION SYSTEM

2.1 The Injection Laser

In the field of quantum electronic devices the GaAs injection laser diode is strategically positioned between the light emitting diode and the conventional gas or solid state laser. Whereas in the early sixties, the laser emerged as a solution in search of a problem, gallium arsenide for many years remained a semiconductor in search of an application. The phenomenon of electroluminescence in p-n junctions due to the recombination of electrons and holes was known for over fifty years. However, in most semiconductors this process was very inefficient and most of the recombination energy was wasted as heat. Soon after the advent of the laser, it was discovered that the recombination efficiency was very high in GaAs semiconductors. In 1962, three different research teams [13] almost simultaneously demonstrated lasing action in GaAs p-n junctions and since then, injection laser diodes have received a great attention because they are the simplest to operate and the most compact of the known lasing sources.

A brief theory of the device, along with its important properties and characteristics pertinent to communication applications are presented in the following pages.

2.1.1 Structure. Basically, an injection laser diode is a p-n junction with a precisely controlled impurity profile in a direct bandgap semiconductor material.

By definition, the laser is a device with amplifies light by stimulated emission of radiation. It therefore demands the existence of a suitable amount of stimulated

emission and the provision of some form of feedback mechanism to ensure that the radiation passes through the device many times and undergoes amplification. In the injection laser, the first of these requirements is achieved by forward biasing the p-n junction so that population inversion is attained at a particular threshold value, and the second is achieved by the construction of a resonant structure known as the Fabry-Perot cavity. The Fabry-Perot cavity in an injection laser is formed by cleaving the opposite ends of the semiconductor crystal and roughening the adjacent sides. This enhances the optical gain of the system and at the same time suppresses the undesirable modes.

Most of the modern injection lasers, including the one used in this experiment, are manufactured using the so-called close confinement (CC) process. Figure 2-2 shows the close confinement structure of a single heterojunction injection laser. The basic CC laser structure consists of three regions. Region 1 is a p^+-type epitaxial layer of GaAlAs on an n-type GaAs substrate. The lasing region 2 is a compensated p-type material and region 3 is the n-type substrate. In the CC structure a wave guide effect is accomplished by suitable engineering of the index of refraction profile perpendicular to the junction plane. The wave guiding sharply reduces internal optical loss by preventing light leakage into the highly absorbing p^+-region adjoining the lasing region. Another benefit of this

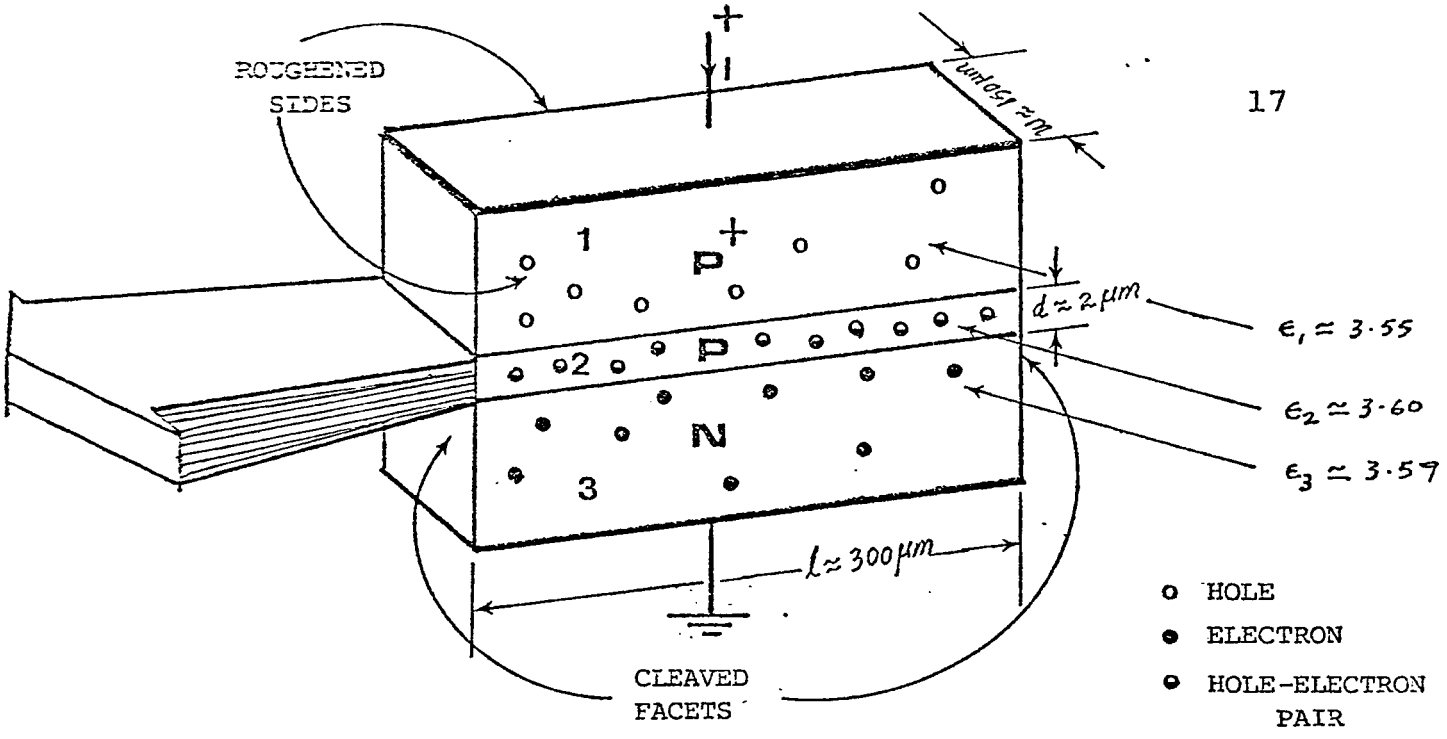

FIGURE 2-2

CLOSE CONFINEMENT STRUCTURE OF INJECTION LASERS

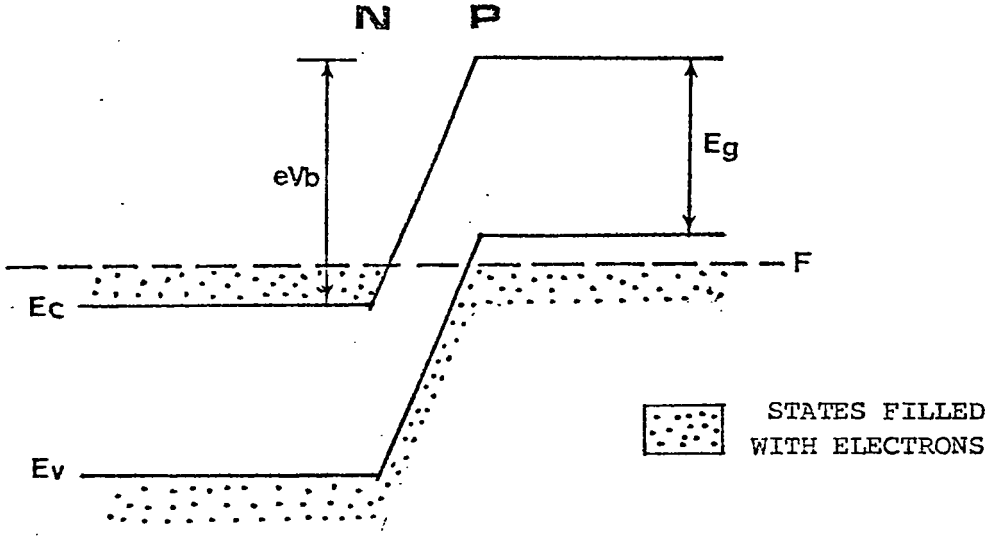

(a) V = 0

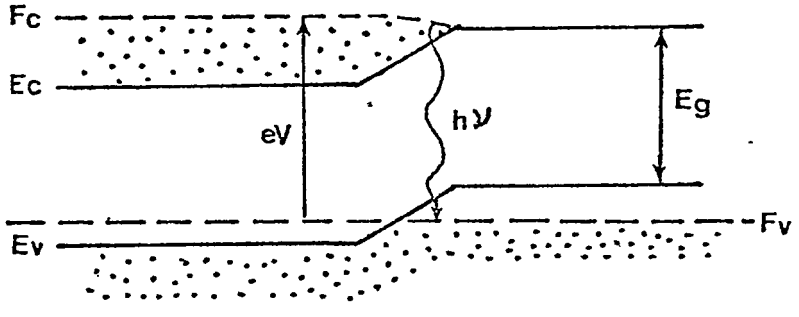

(b) V > 0

FIGURE 2-3

structure is that the electrons injected from the n-region to the active p-region are prevented from diffusing into the p^+ region because of the potential barrier. As a result of this confinement of electrons to the narrow active region, the optical gain for a given current density is increased since most of the injected electrons contribute to lasing.

2.1.2 Principle of operations. The mechanism of lasing in the injection laser diode can best be explained with the help of an energy diagram. Figure 2-3 is a typical plot of energy versus distance of a p-n junction. The n-type region is a semiconductor doped with a donor impurity such as Te and has enough free electrons to fill the conduction band up to the Fermi level F. The p-type material is formed by doping the GaAs with an acceptor impurity such as Zn, and has its valance band filled to level F with the free holes. With no applied voltage, the electrons diffuse from the n-side to the p-side and the holes from the p-side to the n-side until a potential barrier V_b is built up across the junction to prevent further current flow. If a forward voltage, V, is applied across the junction to overcome the potential barrier or to raise the n-side energy bands relative to the p-side energy bands as shown in Figure 3-2 (b), then electrons cross the junction to the p-side, or in other words, the "carrier injection" takes place. As they reach the p-side, the electrons make a transition to an empty state in the valance band to recombine with the holes and emit photons with energy approximately equal to E_g.

At low values of forward voltage, the diode emits a small incoherent radiant flux. However, if the diode is biased beyond a certain threshold value, a situation results where the upper energy level is occupied with a greater probability than the lower energy level. Under this condition, known as the "population inversion", the probability of radiative downward transition exceeds that of upward transition leading to a net stimulated emission. The condition for stimulated radiation is given by

$$F_c - F_v > h\nu \tag{2-1}$$

where, F_c and F_v are the quasi-Fermi levels[1] associated with the upper and lower energy states, h is the Planck's constant and ν is the frequency of emission. Of course, for a sustained laser action the presence of a resonant cavity with sufficient gain to overcome the optical losses is necessary.

The threshold current density necessary for the population inversion greatly depends on the temperature. At 0°K it is given by

$$J_t = \frac{1}{\beta}\left[\frac{1}{\ell} \ell_n\left(\frac{1}{r_1}\right) + \alpha\right] \tag{2-2}$$

where β is a constant for the device, ℓ is the length of the resonant cavity, r_1 is the reflectivity of the cavity and α is the absorption coefficient. The laser spectra above and below the threshold are shown in Figure 2-4.

---

[1]The quasi-Fermi level is the energy at which the probability of a state being occupied is equal to one-half.

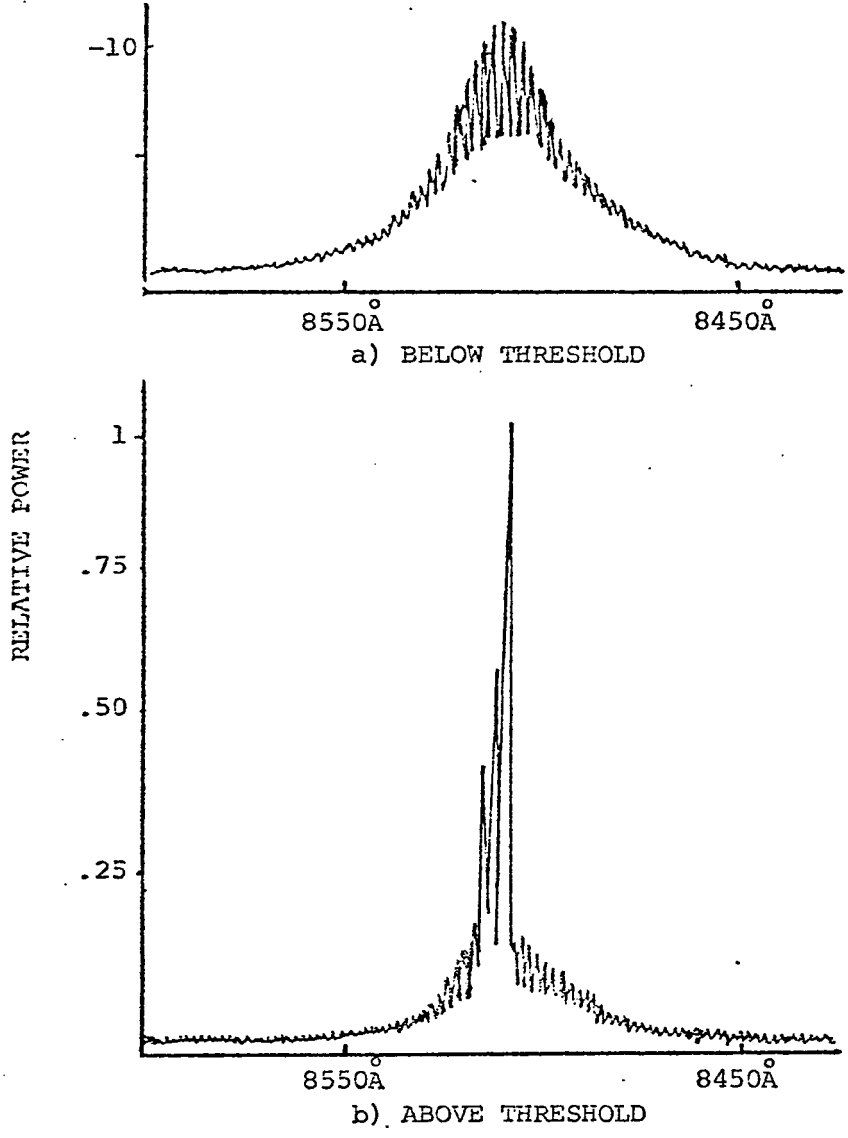

FIGURE 2-4

LASER SPECTRA NEAR THRESHOLD AT 77°K

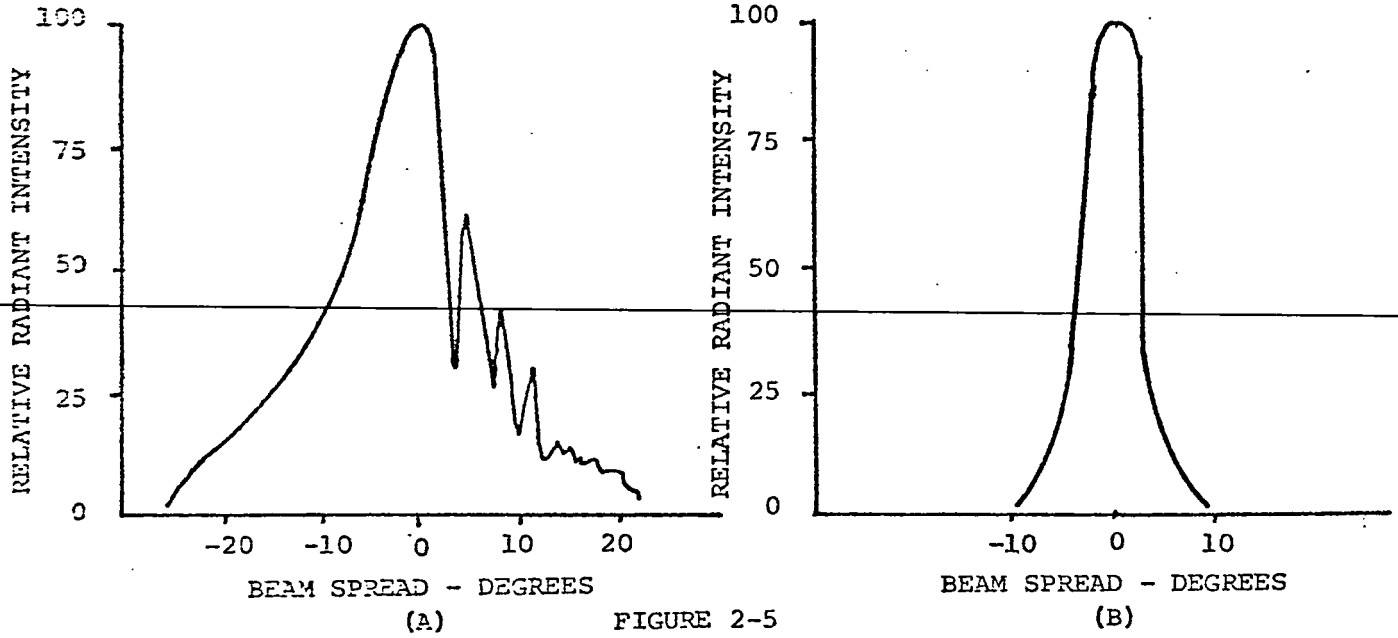

FIGURE 2-5

TYPICAL RADIATION PATTERN OF INJECTION LASER A) IN A PLANE PERPENDICULAR TO THE PLANE OF JUNCTION AND B) IN A PLANE PARALLEL TO THE PLANE OF JUNCTION

Due to the very small dimensions of the active region of the device, the light emitted from an injection laser does not have the highly directional properties of other laser beams. The angle of divergence of the beam in a given direction varies inversely as the dimension of the active region in that direction. A typical radiation pattern is shown in Figure 2-5.

2.1.3 Laser output and efficiency. As described in the last section, laser radiations in an injection laser are emitted due to the recombination of the minority carriers (electrons) injected into the conduction band of the p-type material, with the majority carriers (holes) of the valance band in the junction regions. In a direct band gap GaAs semiconductor, the probability that this recombination will be radiative is almost 100% at 77°K and up to 70% at room temperature. The number of photons emitted from the laser cavity per injected electron is termed the "external quantum efficiency", and is defined as

$$\eta_{ext} = \frac{\text{Number of photons emitted}}{\text{Number of electrons injected}} = \frac{P/h\nu}{I/q} \qquad (2\text{-}3)$$

where P is the output power and I is the current through the device. Since

$$h\nu \simeq E_g \simeq eV \qquad (2\text{-}4)$$

the external quantum efficiency can be written as

$$\eta_{ext} = \frac{P}{IV}. \tag{2-5}$$

If the device is operated above the threshold current I_o, stimulated emission is obtained and the laser output increases linearly with the current. In this particular case the external quantum efficiency is denoted by $\Delta\eta$ and is called the incremental quantum efficiency. At a given temperature

$$\Delta\eta = \frac{P}{(I - I_o)\ V}. \tag{2-6}$$

The incremental quantum efficiency of a close confinement injection laser could be as high as 50% at room temperature.

The power conversion efficiency or the radiant efficiency of the device is simply the ratio of the output power to the forward power dissipation

$$\eta = \frac{(I - I_o)\ V\ \Delta\eta}{IV + I^2 r} \tag{2-7}$$

where, r is the forward resistance of the diode. Typical values of radiant efficiency are 5% at room temperature and 50% at 77°K.

2.1.4 Temperature effects on injection laser characteristics. Since an injection laser must be operated at high current densities, it must be operated only in pulse service and within the specified maximum pulse durations and duty factors in order to keep the power dissipation in the device

down to an acceptable level. Thermal effects profoundly influence the operation of the device. The junction temperature rise is proportional to the average power dissipated in the device, and is given by

$$\Delta T = \Theta(IV + I^2 r)\delta \qquad (2\text{-}8)$$

where δ is the duty cycle of operation and Θ is the thermal impedance [14] of the device. Θ depends upon the device geometry and the thermal conductivity of the heat sink on which the junction is mounted. The adverse effects of temperature on some of the important characteristics of the laser diode are considered in the following paragraphs.

A) Threshold:

The lasing threshold current is a cubic function of the temperature so that [15]

$$I' = I_o\left(1 + \frac{\Delta T}{T_o}\right)^3$$

where I' is the threshold current at a temperature ΔT above the ambient temperature T_o. Figure 2-6 shows a typical plot of the threshold current density versus temperature.

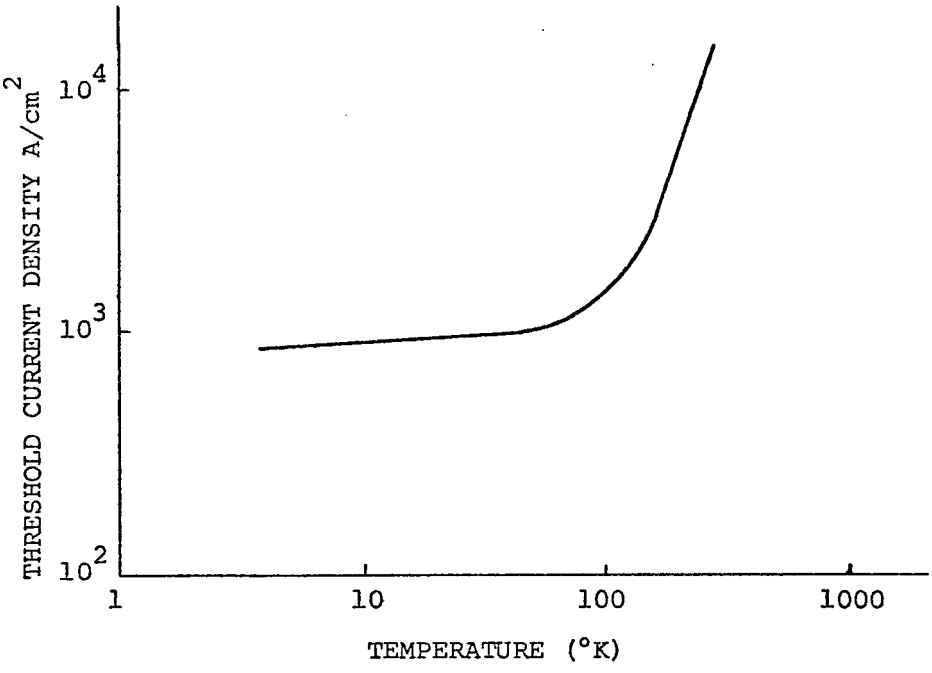

FIGURE 2-6

THE THRESHOLD CURRENT AS A FUNCTION OF TEMPERATURE

B) Output and Efficiency:

Figure 2-7 shows the output of a typical injection laser as a function of current at different temperatures. Figure 2-8 is a typical plot of efficiency versus temperature. Although the incremental quantum efficiency is relatively insensitive to temperature, the power efficiency decreases rapidly with temperature rise, because at high temperatures the devices must be operated at high current densities in order to exceed the threshold current.

C) Spectral Properties:

The energy of a photon emitted in the recombination process is approximately equal to the band gap energy of the semiconductor (Equation 2-4). At 77°K, the band gap energy of gallium-arsenide is about 1.51 eV and it varies with the temperature according to the relationship [16],

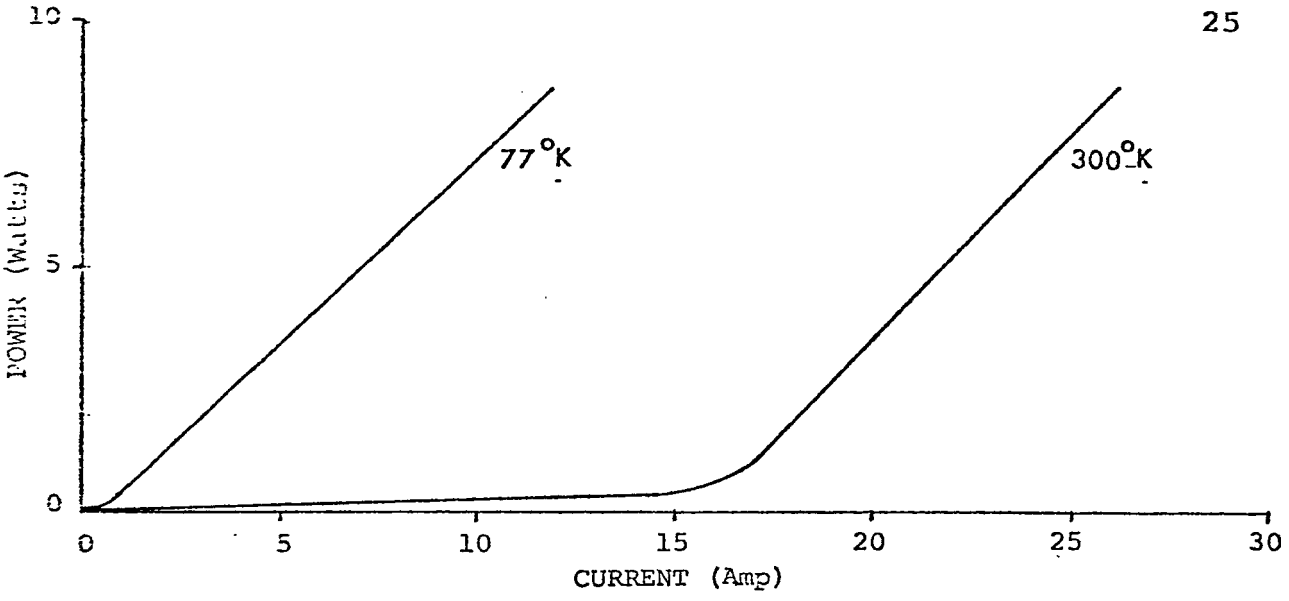

FIGURE 2-7

INJECTION LASER OUTPUT AS A FUNCTION OF CURRENT, AT DIFFERENT TEMPERATURES

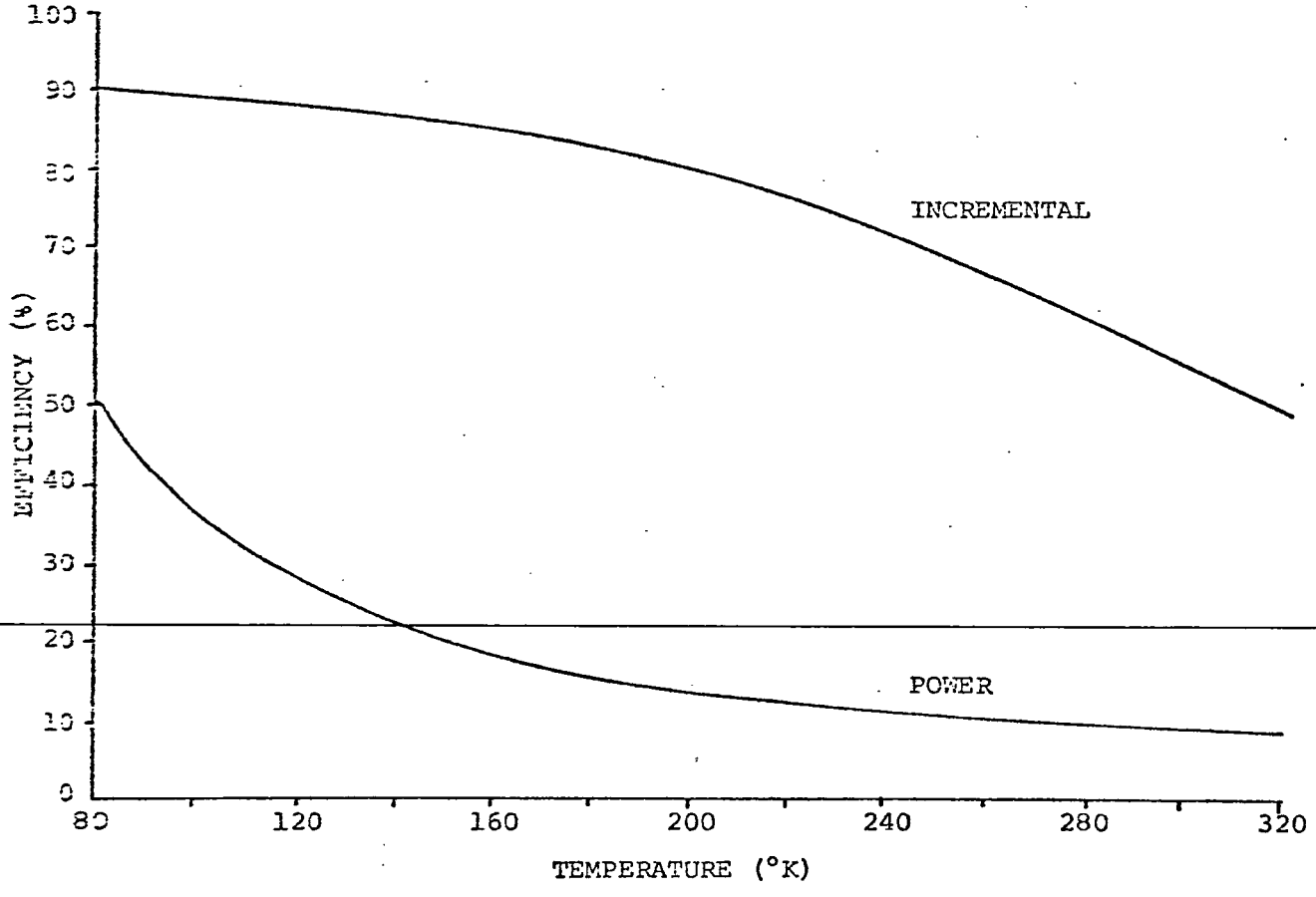

FIGURE 2-8

VARIATION OF EFFICIENCY WITH TEMPERATURE

$$\frac{dE_g}{dT} \simeq -5 \times 10^{-4} \text{ eV/°K} \qquad (2\text{-}10)$$

It has been shown that the energy of the photon remains about 0.07 eV less than the band gap energy over a wide temperature range [14]. The peak wavelength of emission is, of course, related to the photon energy by,

$$\lambda = \frac{hc}{E_p} = \frac{1240}{E_p} \text{ nm.} \qquad (2\text{-}11)$$

where c is the velocity of light and E_p is the energy of a photon. It follows that the wavelength increases approximately 0.23 nm/°K with the rise in temperature. Figure 2-9 shows the photon energy and emission wavelength as a function of temperature. At higher temperatures several modes are generated in the laser cavity [15] and the spectral bandwidth therefore increases. Figure 2-10 shows the effect of temperature on the spectral shape.

2.1.5 Communication application of the injection laser. The fundamental problem in any optical system is to direct sufficient power to the detecting element and in this regard, an important property of the optical source is its brightness. Higher brightness means higher antenna gain which in turn results in reduction in the size of the optics. Brightness is expressed in $W/cm^2 \cdot$sterad and depends on the radiant power density at the emitting aperture and the beam width into which the power is emitted. A typical peak value of brightness for a single laser diode is 2×10^7 W/cm^2.

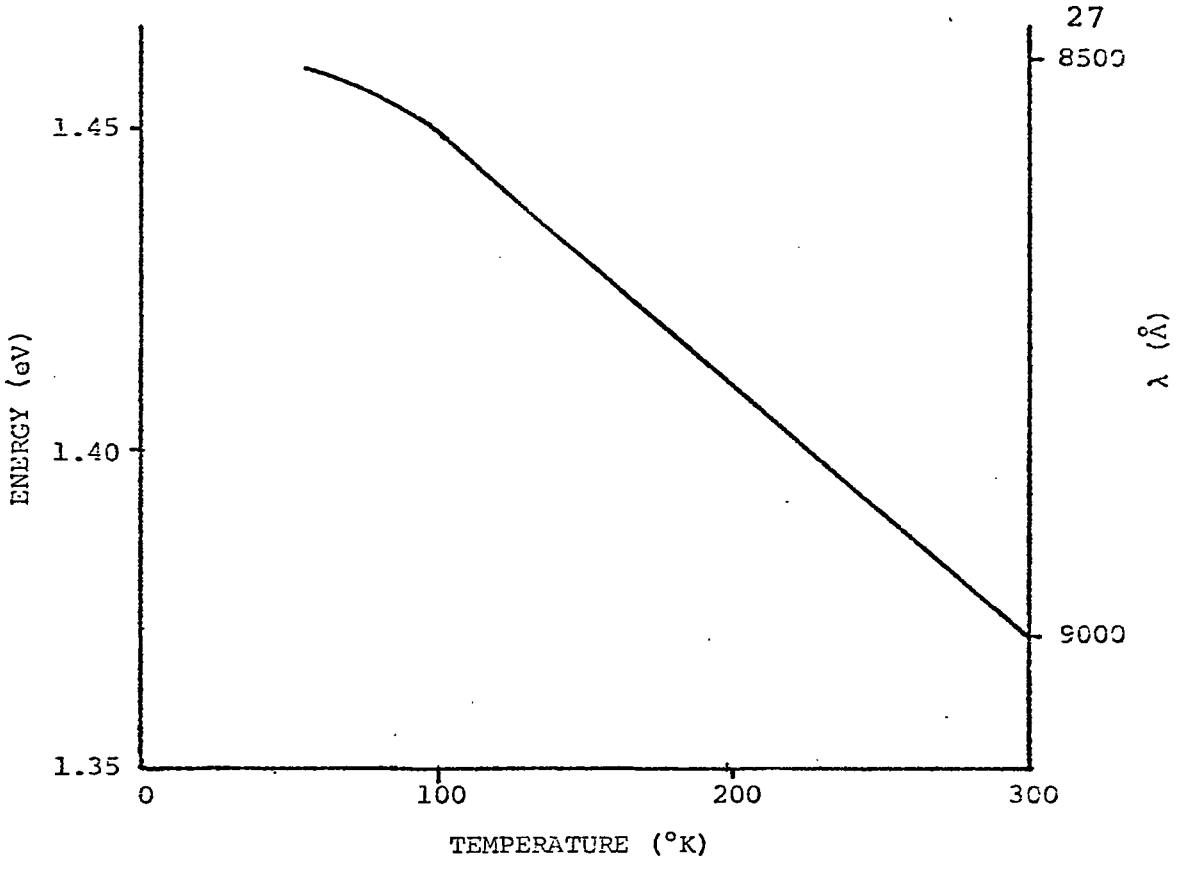

FIGURE 2-9

LASER PHOTON ENERGY AS A FUNCTION OF TEMPERATURE

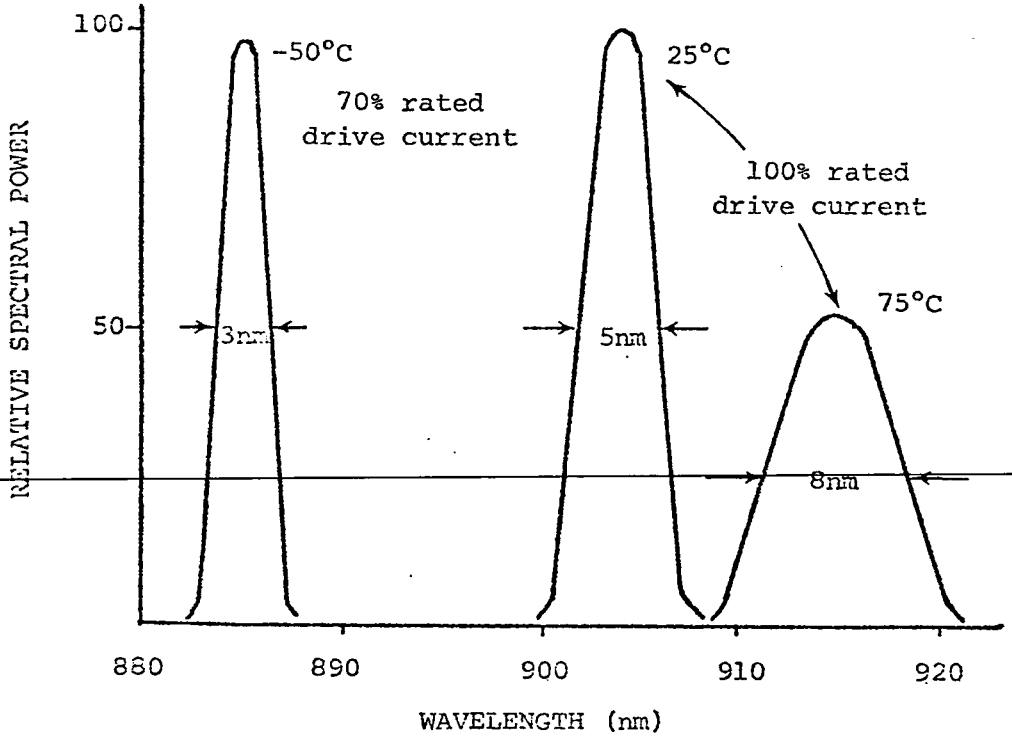

FIGURE 2-10

TEMPERATURE EFFECTS ON LASER SPECTRUM [17]

sterad. Although solid state lasers offer much higher peak powers and brightness than injection lasers, it is instructive to compare its brightness with other sources of radiation. If a tungsten filament is operated almost to its melting point, the brightness is about 100 W/cm^2. sterad, and the hottest carbon arcs reach about 1000 W/cm^2. sterad [14].

Due to the power dissipation limitations, gallium-arsenide lasers in most practical applications are used in a pulsed mode of operation. A detailed analysis of the rate at which the temperature of the diode rises during the pulse operation is a complex problem which depends on the structure of a particular diode. Heat is generated both at the junction and due to the resistivity of the semiconductor, in the bulk of the device. For the high duty cycle, heat will not have time to diffuse away, and the junction temperature will continue to rise until a thermal equilibrium is reached. However, the temperature at this point could be so high that the laser action would be no longer possible. This calls for a low duty cycle operation allowing sufficient time for cooling between the successive pulses. In this mode of operation a single laser diode can give reasonably high peak output power although the average power will be small since

$$P_{av} = P_{Pk} \times \delta \qquad (2\text{-}12)$$

where δ is the duty cycle. With the current technology

laser diodes giving peak output powers up to 100 W at room temperature are available. To obtain higher power outputs, lasers can be used in series combinations. Fabricated in stacks on a single substrate, this arrangement offers the possibility of obtaining kilowatts of peak power, however, the average power is again severely limited by the problem of heat removal from the closely packed devices.

Injection lasers are at their best at cryogenic operations. Most notably the threshold current reduces by more than an order of magnitude and the power efficiency jumps almost by the same factor. Continuous power output of 1 W or more can be readily obtained with the laser operated at liquid-nitrogen temperature (77°K). Seven watt continuous power has been reported with the device cooled to 4.2°K [18]. However, the complexity associated with the cryogenic operation is warranted only in specialized communication applications such as the links carrying multichannel information, or very high data rate space communications.

One of the chief advantages which semiconductor lasers possess over other lasers is that the light output can be modulated up to high frequencies simply by varying the current through the device. The modulation frequency is ultimately determined by the turn-on characteristics of the laser diode. There is a definite delay between the onset of the current pulse and the turn on of the

stimulated emission, due to the finite time required to build up the population inversion. This delay decreases with the amplitude of the current pulse. In general, it is a few hundred nanoseconds at the room temperature and less than one nanosecond at 77°K. There is also a small delay associated with the rise time of the stimulated emission, once it begins. This lag is of the order of a nanosecond at the room temperature but as little as 0.1 nanosecond at 77°K.

For this experiment, an RCA type SG-2004 single GaAs injection laser diode was used. The detailed characteristics of the device were not available. Known parameters are listed in Table 2-1.

Wavelength	904	nm
Emitting region dimensions	6 x 0.08	mils
Series resistance	0.35	Ω
Threshold current	15	A
Peak forward current	25	A
Maximum pulse duraction	200	ns
Maximum duty cycle	0.1	%
Peak radiant power output - max	9	W
Peak radiant power output - min	5	W
*Incremental quantum efficiency	8	%
*Power efficiency	4	%
Voltage drop at peak current	9	V

*Approximate

Table 2-1

Characteristics of SG-2004 GaAs Laser Diode at Room Temperature

2.2 Optical Detectors

Optical detectors in an optical communication system transform the optical signal into electrical signal by converting incident photons to electrons. Photodetectors are square-law devices that respond to the intensity which is the square of the amplitude of the electromagnetic field. This section contains a discussion of the photodetection techniques and a summary of the detector performance criteria. The operation of the particular kind of detector chosen for this experiment has been described. Detection noise is considered in Chapter 3.

Before considering the photodetecting device itself, it will be worthwhile to discuss the techniques commonly used in the detection of optical signals.

2.2.1 Detection techniques. Two basic techniques are available for detecting an optical signal.

A) Optical Heterodyne Detection:

In an optical heterodyne or coherent detection scheme two optical fields at different frequencies are mixed at the input of a photodetector as shown in Figure 2-11 and an electrical signal at the intermediate or difference frequency is recovered at the output of the photodetector. Optical photomixing is made possible because of the narrow spectral lines and high powers available from laser sources.

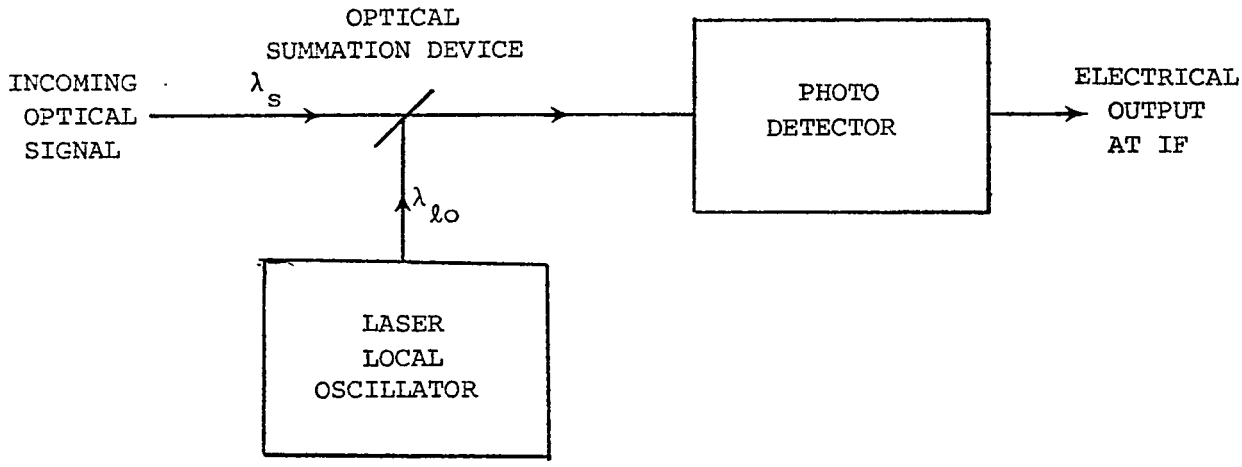

FIGURE 2-11

COHERENT DETECTION SYSTEM

The mean value of the photocurrent generated at the intermediate frequency is

$$I_{IF} = R\sqrt{2P_{lo}P_s} \qquad (2\text{-}13)$$

where R is the responsivity of the detector, P_{lo} is the local oscillator power and P_s is the received signal power. The photomixing action takes place over the detector surface area. The maximum IF signal is obtained only when the signal and local oscillator beams bear the same phase relationship over the complete area of coincidence. It is therefore implied that the optical phase must be uniform over the complete wavefront of each beam. In order to meet this requirement, the following conditions must be satisfied [19].

1) The two beams must have the same mode structure.
2) The two beams must be coincident and to provide maximum signal-to-noise ratio, their diameters must be equal.
3) The beams must propagate in the same direction.
4) The two wavefronts must have the same curvature.
5) The beams must be identically polarized.

These requirements are extremely severe and difficult to meet in practice. However, coherent detection offers many advantages. The conversion gain of a heterodyne detector, defined as a ratio of the IF output power to signal input power depends upon the local oscillator power. High gain is therefore possible, even with a detector having no internal current gain, by using a local oscillator with sufficient power. Heterodyne detection systems have a diffraction limited field of view [20] and small spectral acceptance bandwidth. Effective background discrimination is thus obtainable. The operation of a heterodyne detector is limited by the quantum noise of the local oscillator source. It therefore allows the realization of optical receivers with wide bandwidths and high sensitivity almost equal to the theoretical quantum noise limit. In addition, photomixing preserves the frequency and phase information of the input signal and can be used for intensity, phase and frequency modulated signals.

In spite of all these advantages, the critical requirements outlined above place severe restrictions on

the application of heterodyne technique. This technique is very inefficient and unstable for atmospheric optical communication systems due to the random phase fluctuation arising from the atmospheric turbulence (Chapter 3).

Besides, the heterodyne detection technique is very inappropriate for the injection laser system being considered for this experiment because of the relatively wide spectrum and the lack of adequate coherence of the laser source. The direct detection technique was used in the experiment and is described below.

B) Direct Detection:

As shown in Figure 2-12, the direct photodetection technique consists simply of detecting the incident energy within the spectral response of the filter, with the resultant detected signal being able to follow the amplitude variations induced by the incoming signal modulation.

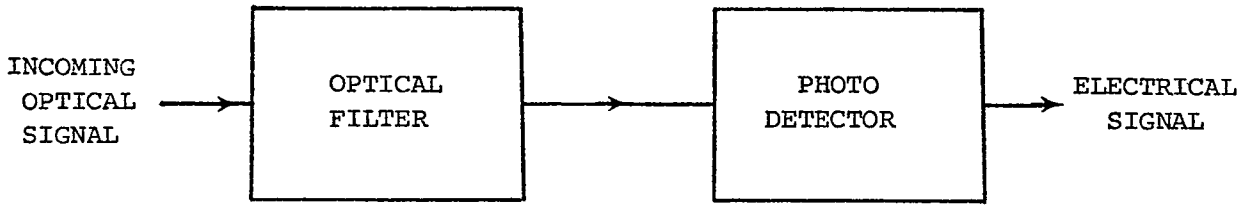

FIGURE 2-12

DIRECT DETECTION SYSTEM

In direct photodetection, all optical frequency and phase information is lost. The detector responds to

individual photons, producing η electrons for every received photon, where η is the quantum efficiency of the detector. The direct detector therefore acts like a photon counter. The photocurrent at the output of the detector having a responsivity, R, is

$$I_s = R\ P_s. \tag{2-14}$$

The direct detector does not provide the effective background noise discrimination that is obtainable in the heterodyne detector. To achieve spectral discrimination, an optical filter must be used, and to achieve spatial filtering, the field of view must be restricted. Also the direct detector cannot provide detection gain unless a post-detection secondary emission multiplication device is used as a photodetector. The main advantage of direct detection is its simplicity, which results in reduced cost, weight, size and power consumption. The direct detector reproduces amplitude variations of the incident power. The loss of coherence is not critical in a direct detection system.

2.2.2 Photodetector performance criteria. The major requirements imposed on photodetectors and detection systems for optical communication applications include, 1) large response to the incident optical signal, 2) sufficient instantaneous bandwidth to accommodate the information bandwidth of the signal, and 3) a minimum of noise added by the demodulation process.

The basic performance criteris to evaluate an optical detector are the following.

A) Responsivity:

The responsivity of an optical detector is the measure of its sensitivity and is expressed as a ratio of the rms value of the photocurrent to the rms incident optical power.

$$R = \frac{GI_s}{P_s} = \frac{G\eta q}{h\nu} \quad \text{amps/W} \tag{2-15}$$

where η is the quantum efficiency of the detector, q is the electronic charge, h is the Planck's constant, ν is the frequency of radiation and G is the gain in the detector.

B) Quantum Efficiency:

The quantum efficiency of an optical detector is simply the ratio of the average number of electrons generated in the detector to the average number of incident photons. It is just another way of measuring the effectiveness of the detector in converting light to current, and is given by

$$\eta = \frac{1.24R}{\lambda G} \tag{2-16}$$

where λ is the wavelength in microns.

C) Noise Equivalent Power:

The NEP of an optical detector is a measure of the minimum power that can be detected and is defined as the minimum radiant power necessary to give a signal-to-noise ratio of unity, when the noise is normalized to unit

bandwidth. The units of NEP are Watts/$\sqrt{Hz}$.

The Total Noise Equivalent Power is the minimum radiant power in watts necessary to give a signal-to-noise ratio of unity for a specified electrical bandwidth, B.

$$TNEP = NEP \times \sqrt{B} \quad \text{in watts} \tag{2-17}$$

The reciprocal of NEP is called the detectivity, D.

D) Detector D*:

D* is obtained by multiplying the detectivity by the square root of the sensitive area of the detector.

$$D^* = D\sqrt{A} = \frac{\sqrt{A}}{NEP} \quad \text{in } cm\sqrt{Hz}/\text{watts} \tag{2-18}$$

D* is specified at a given temperature and modulation frequency.

E) Dark Current:

The dark current in an optical detector is the current flowing when the detector is shielded from optical radiation. It constitutes one of the important noise sources in a detection process.

2.2.3 Choice of detector for GaAs laser systems. The most important parameter in the choice of a photodetector in any optical system is the wavelength of operation. At the wavelength of gallium-arsenide lasers, the choice usually lies between a photomultiplier tube, a silicon photodiode and a silicon avalanche diode.

A photomultiplier tube is an excellent detector particularly at the visible and ultraviolet spectrum and

has the built-in advantage of being an excellent wide band, low noise-high gain amplifier. On the other hand, a photomultiplier has a poor quantum efficiency and low responsivity at 0.9 μm. The best cathod surface available for 0.9 μm wavelength has a sensitivity of about 10 mA/watt and the efficiency of 1% [21]. Besides, photomultipliers have low lifetime stability. They exhibit a certain degree of hysteresis and degradation with time. Photomultipliers require a stable high voltage power supply for their operation and tend to be very expensive.

Avalanche photodiodes offer higher quantum efficiency and sensitivity than the photomultiplier at the same time retaining the feature of internal gain mechanism. In addition they are much more compact and rugged in comparision with the photomultipliers. However, the avalanche process is an unavoidably noisy one. If the signal current is multiplied by m, the signal power is multiplied by m^2, but the shot noise power is multiplied by m^{2x} where the value of x lies between 1.15 and 2 depending on the ionization coefficients for electrons and holes [22].

Although the silicon photodiodes have no internal gain mechanism, they are very well suited for the wavelength of GaAs lasers and possess several other advantages. Their quantum efficiency is as high as 90% and they have peak response at about 0.9 μm, which is the wavelength emitted by the GaAs laser. Silicon photodiodes exhibit excellent linearity of output over a wide input range and have very

good long term stability. They are quite inexpensive compared to the other types of detectors. All these features along with their compact and rugged structure make silicon photodiodes a top choice for photodetection applications in injection laser systems.

For this experiment an RCA silicon p-i-n photodiode (C-30807) was selected. The important characteristics of the device at room temperature and rated bias are listed in Table 2-2. Figure 2-13 shows the spectral response of the device.

2.2.4 p-i-n photodiode. Basically the photodiode is a silicon p-n junction. Silicon has a bandgap energy of 1.1 eV. Radiations having wavelengths up to about 1200 nm are absorbed in silicon and create electron-hole pairs in the junction region. Because of the internal potential barrier at the junction, the electrons tend to move toward the n-type material and the holes tend to move toward the p-type material. The excess of free charge carriers makes the n-side negatively charged and the p-side positively charged so that an open circuit voltage appears at the detector output. This is known as the photovoltaic effect. If the diode is externally reverse biased then a continuous current can flow, and it can be used to develop a voltage across an external load resistance. The voltage will be proportional to the intensity of the light. This is known as the photoconductive mode of operation (Figure 2-14(b)). The photovoltaic mode eliminates the dark current and hence,

Photosensitive surface		
(Circular window) Area	0.8	mm^2
Diameter	1.0	mm
Spectral response range (10% points)	400-1100	nm
DC reverse operating voltage	45	V
Radiant responsivity at 900 nm	0.65	A/W
Quantum efficiency	90	%
Dark current	10^{-8}	A
Noise current	6×10^{-14}	$A/Hz^{\frac{1}{2}}$
NEP at 900 nm (1 kHz)	1×10^{-13}	$W/Hz^{\frac{1}{2}}$
Peak photocurrent (max)	100	mA
Capacitance	2.5	pf

Table 2-2

Characteristics of C-30807 p-i-n Photodiode

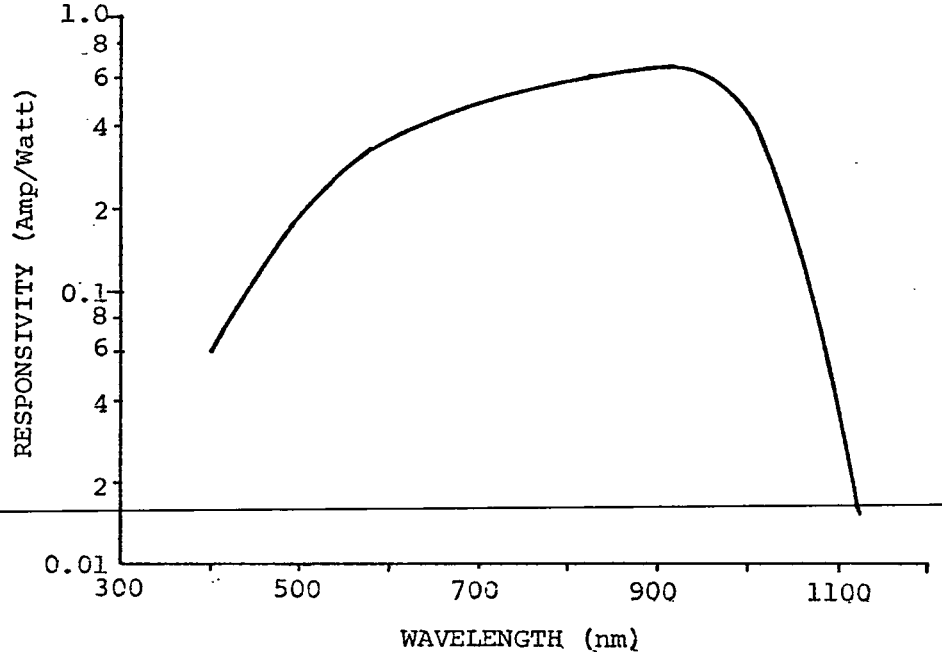

FIGURE 2-13

SPECTRAL RESPONSE OF C-30807 p-i-n PHOTODIODE

has a distinct advantage at low level light signal detection. The photoconductive mode, however, offers the advantages of greater responsivity and much faster response time over the photovoltaic mode.

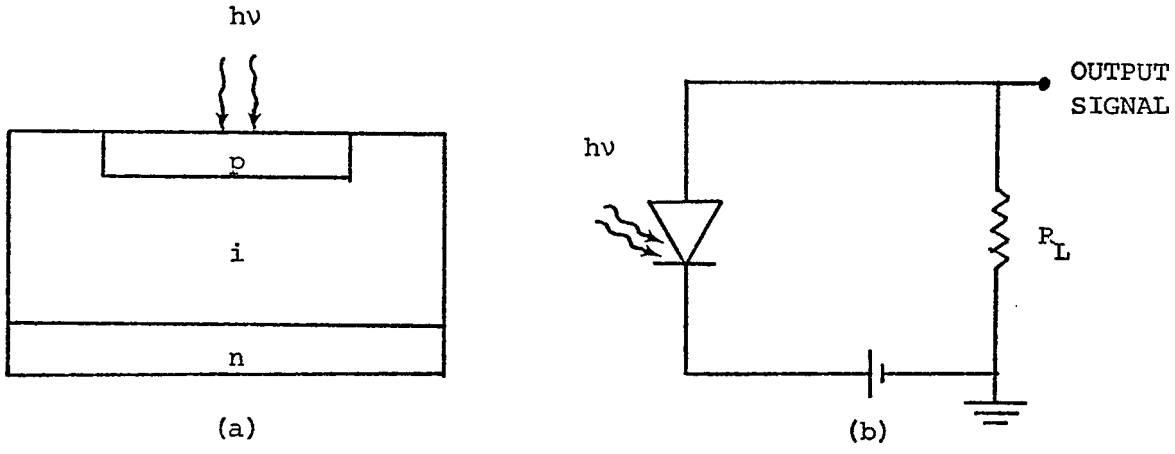

FIGURE 2-14
a) STRUCTURE OF p-i-n PHOTODIODE AND
b) BASIC SOLID STATE PHOTODETECTOR CIRCUIT

A p-i-n structure consists of a thin heavily doped p region and a heavily doped n-substrate separated by a nearly intrinsic "i" region, as shown in Figure 2-14(a). In a photoconductive mode the "i" region is swept free of carriers by the reverse bias so that it becomes a region of high and nearly constant field. This high electric field sweeps across the carriers more effectively as soon as they are produced at the p-i junction by the incident radiation. The p-i-n structure offers improved response time, responsivity and linearity [23].

The photocurrent I_s due to the incident optical power P_s is given by

$$I_s = R\ P_s. \qquad (2\text{-}14)$$

Since the responsivity is constant for a given detector, a linear relationship exists between the photocurrent and the incident power. It is also evident that for a given power level, the photodetector acts like a constant current generator.

The AC characteristics of a photodiode can be described in terms of an equivalent circuit (Figure 2-15) that contains a constant current source I_s, junction depletion layer capacitance C_d, shunt resistance R_d and a series resistance R_s, which is the resistance of undepleted silicon and lead resistance. R_L is the load resistance.

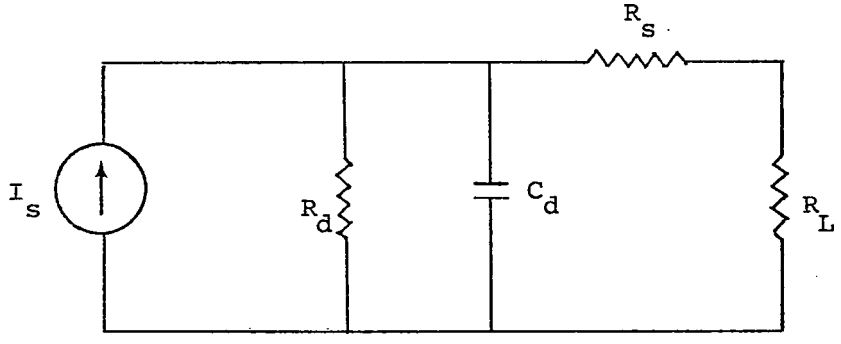

FIGURE 2-15
EQUIVALENT CIRCUIT OF A PHOTODIODE

For maximum signal across the load, $R_s << R_L$ and $R_d >> R_L$. Typically R_s is in the range of 50 to 500Ω and R_d is greater than 10 MΩ.

Response Time of a Photodiode:

A photodiode cannot follow the variations of light pulse instantaneously. The delays are involved due to

1) transit time of photogenerated carriers within the silicon crystal, 2) trapping of photogenerated carriers within the crystal and 3) rise and decay time due to the equivalent circuit RC time constant. The delays due to the first two reasons are made very short in a p-i-n photodiode and are of the order of a few nanoseconds.

If the photodiode is irradiated with a step input of radiant flux, the rise time of the detector is given by,

$$t_r = 2.2\ R_L C_d \quad \text{in seconds.} \tag{2.19}$$

The diode capacitance is a function of the reverse bias applied to the diode and it increases as the bias is reduced. To a first order of approximation, the bandwidth of the detector is

$$B = \frac{1}{2\ R_L C_d} = \frac{0.35}{t_r} \quad \text{in Hz.} \tag{2.20}$$

There is thus a trade-off involved in the selection of load resistance for both fast response and high sensitivity. The effect of the load resistance on the detector noise is discussed in the following chapter.

2.3 Optical Components

2.3.1 Transmitting antenna. As described earlier, an injection laser emits a diverging beam from the junction. The output of the laser must be collimated to reduce the beam divergence. The smallest beam diameter results by collimating the beam to its diffraction limit. Figure 2-16

shows the fraction of total transmitted energy contained in the diffraction pattern as a function of distance from the pattern center, for a circular aperture [24].

The angular distance between the first zeros of the diffraction pattern, i.e. the diameter of Airy disk has been shown to be [25]

$$\theta_t = 2.44 \frac{\lambda}{d_t} \tag{2-21}$$

where, λ is the wavelength of the radiation and d_t is the diameter of the transmitting aperture. Therefore the value $\theta = \frac{2.44\lambda}{d_t}$ (radians) represents the full angle diffraction limited divergence of the beam. The diameter of the Airy disk at a distance R is given by

$$d = \frac{2.44\lambda}{d_t} R. \tag{2-22}$$

2.3.2 Receiving antenna. A focusing antenna can be used at the receiver end to gather the laser signal energy and focus it to a spot on the photodiode surface.

As illustrated in Figure 2-17, the photodetector of the diameter d_p is placed at the focal point of the lens and establishes the receiver field of view, θ_r, given by [24]

$$\theta_r = \frac{d_p - d_d}{F} \tag{2-23}$$

where, F is the focal length of the focusing antenna and d_d is the diameter of the focused beam. This spot size, for a diffraction limited lens is simply the Airy disk

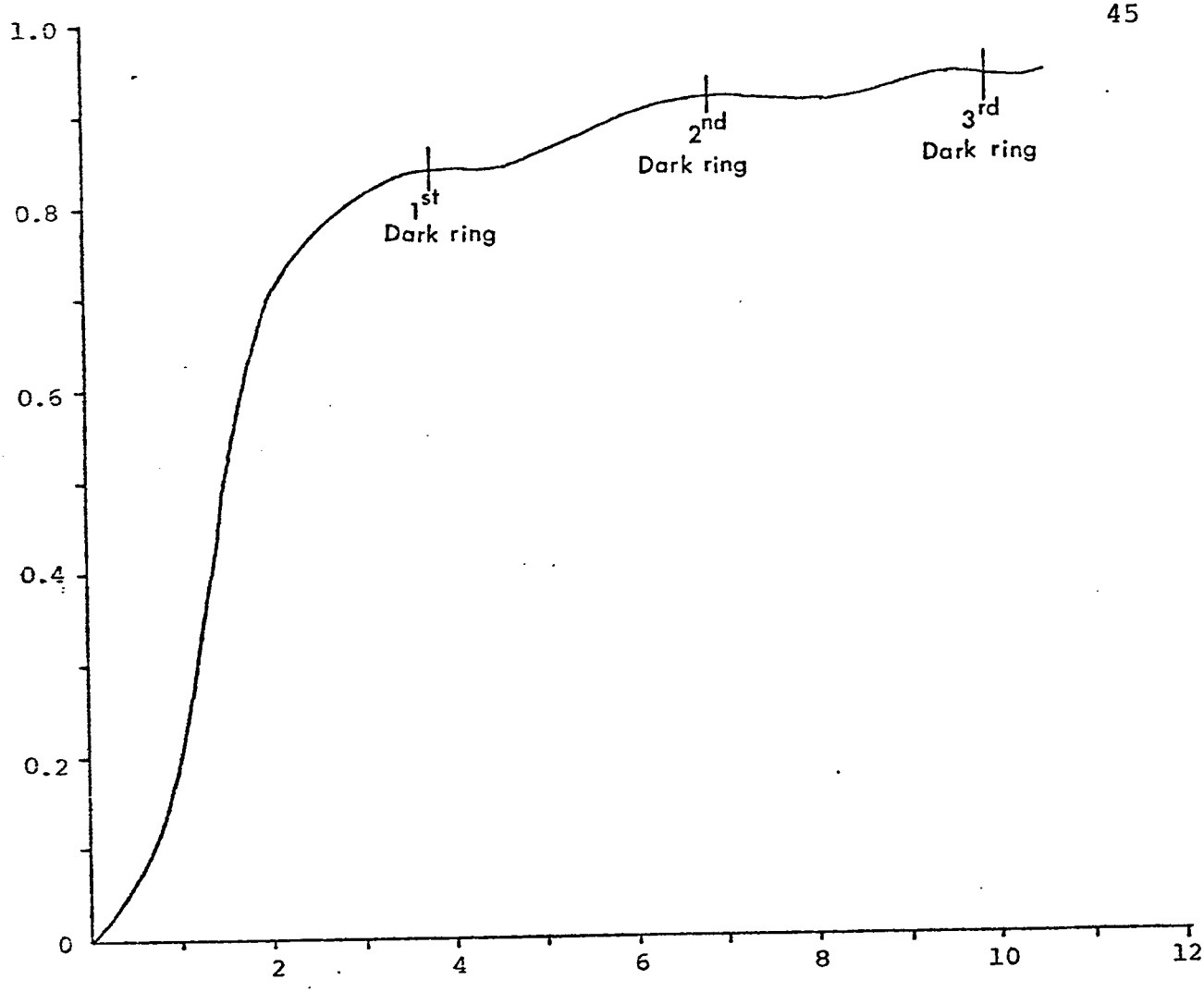

FIGURE 2-16

FRACTION OF LASER POWER IN CIRCLE ABOUT DIFFRACTION PATTERN CENTER

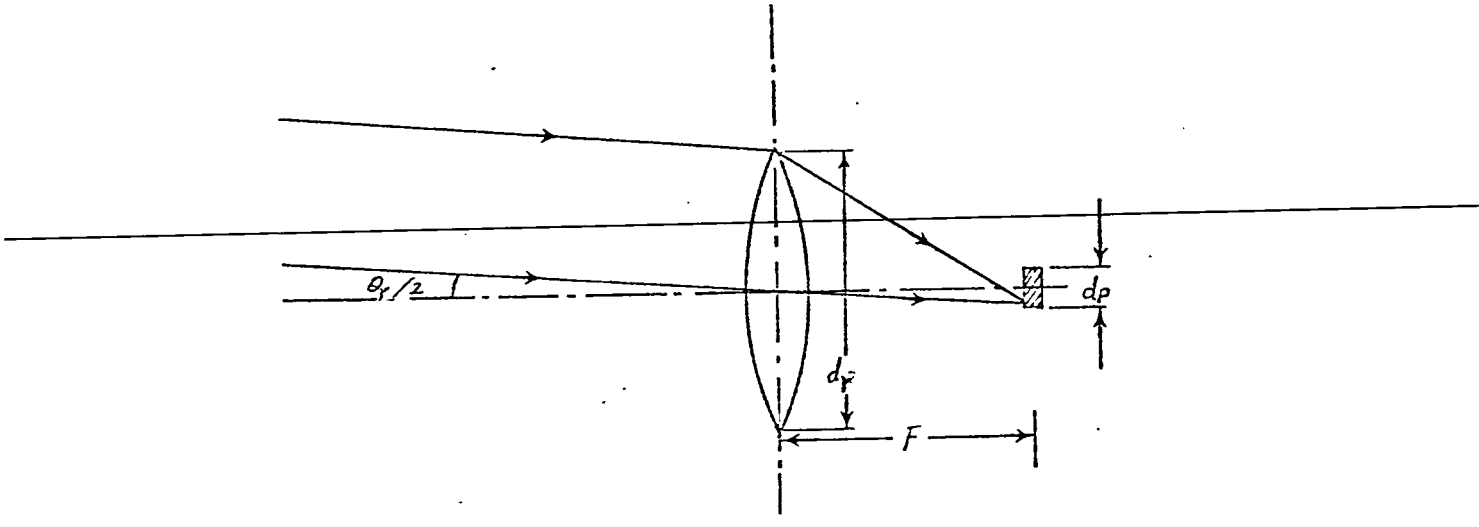

FIGURE 2-17

FIELD OF VIEW OF THE FOCUSING ANTENNA

$$d_d = \frac{2.44\lambda}{d_r} F. \tag{2-24}$$

If d_d is much smaller than d_p, the receiver field of view becomes

$$\theta_r = 2.44\lambda \cdot \frac{d_p}{d_d d_r}. \tag{2-25}$$

Chapter 3

COMMUNICATION SYSTEM ANALYSIS

In the previous chapter the physical aspects of optical communication systems were discussed. In this chapter, the statistical model of the system is explained. Various noise sourses of the system are analyzed and the effects of atmosphere on laser beam propagation are considered. Also included is a discussion on the detection process.

3.1 Communication System: Statistical Model

The statistical model of the optical communication system under consideration is shown in Figure 3-1. The binary optical signal is transmitted over the atmospheric channel. Multiplicative disturbances, consisting of signal attenuation and random phase delays, affect the signal as it passes through the channel. Along with this perturbed signal, the background radiation enters the detector to create external noise. In addition to this, there is the internal detector noise caused by random photoelectron emissions and thermal effects. The receiver thus receives the actual signal corrupted by these various noise signals and determines what signal was actually transmitted. The performance of such digital systems is generally described in terms of the probability of detection error of a data sample or bit.

To specify the measures of system performance theoretically, it is necessary to characterize the optical detection process. Before considering the statistical character of the detection process, however, various inputs to the detector will be analyzed.

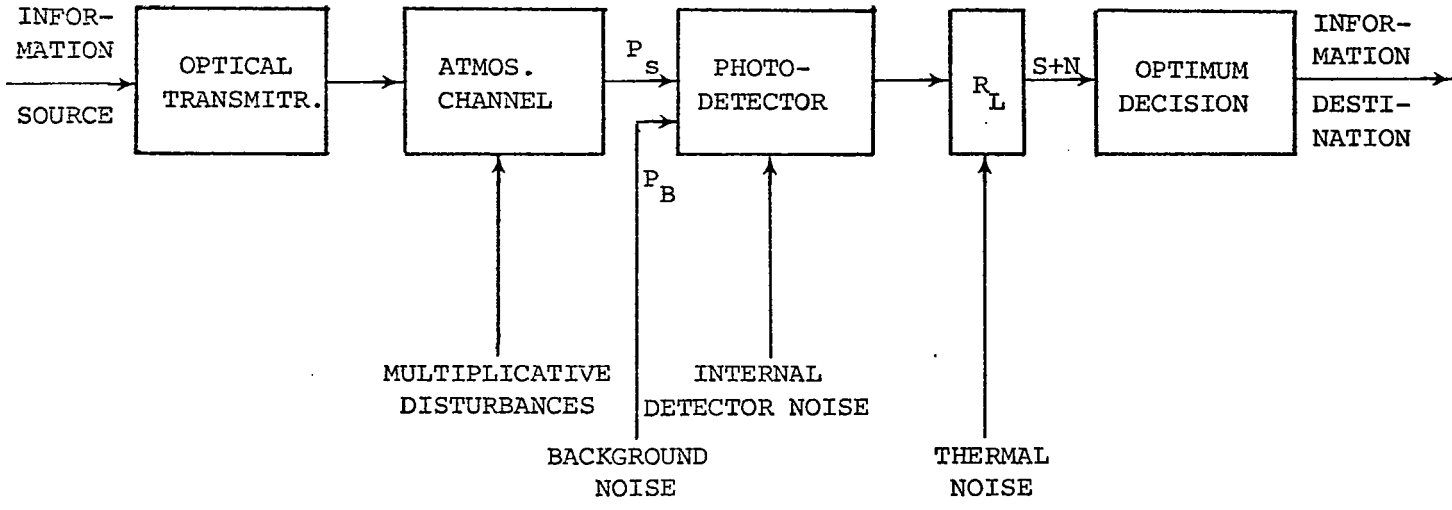

FIGURE 3-1

COMMUNICATION SYSTEM STATISTICAL MODEL

3.2 Received Signal Power

The received optical signal power at the detector depends upon various system parameters and is inversely proportional to the square of the range of the link. The "Range Equation" is given as [26]

$$P_s = \frac{P_L A_r \tau_a \tau_r \tau_t \gamma}{\theta_t^2 R^2} \qquad (3\text{-}1)$$

where, P_L is the peak laser power (W), A_r is the area of the receiver optics (m^2), τ_a is the transmittance of the atmosphere, τ_r is the transmittance of the receiver optics, τ_t is the transmittance of the transmitter optics, γ is the reflectivity of the mirror, θ_t is the transmitter beam width (radians) and R is the range (m).

This equation denotes the theoretical maximum power that can be received with the given system parameters and does not take into account any pointing errors. The transmitter beam width, θ_t is taken to be the angular distance between the first zeros of the diffraction pattern, i.e.

$$\theta_t = 2.44\ \lambda/d_t \qquad (2\text{-}21)$$

3.3 Photodetector Noise Sources

Noise in the detection process of a laser communication system arises from radiations externally entering the detector and from the internally generated noise. The various types of detection noise are listed in Figure 3-2.

DETECTOR NOISE SOURCES

Internal	External
Thermal noise	Photon fluctuation or generation recombination noise
Current noise	Amplifier noise
Flicker noise	Phase noise
Dark current noise	Intensity fluctuation noise
	Background noise

FIGURE 3-2

The dark current noise, photon fluctuation noise and background noise are often collectively called the "shot noise". In most practical applications only the thermal noise, the shot noise and the noise due to the amplifier following the detector are significant. These noise sources are described in this section. The phase noise and the intensity fluctuation noise arise from the atmospheric turbulence effect. They are described in a later section.

3.3.1 Thermal noise. The thermal noise in an optical detection system is caused by the thermal fluctuations in a detector load resistance. Pratt [24] has shown that the two sided thermal noise power spectral density is given by

$$G_{VT} = 2kTR_L \text{ in volts}^2/\text{Hz} \qquad (3\text{-}3)$$

where, k is the Boltzmann constant and T is the temperature. The electron fluctuations in the noisy resistor occur in very short times compared to the response time of the detector. Thus the spectrum of the thermal noise source may be assumed to be flat, in the passband of the detector. The mean square noise voltage is given by

$$\overline{V_T^2} = 4kTBR_L, \qquad (3\text{-}4)$$

and the mean square noise current is given by

$$\overline{i_T^2} = \frac{4kTB}{R_L} \qquad (3\text{-}5)$$

The thermal noise voltage and current sources are Gaussian random variables under thermal equilibrium, hence their probability distributions are the Gaussian distributions.

Due to the lack of an internal gain mechanism in the photodiodes, the thermal noise predominates over the shot noise at low signal levels. Therefore, the photodiode performance is often limited by the thermal noise.

3.3.2 Dark current shot noise. Even when a detector is shielded from light, there is a small current flow due to the thermally generated charge carriers. This constitutes the dark current noise in the optical detector. The noise power spectral density of the dark current is composed of a flat spectrum plus a DC component [24]. The total noise power at a load resistance R_L due to the random fluctuations in the dark current is given by the Schottkey noise formula

$$N_D = 2\, qI_D BR_L \quad \text{in watts} \tag{3-6}$$

where I_D is the average value of the dark current. The mean-square noise current is given by

$$\overline{i_d^2} = 2\, G^2 qI_D B. \tag{3-7}$$

The dark current electronic emissions are time independent and obey Poisson statistics.

3.3.3 Background noise. Along with the transmitted signal, an optical detector receives background radiations from the sun, sky and reflected light from other objects. A direct detector does not discriminate against the background noise and in some systems it can become a significant factor in the signal-to-noise ratio and hence the performance of the system. In such cases measures must be taken to reduce the background effect by limiting the field of view of the receiver and by using an optical filter to restrict the input spectral bandwidth.

Background radiations are usually expressed in radiometric quantities. The characterizations most often used in laser communication systems are tabulated in Table 3-1.

Symbol	Name	Definition	Units
S	Area		m^2
Ω	Solid angle	$\pi\alpha^2$	S_r
α	Plane angle		rad
U	Radiant energy		J
P	Radiant power	Rate of transfer of radiant energy, $\frac{\partial U}{\partial t}$	W
W	Radiant emittance	Radiant power per unit area emitted from S, $\frac{\partial P}{\partial S}$	Wm^{-2}
W_λ	Spectral radiant emittance	Radiant emittance per unit wavelength interval $\frac{\partial W}{\partial \lambda}$	$Wm^{-2}\mu m^{-1}$
H	Irradiance	Radiant power per unit area incident upon S, $\frac{\partial P}{\partial S}$	Wm^{-2}
H_λ	Spectral irradiance	Irradiance per unit wavelength interval $\frac{\partial H}{\partial \lambda}$	$Wm^{-2}\mu m^{-1}$

Table 3-1
Radiometric Quantities and Units

Several forms of the expression for background noise power exist [24]. In terms of the spectral irradiance the average power due to background radiation at the detector surface is given by

$$P_B = \frac{\tau_a \tau_r B_{opt} A_r \theta_r^2 \xi}{4} H_\lambda \quad \text{in watts} \tag{3-8}$$

where τ_a is the atmospheric transmittivity, τ_r is the receiver transmittivity, B_{opt} is the input filter bandwidth, A_r is the receiver antenna aperture area and ξ is the reflection coefficient of the background.

The sun is the most important source of the background radiation from optical communications point of view. At 0.9 μm, the solar spectral irradiance is about 0.1 $W/m^2 \cdot \mathring{A}$, when the sun is at the zenith [28]. The background noise can be considerably minimized by restricting the field of view of the receiver and by using a narrow band filter to reduce the input spectral bandwidth to the detector.

3.3.4 Photon fluctuation noise. Photodetectors are subject to noise caused by emission fluctuations of the optical radiation incident upon a photodetector, even when the mean radiation intensity is constant. This phenomenon, often called photon fluctuation noise, manifests itself as shot noise for a photoemissive detector or as generation-recombination noise for a semiconductor detector. Since this is the noise due to the optical radiation

fluctuations incident upon the detector, there are two external sources responsible for the noise 1) the signal source itself and 2) the background radiations.

It has been shown that the probability distribution of photoelectron counts due to both the background as well as the laser source is Poisson [24]. The mean and variance of this distribution are both equal to $\bar{n} = \tau\frac{I}{q}$ photoelectrons, where I is the average detector current due either to background or the signal in time interval τ. Photon fluctuation noise has a flat spectrum and its power spectrum density is given by

$$G_{i_{shot}} = 2\ q(I_s + I_B)\ \text{in amps}^2/\text{Hz} \qquad (3\text{-}9)$$

where I_s is the average detector current due to the laser radiation = $q\bar{n}_s/\tau$ and I_B is the average detector current due to background radiations = $q\bar{n}_B/\tau$. Therefore, the noise in bandwidth B is

$$N = 2\ q(I_s + I_B)R_L B \quad \text{in watts.} \qquad (3\text{-}10)$$

From equations (3-6) and (3-10), the total shot noise in a direct detection system is

$$N_{shot} = 2\ q(I_s + I_B + I_D)R_L B \quad \text{in watts.} \qquad (3\text{-}11)$$

3.4 Signal-to-Noise Ratio in a Direct Detection System

The signal power across the equivalent load resistor R_L due to the signal photocurrent, I_s, in a photodiode without an internal gain mechanism is simply,

$$P_s = I_s^2 R_L. \tag{3-12}$$

The noise power resulting due to the effects of shot noise, thermal noise and amplifier noise will be given by

$$N_s = 2\ qB(I_s + I_B + I_D)R_L + 2FkTB \tag{3-13}$$

where F is the noise factor of the amplifier. The signal power to noise power ratio is then given by [26]

$$\frac{S}{N} = \frac{I_s^2 R_L}{2\ qB(I_s + I_B + I_D)R_L + 2FkTB} \tag{3-14}$$

3.5 Atmospheric Effects in Optical Communication Systems

The deleterious effects of the atmosphere on the propagation of optical beams impose the most serious limitations on the practical use of optical communication links. An attempt is made to outline the adverse role played by the constituents of the atmosphere at optical frequencies. Theory and the effects of atmospheric turbulence are considered. The basic phenonema responsible for the atmospheric degradation of laser radiation are the turbulence, molecular absorption and scattering. Turbulence results due to the refractive index inhomoginities. While

the predominent influence of absorption and scattering is signal attenuation, the turbulence, among other things, causes intensity scintillations and coherence degradation.

3.5.1 Atmospheric attenuation. It is a common experience that when a signal, whether radio or optical, is transmitted over an atmospheric channel, it loses its power. The signal attenuation is attributed to two phenomena.

A) Molecular Absorption:

The loss of optical signal strength by absorption in the atmosphere is due to molecular constituents, mainly water vapor, carbon dioxide and ozone. They have both narrow and broad band absorption spectra, some of which may coincide with laser wavelengths. Hence, in an optical communication system only those laser frequencies can be used for which the atmosphere is relatively transparent. In a frequency spectrum extending from the visible to the infrared (15μ) there are eight distinct transparent regions or "atmospheric windows" [24]. The emission frequencies of GaAs injection lasers lie in the first window and suffer negligible atmospheric absorption.

B) Atmospheric Scattering:

~~For the spectral regions in an atmospheric window,~~ scattering is the main cause of signal attenuation. Two major types of scattering occur in the atmosphere, distinguished by the size of the particles responsible for scattering. Scattering due to the molecules of air and the particle sizes smaller than the wavelength of the radiation is known

as the Rayleigh scattering. Rayleigh scattering decreases inversely as the fourth power of the wavelength and is therefore not significant for infrared wavelengths. At these wavelengths, Mie scattering is the predominent effect. Mie scattering results from the larger particles such as smoke, haze, fog, dust, water droplets, etc. and is essentially nonselective of wavelength. Mathematical treatment of Mie scattering is quite complex, however, several experimental results are available [27]. Table 3-2 lists the scattering attenuation rate, σ_r, at 0.9 m at different atmospheric conditions.

Atmospheric Condition	Visibility	σ_r(dB/km)
Rayleigh scattering in extremely clear air	"unlimited"	0.08
Light haze	5.2 km	2
Light fog	830 m	12
Heavy fog	170 m	100
Clouds	35 m	600

Table 3-2
Atmospheric Scattering Attenuation at 0.9 μm

C) Horizontal Path Atmospheric Transmittance:

Atmospheric attenuation due to the combined effect of absorption and scattering can be expressed by an exponential law. The transmittance (ratio of transmitted power to incident power) of the atmosphere over a path of length R is

$$\tau_a = \exp\{-\sigma R\} \qquad (3\text{-}15)$$

where σ is the attenuation or extinction coefficient and is equal to the sum of the absorption and scattering coefficients. The atmospheric transmittance τ_a can be calculated for various path lengths, altitudes and atmospheric conditions by the use of Figures 3-3, 3-4 and 3-5 [28]. Figure 3-3 gives the attenuation coefficient σ at sea level as a function of wavelength and atmospheric conditions. Figure 3-4 provides a correction factor for σ as a function of altitude for either a slant or horizontal path. Figure 3-5 is a plot of transmittance against the product of path length and altitude corrected value of σ.

3.5.2 Atmospheric turbulence. Turbulence is a consequence of the refractive index inhomogenities of the atmosphere. The atmospheric refractive index is a random function of time and space. It has been shown that the fluctuations in the refractive index are proportional to the fluctuations in temperature [29]. Part of the solar energy incident upon the earth's surface is absorbed, causing the surface air layer to be heated by the earth. This sheet of warm air becomes less dense and rises to mix turbulently with the surrounding cooler air. The temperature of the air thus varies from point to point in the atmosphere in a random manner. These temperature fluctuations are a function of altitude and wind speed. When a light beam traverses a region in which there is a temperature change

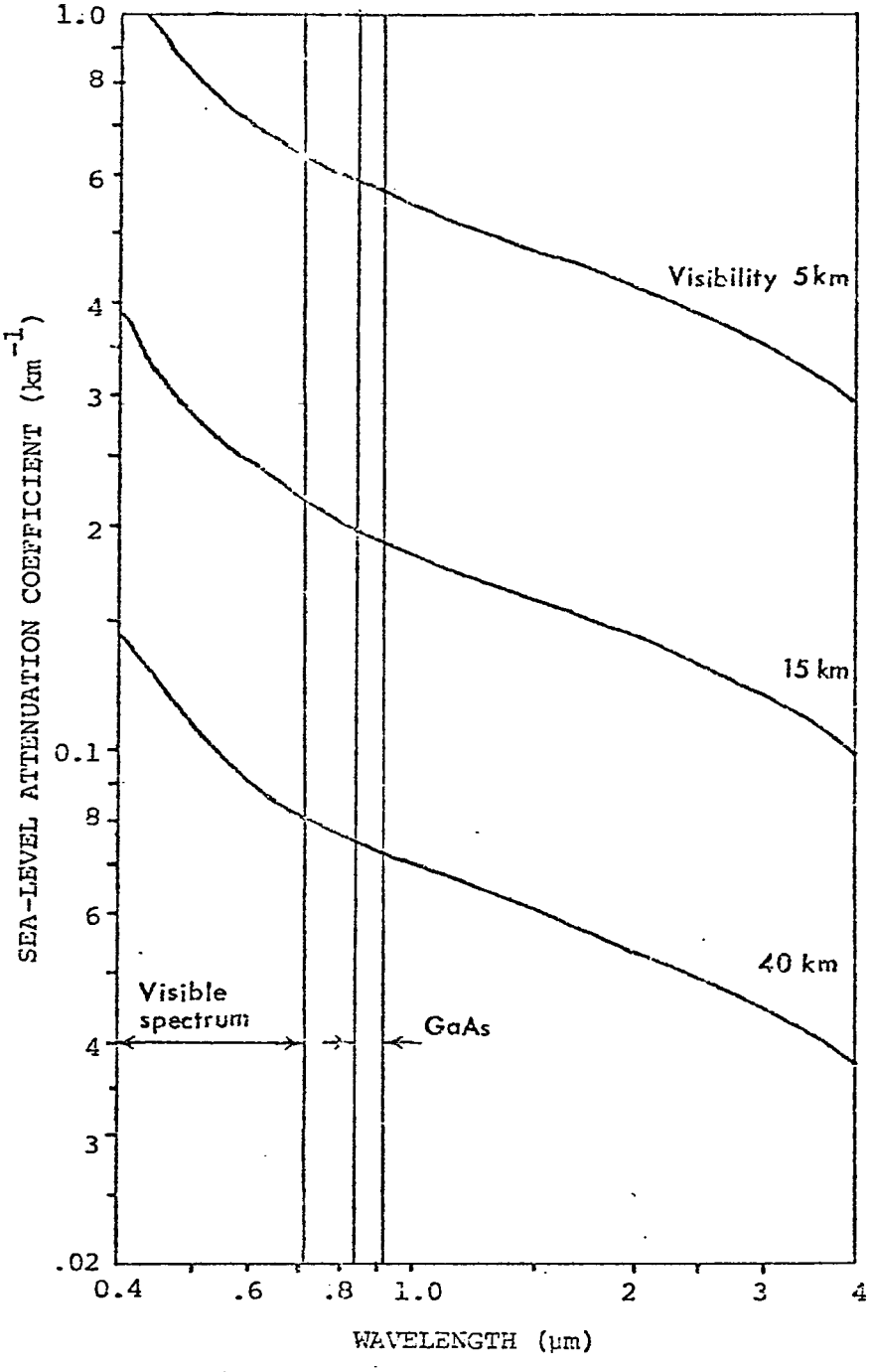

FIGURE 3-3

APPROXIMATE VARIATION OF ATTENUATION COEFFICIENT WITH WAVELENGTH AT SEA-LEVEL FOR VARIOUS ATMOSPHERIC CONDITIONS

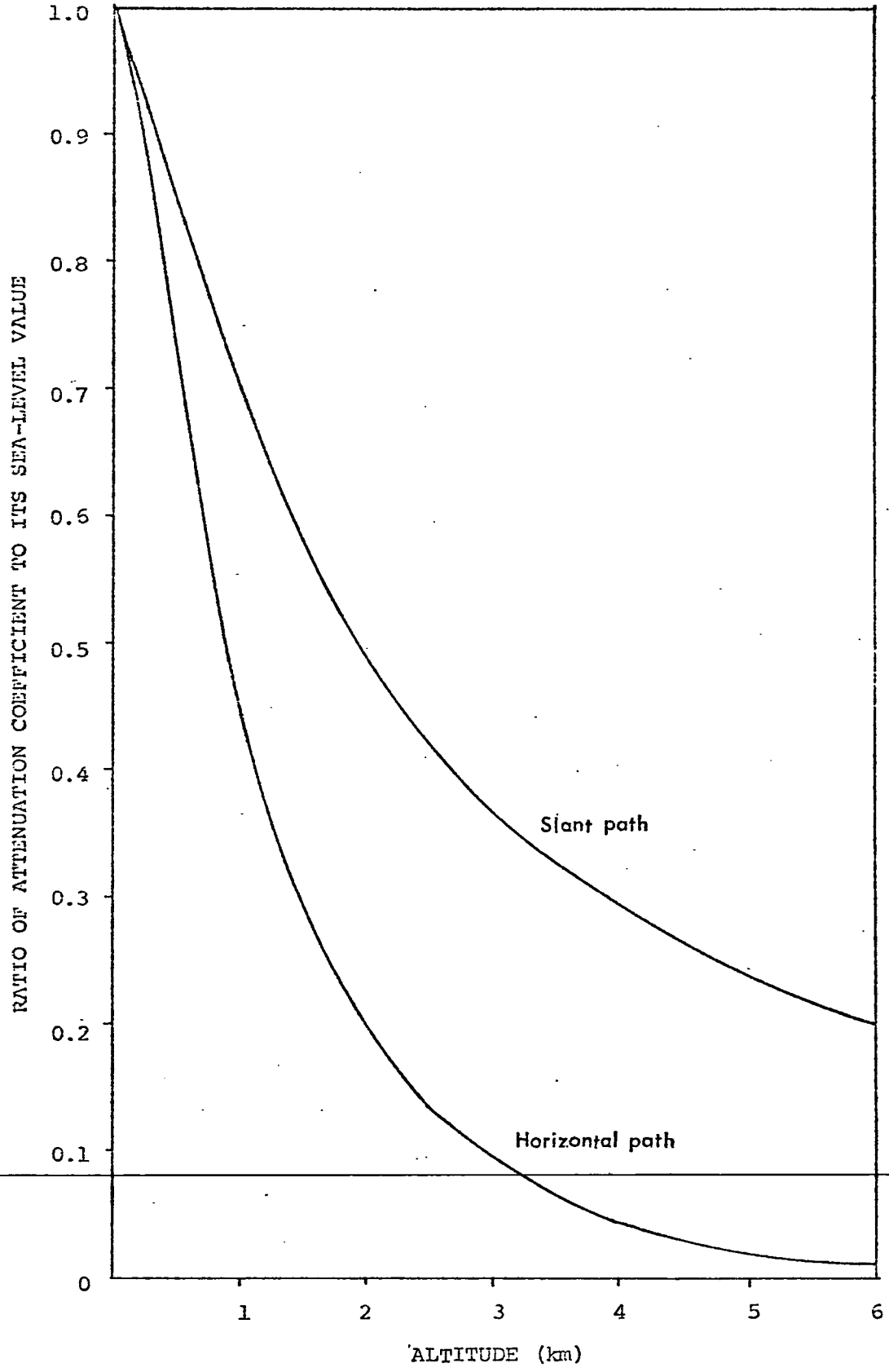

FIGURE 3-4

APPROXIMATE RATIO OF ATTENUATION COEFFICIENT TO SEA-LEVEL VALUE FOR SLANT PATHS AND HORIZONTAL PATHS

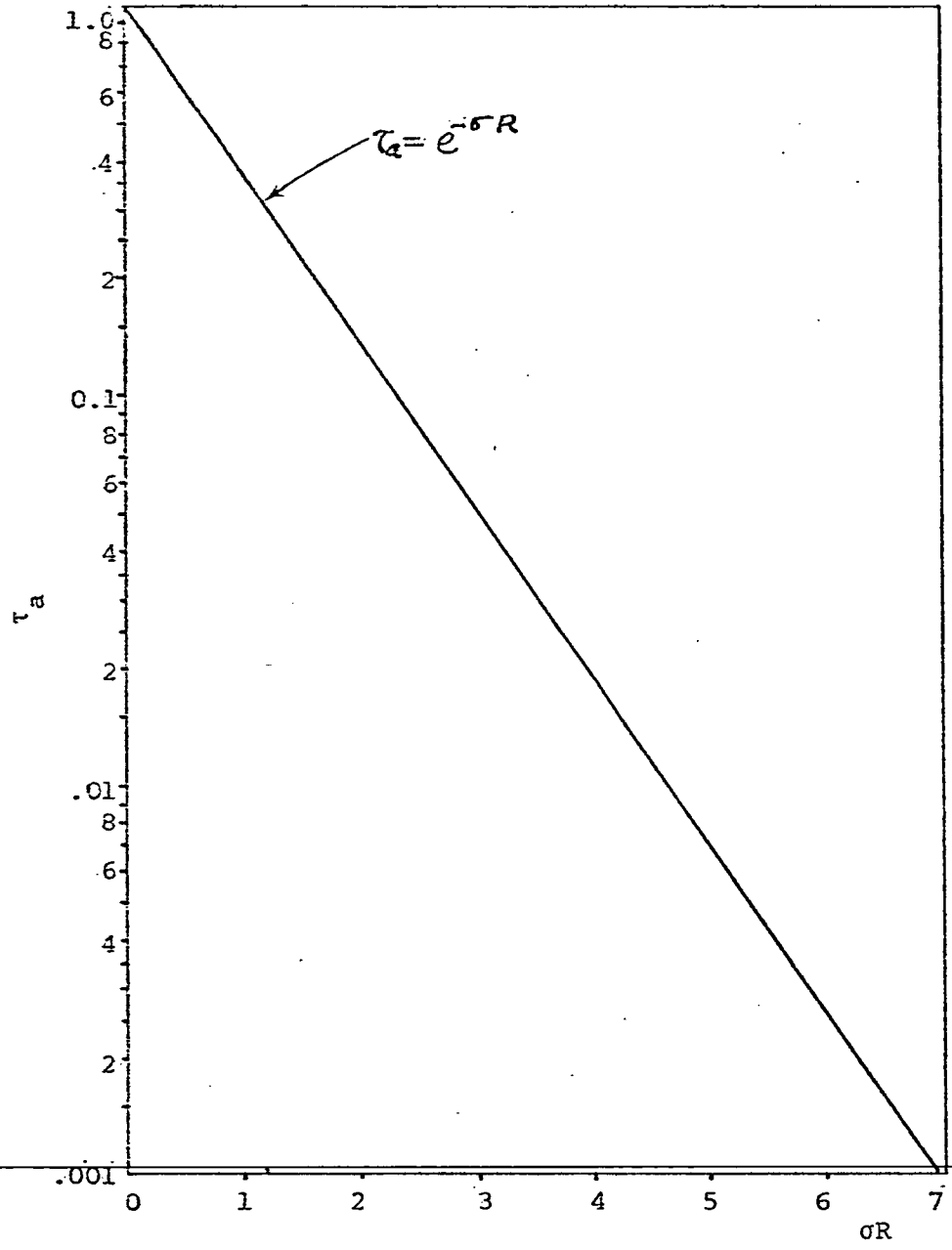

FIGURE 3-5

ATMOSPHERIC TRANSMITTANCE AS AN EXPONENTIAL FUNCTION OF PATH LENGTH TIMES ATTENUATION COEFFICIENT

in the air, the beam is partially or totally deviated, depending upon the relative sizes of the beam and temperature inhomogenity. This interaction of the laser beam with the turbulent medium leads to random amplitude and phase variations along with many other interesting effects.

The consequences of atmospheric turbulence on laser communications are listed below [30].

1) Beam steering - angular deviation of the beam from the line of sight path, causing the beam to miss the receiver.

2) Image dancing - variations in the beam arrival angle, causing the focus point to move in the image plane.

3) Beam spreading - small angle scattering, increasing the beam divergence and decreasing the spatial power density at the receiver.

4) Beam scintillation - small scale destructive and constructive interference within the beam producing local fluctuations in the intensity, so that within the beam cross-section, there appear areas that are bright and dark compared to the average. This leads to fluctuations in received power which are strongly dependent on the receiver aperture.

5) Spatial coherence degradation - losses in phase coherence across the beam phase fronts, degrading the photomixing performance.

6) Polarization fluctuations - variations in the polarization state.

3.6 The Atmospheric Model

All the effects summarized in the last section are attributed to amplitude and phase fluctuations. The quantitative treatment of propagation through a turbulent medium involves a solution of the wave equation in a random medium with boundary conditions appropriate for a laser beam, and a characterization of the medium. Tatarski [31] has proposed a turbulent atmosphere model based upon a perturbation method, called the Rytov method, for the solution of the wave equation. In this model, the turbulent medium is considered to be composed of discrete spheres, each of which is homogeneous but of different refractive index from its neighbors. The spherical inhomogeneities of the refractive index or "eddies" are distributed in the atmosphere and an inhomogeneity dimension ℓ is associated with each eddy. The smallest and largest inhomogeneities are characterized by the dimensions ℓ_o and L_o known as the "inner" and "outer" scales of turbulence, respectively. The dimension between ℓ_o and L_o is called the "inertial subrange". Near the ground, the value of the outer scale is thought to be comparable with the altitude. In the upper atmosphere L_o is often 100 meters or more, but in the presence of stratified layers it does not greatly exceed the layer thickness. The inner scale has a dimension of only a few millimeters [29].

The effect of atmospheric turbulence depends

upon the relative sizes of the beam diameter, D, and the inhomogeneity dimension, ℓ. In particular,

a) If $D << \ell$, the major effect of turbulence is to deflect the beam as a whole. At long ranges the beam appears to execute a two-dimensional random walk in the receiver plane. Under this condition, image dancing and beam steering are predominantly noted. This situation exists for an earth transmitter and deep-space receiver system.

b) If $D \simeq \ell$, the inhomogeneities act like lenses which focus or defocus the beam, imparting a granular structure to the beam cross-section. The steering and spreading are both small in this case. If the transmission range is shorter than the far field range, the scintillation will also be small.

c) If $D >> \ell$, small portions of the beam are independently diffracted and scattered. The beam phase fronts are badly distorted and the intensity fluctuations are strong. This case applies for communications from a deep-space transmitter to an earth receiver.

In the atmosphere there are inhomogeneities of all dimensions ($\ell >> D$, $\ell \simeq D$, $\ell << D$), but those within a certain subrange often contribute most to the turbulence spectrum. For example, Tatarski showed that in the case of an infinite plane wavefront incident on the turbulent medium, the inhomogeneities which make the greatest contributions to amplitude fluctuations have dimensions of the order of $\sqrt{\lambda R}$, where R is the range. This dimension

of $\sqrt{\lambda R}$ is known as the "correlation length" and is generally of the order of tens of centimeters [30].

Assuming the atmosphere to be locally homogeneous, as postulated by the model, the refractive index fluctuations at any point $\bar{r}$ in space can be statistically described by a quantity called the "structure function", such that

$$D_n(\bar{r}) = C_n^2(\bar{r}) f(r, \ell_o, L_o). \tag{3-16}$$

The quantity C_n is called the "structure constant" and is a measure of the strength of turbulence. The structure constant decreases roughly as the negative one-third power of altitude within about the first 100 meters of the earth's surface. Hence, theoretically a significant reduction in turbulence intensity is possible with elevated laser systems.

3.6.1 Optical intensity fluctuations (scintillation). Tatarski postulates that the logarithm of the amplitude of a distorted wave has a Gaussian probability density function, so the strength of the scintillations is described in terms of "log-amplitude variance". For the horizontal paths, the log-amplitude variance is given by

$$\sigma_\ell^2 = \left\langle \left(\log \frac{A}{A_o}\right)^2 \right\rangle \simeq 0.31\, C_n^2 k^{7/6} R^{11/6} \tag{3-17}$$

where, A is the instantaneous amplitude of the optical field, A_o is the initial amplitude, k is the wave number and R is the range through the turbulent medium. The

fluctuation in the logarithmic level of intensity is given by,

$$\sigma_I^2 = 4\sigma_\ell^2 \tag{3-18}$$

A typical diurnal variation of scintillation consists of a broad maximum throughout daylight hours, sharp minima near sunrise and sunset, and highly variable effects at night. The daytime maximum reaches a broad, smooth peak soon after noon, but cloud cover, either intermittent or continuous, produces a sharp drop in scintillation activity. Activity increases with wind velocity for light winds, but decreases again as the wind becomes strong, mixing the air to produce an adiabatic lapse rate. Sharp minima at sunrise and sunset occur when the lapse rate, changing because of the rapidly varying solar radiation, passes through the adiabatic condition [32]. In the case of strong turbulence, σ_I^2 saturates at a value approximately equal to ℓ_n 2. Until saturation occurs, the log intensity variance of scintillations varies inversely as the 7/6 power of the optical wavelength. Details of the scintillation pattern are relatively broadband, differing little with a wavelength change of a few tens of nanometers, but they become quite uncorrelated when the wavelength changes by a factor of 2.

Figure 3-6 shows the frequency spectra of scintillation for different atmospheric conditions [33]. The frequency spectrum is caused by the motion of the

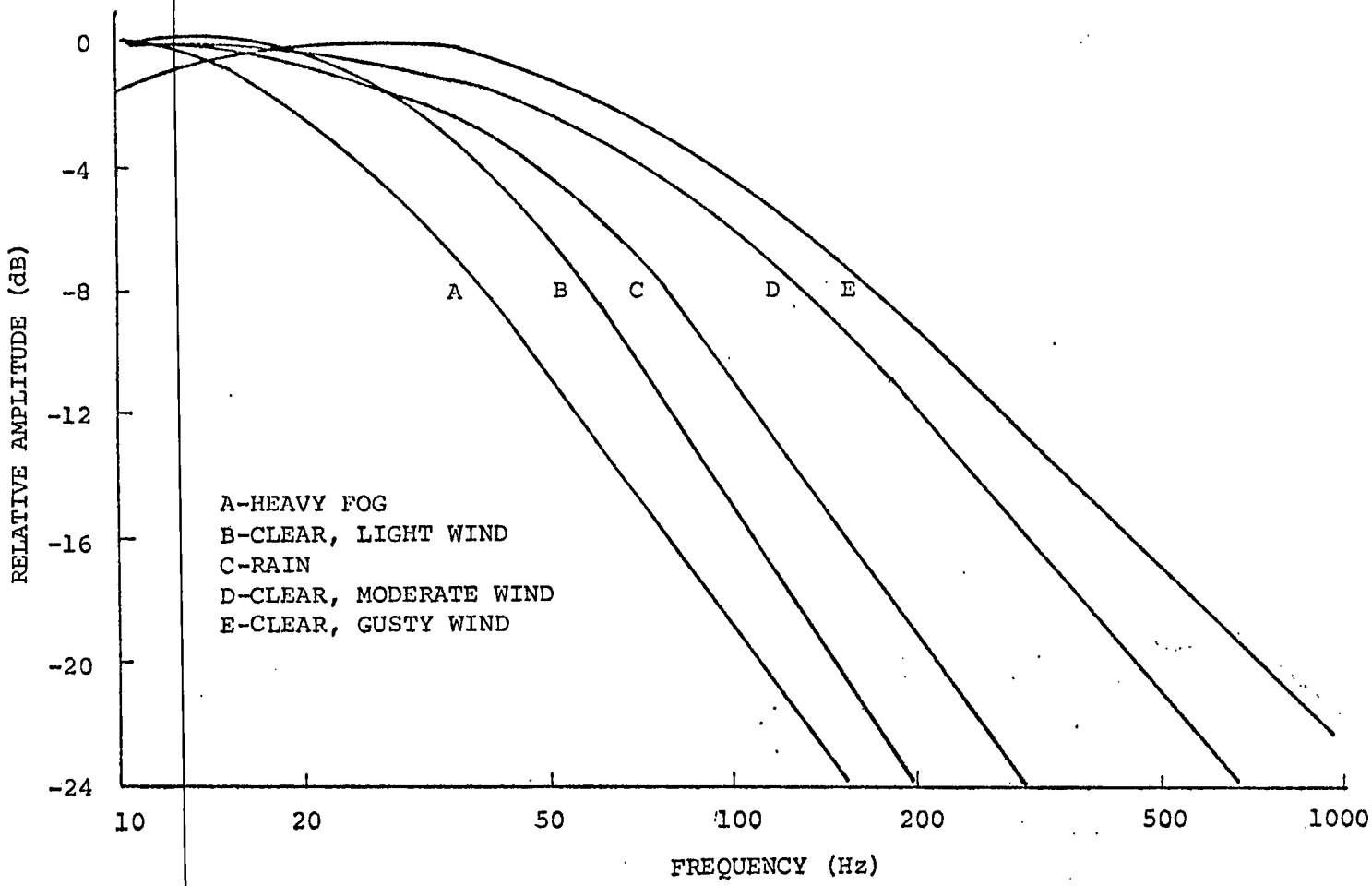

FIGURE 3-6

FREQUENCY SPECTRA OF SCINTILLATIONS

atmosphere. In this respect the factors that affect the temporal frequency of scintillation are 1) the transverse component of wind that moves the turbulence across the beam, 2) changes in wind direction and 3) the internal "mixing" motions of the atmosphere due to the evolution of turbulence. From the figure it is seen that, in general, the predominant temporal frequencies occupy the range from 1 to 100 Hz. The spectrum gets wider as the wind gets stronger.

In an optical communication system the effect of beam scintillation is to introduce multiplicative noise by creating random fading in the carrier beam intensity and thus decreasing the S/N ratio of an optical receiver. For a direct detection receiver, studies indicate that the carrier signal variance is approximately inversely proportional to the receiver antenna area. As the antenna diameter to laser beam diameter ratio increases, the magnitude of the variations decreases. This is the so-called "aperture averaging" effect. Thus in a direct detection system increasing the antenna diameter not only increases the average signal level but also decreases the signal fluctuation [34].

3.6.2 Optical phase fluctuations. While the intensity scintillations are caused by turbulence with a scale of the order of $\sqrt{\lambda R}$, it is believed that the phase fluctuations are mainly produced by the larger scales and so depend upon the "outer scale" of turbulence. Tatarski has postulated a

normal distribution for the phase variation between points separated by a distance ρ in the receiver plane, and he has shown that for a horizontal path, the fluctuation in phase is given by

$$\sigma_\phi^2(\rho) = \begin{cases} 1.46\ k^2\rho^{5/3}C_n^2R, & \ell_o << \rho << \sqrt{\lambda R} \\ 2.91\ k^2\rho^{5/3}C_n^2R, & L_o >> \rho \gtrsim \sqrt{\lambda R}. \end{cases} \tag{3-19}$$

The dimension ρ_o, such that, $\sigma_\phi(\rho_o) = \pi$ is known as the "lateral phase coherence length". The phase fluctuations arise from either of the two processes. First, the wavefront is distorted such that over dimensions ρ satisfying the condition $\sigma_\phi(\rho) > \pi$, the phase correlation is essentially zero. Second, the wavefront remains a plane but is tilted through an angle $\sigma_\theta = \sigma_\phi/k\rho$. The first cause leads to such effects as the beam spreading, image blurring and spatial coherence degradation. The second cause results in the angle of arrival fluctuations which increase the receiver field-of-view and contribute to beam steering and image dancing.

Optical phase fluctuation and especially the coherence degradation, is of no consequence in a direct detection receiver, but these effects play a major role in the design of an optical heterodyne receiver. From the direct detection point of view the side effects of the phase fluctuation are important. These effects are briefly described here.

Beam Steering:

If the beam dimension is much less than the inhomogeneity dimension (i.e., $D << \ell$), the entire beam will be deviated by an angle, $\delta_\theta = \sigma_\theta/\sqrt{2}$. Experimental studies by Whatley and Smith [33] illustrate a typical example of beam pointing variations over a period of twenty-four hours for a 5 km path (Figure 3-7). Beam wandering may be somewhat compensated by using diverging optics to increase the beam divergence, of course, at the expense of spatial power density and hence the antenna gain.

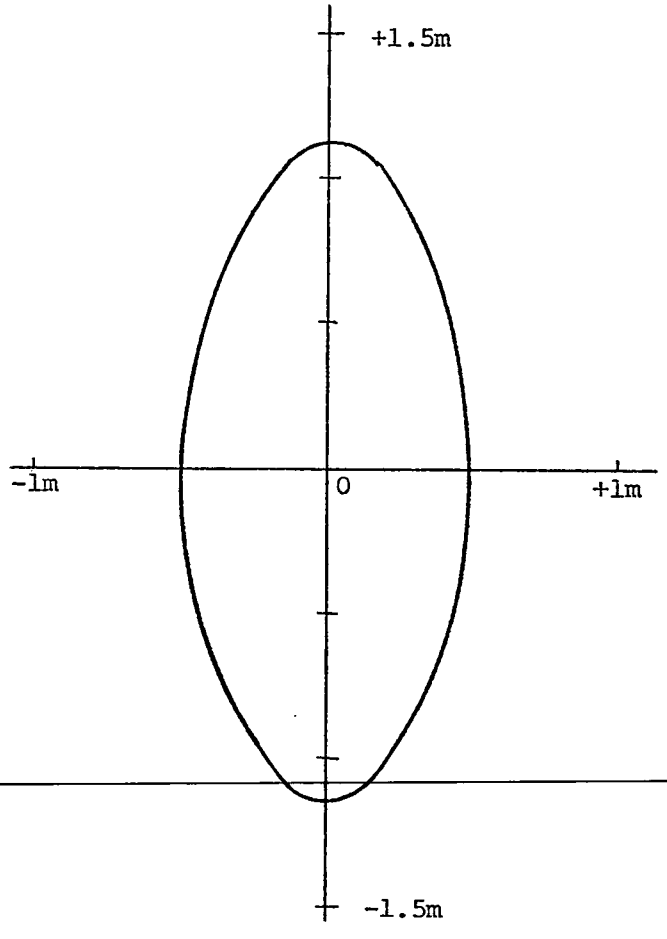

FIGURE 3-7

AREA COVERED BY BEAM MOVEMENT ON A 5 km PATH

Image Dancing:

The rms displacement of the beam focus from the focal point of the receiver antenna is equal to $F\sigma_\theta$, where F is the focal length of the receiver optics. Image dancing could be compensated by providing a larger detector area, but this may increase the receiver field of view and therefore the background noise.

Beam Spreading:

Beam spreading results when the beam wavefront is distorted such that $\sigma_\phi(\rho) > \pi$ over some lateral beam distance ρ. Corresponding to each phase coherent portion of the beam defined by the coherence length ρ_o, there is a ray deviation angle δ_θ which is relatively independent between different coherence areas. The beam energy is thus randomly spread in the receiver plane, therefore reducing the antenna gain. Experimental results show that a diffraction-limited beam with an ideal divergence of 5 μradians will experience an increase due to turbulence of from 0 to 150 μradians depending on the time of day [35]. The spread is typically proportional to $R^{1.2}$, R being the path length.

3.6.3 Techniques for overcoming turbulence probelms in direct detection systems. The best known and simplest technique for overcoming turbulent scintillations in a simple direct detection receiver is "aperture averaging". Increasing the size of the receiver optics to a diameter which is substantially greater than the correlation length,

$\sqrt{\lambda R}$, results in the simultaneous reception of a number of independently scintillating portions of the beam and substantially reduces the variance of the total received signal.

Another technique for reducing received signal variations is to increase the transmitter size. A large improvement is predicted when the receiver is in the near field of focused transmitter [36].

Spatial diversity receiver configurations utilizing detector arrays have been suggested for optimum communication in the presence of log-normal fading [35], however, the trade-off between complexiety and performance is not known.

3.7 Statistics of the Photodetection Process

Having considered the various noise sources, the background effects and the atmospheric effects which form the principal objections to terrestrial optical communication systems, we now return to the statistical model of such a system which was introduced at the beginning of this chapter. The following section deals with the theoretical evaluation of a receiver that yields the best performance in the reception of optical signals. These theoretical predictions form the basis of comparison with the experimentally obtained results.

3.7.1 Photodetector output probability density. As illustrated in the statistical model (Figure 3-1), signal photoelectrons combine with the background and dark current

emissions at the photodetector summation point. The noise due to atmospheric turbulence does not affect the system performance in the same way as the background and inherent detector noise does, and consequently cannot be lumped together with the rest of the noise. Its effect will be considered separately.

The total energy incident on the photodetector surface due to the background radiation and the laser signal does not remain absolutely constant all the time, but rather it randomly fluctuates from time to time. These random fluctuations are recognized as detection noise. The photon fluctuation statistics can be mathematically described in terms of the photodetector output probability density functions due to the above mentioned photoelectron sources.

It has been shown [24] that the background and dark current photoelectron emissions are independent Poisson[1] processes, so that the resultant distribution due to their combined effect is also Poisson. Hence,

$$P(k_1\tau) = \frac{(\bar{n}_e)^k \, e^{-\bar{n}_e}}{k!} \qquad (3\text{-}20)$$

---

[1]The Poisson distribution theorem states that, if a set of points is distributed individually and collectively at random in the interval (a,b), the probability that n points will lie within any subinterval of length x is

$$P(n,x) = \frac{(kx)^n}{n!} e^{-kx},$$

where kx is the expected number of points within the subinterval [4].

where, $\bar{n}_e = \bar{n}_d + \bar{n}_b$ is the average number of non-signal photoelectrons in the time period τ.

At low input levels, the photon fluctuations at the detector output due to the laser emission statistics have been shown to be a time-varying Poisson process where the time variation is a random process related to the bandwidth of the source and is independent of the noise photoelectron emissions [4]. Therefore, the statistical distribution of the laser signal can similarly be represented by the Poisson law,

$$P(k,\tau) = \frac{(\bar{n}_s)^k \, e^{-\bar{n}_s}}{k!} , \qquad (3\text{-}21)$$

$\bar{n}_s$ being the average number of signal electrons in the time period τ.

3.7.2 Shot noise limited detection. At low signal levels, the photodetector performance is usually limited by the shot noise, especially if the detector employs high gain photomultiplication [24]. The probability distribution of photoelectron emission due to both the signal and the noise is then given by

$$P(k,\tau) = \frac{(\bar{n}_s + \bar{n}_e)^k \, e^{-(\bar{n}_s + \bar{n}_e)}}{k!} . \qquad (3\text{-}22)$$

The probability density functions of noise and signal plus noise photoelectron counts are shown in Figure 3-8.

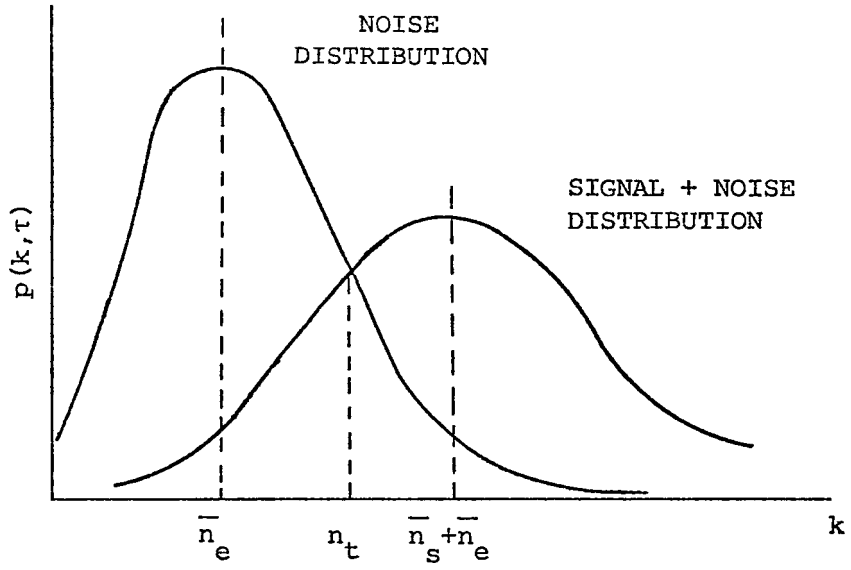

FIGURE 3-8

POISSON DISTRIBUTIONS OF NOISE AND SIGNAL

It is at once evident that some decision making is involved. If the number of phtotelectron counts exceed a certain threshold, the receiver recognized the signal (one bit); if the count is below the threshold value no signal (zero bit) is recognized. During each bit period, there is a probability that the threshold will be exceeded by noise electrons and "one" will be recognized when "zero" was intended. This is the probability of "false detection". Similarly there also exists a probability that the threshold may not be exceeded at all when the pulse was transmitted, and the intended "one" will be recorded as a "zero". This is called the probability of "no detection". The total probability of error resulting due to both the probability of false detection and the probability of no detection is given by,

$$P_E = P(1) \cdot P_{ND} + P(0) \cdot P_{FD} \tag{3-23}$$

where P(1) is the apriori probability of transmitting a pulse or "one" bit and P(0) is the apriori probability of transmitting no pulse or "zero" bit. Minimum P_E results when the threshold is set at an optimum value. Curran and Ross have shown that the value of the optimum threshold count is mathematically given as [37],

$$n_t = \frac{\bar{n}_s + \log \left[\frac{P(0)}{P(1)}\right]}{\log \left(1 + \frac{\bar{n}_s}{\bar{n}_e}\right)} . \tag{3-24}$$

In terms of the signal and noise electron counts, the theoretical minimum probability of error is given by,

$$P_E = P(1)\left[1 - \sum_{k=n_t}^{\infty} \frac{(\bar{n}_s + \bar{n}_e)^k \, e^{-(\bar{n}_s + \bar{n}_e)}}{k!}\right] + P(0) \cdot \sum_{k=n_t}^{\infty} \frac{(\bar{n}_e)^k \, e^{-\bar{n}_e}}{k!} \tag{3-25}$$

Figure 3.9 is a typical plot of the minimum probability of error against the signal level.

3.7.3 Thermal noise limited detection. Thermal noise added at the detector output has a Gaussian distribution with zero mean and variance proportional to the total

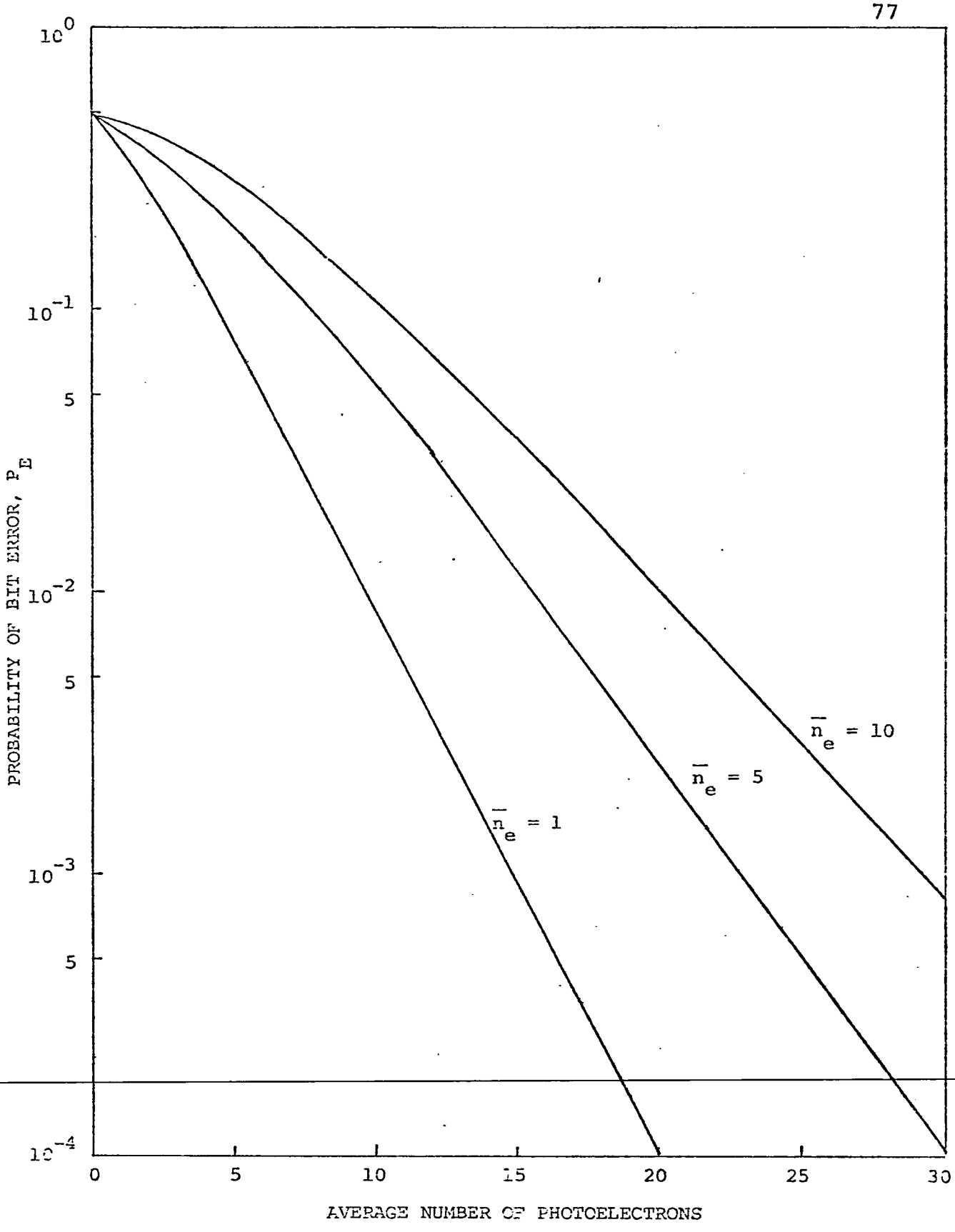

FIGURE 3-9

PROBABILITY OF DETECTION ERROR FOR PCM DIRECT DETECTION LASER COMMUNICATION SYSTEM - SHOT NOISE LIMITED OPERATION

thermal noise power. The probability density of the themal noise current source is

$$p(i_T) = \sqrt{2\pi\sigma_{i_T}^2}\ \exp\left[-\frac{i_T^2}{2\sigma_{i_T}^2}\right] \qquad (3\text{-}26)$$

where i_T is the thermal noise current and σ_{i_T} is the variance of the Gaussian noise.

The thermal noise limited operation results when there is a large number of photon counts. The photoelectron emissions due to the dark current and background radiation then become negligible compared to the thermal noise. With large signal photoelectron counts the signal current probability distribution may be considered Gaussian [24]. The probability density of the total photodetector current, $i_s + i_T$, is the sum of two Gaussian variables and is therefore Gaussian.

Figure 3-10 shows the typical probability of error curve in a thermal-noise-limited system.

3.7.4 The effect of atmospheric turbulence on the error rate in binary communications. Fried and Schmeltzer [38] have shown that the log-normal scintillation, except at the very weakest level, can have a very adverse effect on the performance of an optical link. There is a high probability in a log-normal distribution of values much smaller than the mean value. Occurrence of such deep fade in the channel, results in a very low signal-to-noise

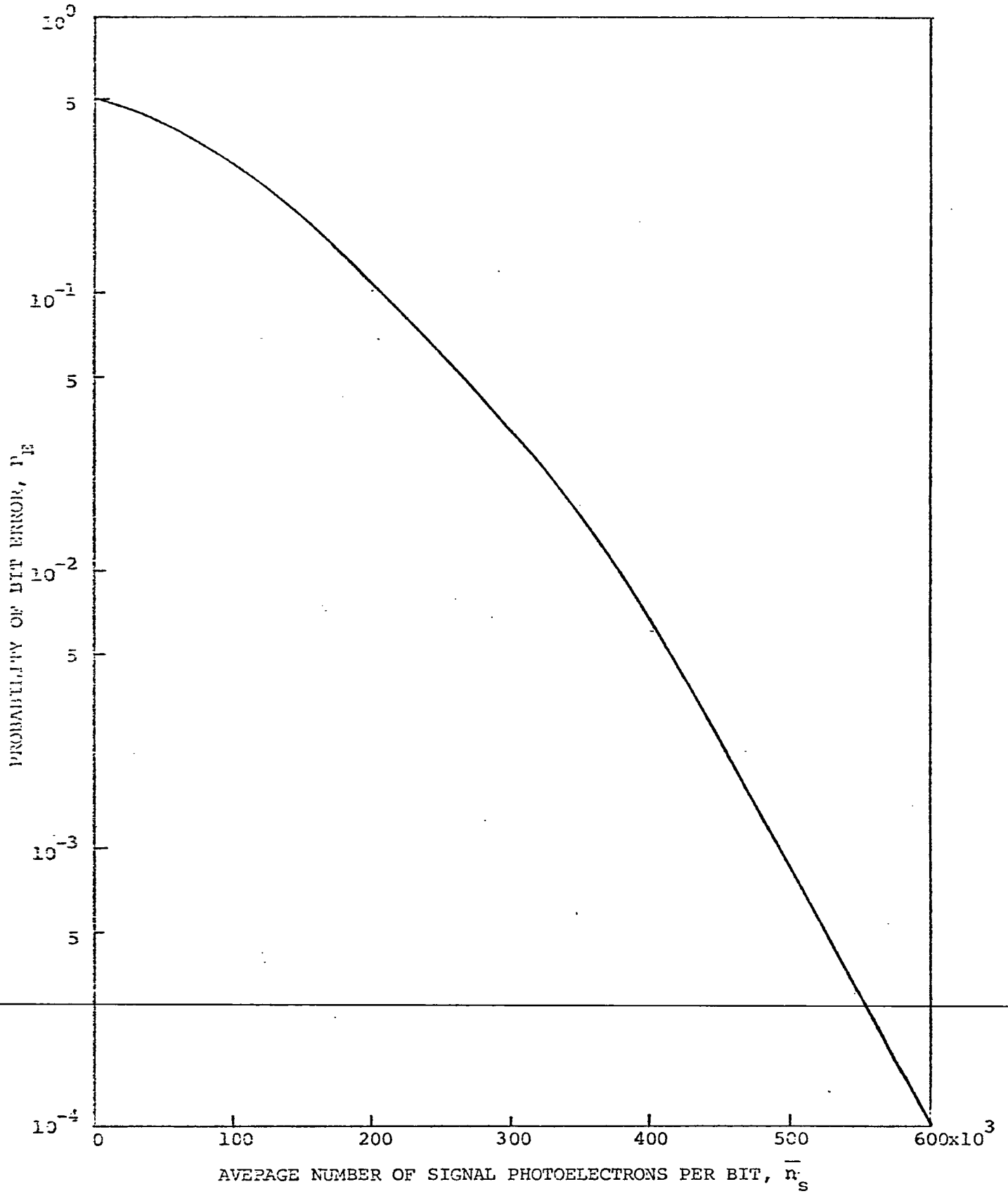

FIGURE 3-10

PROBABILITY OF DETECTION ERROR FOR PCM DIRECT DETECTION LASER COMMUNICATION SYSTEM - THERMAL LIMITED OPERATION

ratio and high error rate. To avoid this, the mean value of the signal must be very far removed from the deep fades, i.e., the system must have a very large signal-to-noise ratio. Fried and Schmeltzer define a "loss factor" which is the extra signal-to-noise ratio in decibels required above that needed because of the regular noise of the system to compensate for the adverse effect of scintillation. Table 3-3 lists the loss factor required at different turbulent conditions to maintain a probability of error of 10^{-5}. This gives an idea of the effect of turbulence on the performance of a binary optical communication link.

Turbulence	Log amplitude variance, σ_ℓ^2	Loss factor in decibels
very weak	0.002	0.5
weak	0.01	3
intermediate	0.10	15
strong	0.50	50
very strong	2.0	100

Table 3-3
Effect of Turbulence on the Error Rate

Chapter 4

SYSTEM SYNTHESIS

4.1 The Experimental Setup

An experimental infrared digital communication system utilizing a single GaAs laser diode was established between the Engineering and Science-and-Research Buildings on the University of Houston campus over a total transmission path of about 750 meters. A sketch of the link is shown in Figure 4-1. Narrow laser pulses were collimated and transmitted through a serveying transit mounted in the optical communication laboratory on the third floor of the Engineering Building. These pulses passed through the glass window of the laboratory and were pointed at an eight inch plane mirror securely mounted on the roof of the six story Science-and-Research Building. The mirror reflected the beam back to a ten-inch diameter receiver antenna placed beside the transmitter. The beam thus traversed the glass window twice at an angle of about thirty degrees. An appreciable amount of power was lost in this process since the glass essentially acted as a beam splitter.

The received beam was focused by an f:2 plano-convex lens on the surface of a silicon photodiode having a sensitive area of 0.8 mm^2. The current pulses generated by the light pulses were converted to voltage pulses by a

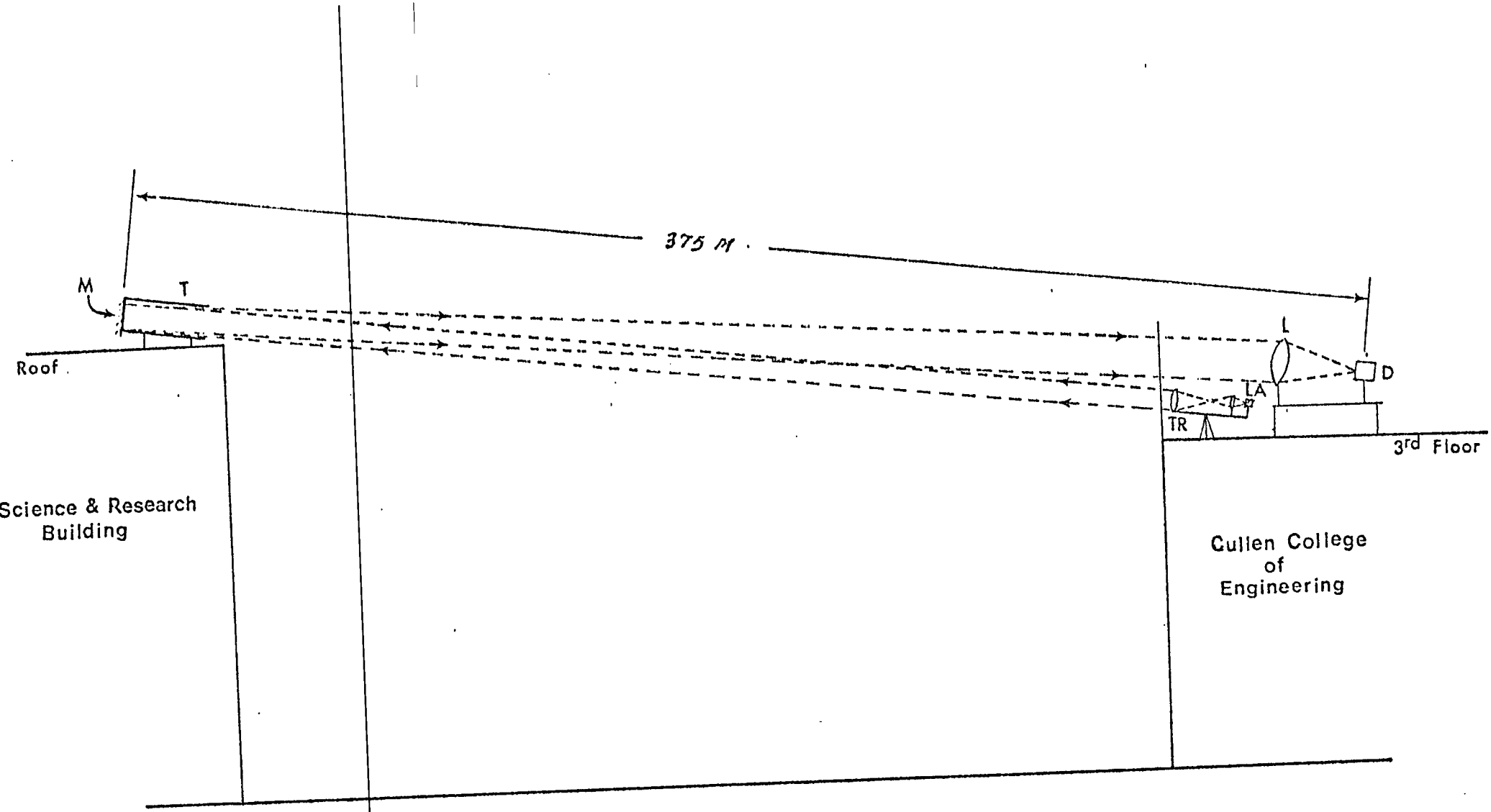

FIGURE 4-1

THE EXPERIMENTAL SETUP

M - MIRROR
T - TUBE
TR - TRANSIT
LA - LASER
L - FOCUSING LENS
D - PHOTODIODE

transimpedance amplifier and were fed to an integrator which acted as a matched filter receiver [39] for the binary signal. The integrator output was sampled and compared with a threshold voltage level, and a decision was made about the state of the signal. A TTL pulse was generated every time the receiver recognized the signal. This TTL output was then compared with the actual signal transmitted at that particular instant. The synchronization was achieved by gating the receiver decision pulses with the laser trigger pulses. Every time the trigger and the received signal differed, an error pulse was generated and was recorded on an electronic counter.

The block diagram of the physical model of this communication system is shown in Figure 2-1. It is evident that if the presence of the pulse represents a binary "one", for example, and the absence of the pulse represents a binary "zero", then the scheme described above can be used to transmit a PCM(IM) data between two points through the atmospheric channel.

4.2 Design of Building Blocks

4.2.1 Design of the laser modulator. An important step in synthesizing the link was developing a modulator to provide the narrow, high current pulses at a reasonably high repetition rate to trigger the injection laser. At room temperature, the laser must be operated within a specified duty cycle. The pulser must provide current

rise times of several amperes per nanosecond. However, the maximum speed is limited due to the difficulty of driving very fast, high current pulses into a low impedance presented by the forward-biased laser diode. The laser can tolerate only a very small amount of reverse current, therefore, any current undershoot must be held to a minimum. Since a current pulse with incorrect waveform can damage or even destroy the laser, a reasonable degree of care and sophistication is necessary in component selection, circuit layout and wiring.

The block diagram of a basic pulse generator for the injection laser application is shown in Figure 4-2.

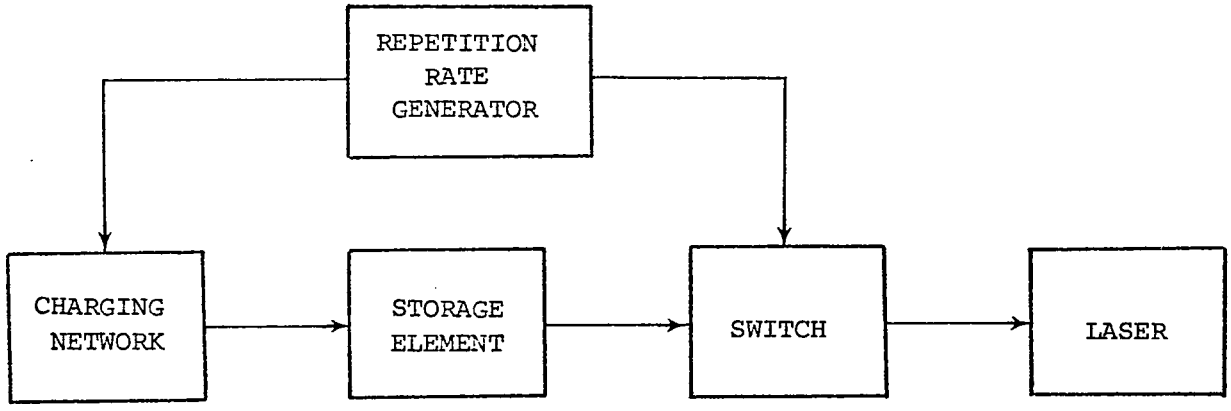

FIGURE 4-2

BLOCK DIAGRAM OF INJECTION LASER PULSER

The storage element which may be a capacitor or a transmission line can be charged through a resistor, an inductor or a transistor. The storage element must be capable of holding sufficient energy for at least a

single pulse. The rate of which this energy is released when the switch is closed, and hence the pulse shape, is determined by the electrical structure of the storage element.

The important properties of a switch for this application are the closing speed, the current handling capability, the "on" resistance and the recovery time. For high repetition rates, an avalanche transistor or a SCR can be used for switching.

Circuit layout and the lead lengths are very important to the performance of the injection laser pulser. The initial rate at which the current rises is V/L, L being the stray inductance in the circuit. This indicates the importance of keeping the stray inductance as low as possible. In addition to the rise time, the inductance decreases the peak value of the current and can also produce the undesirable ringing and undershoot in the current pulse. A modulator to give 25A peak current required by the injection laser SG-2004 at 150 ns pulse width was designed and is shown in Figure 4-3. With the limitation of 0.1% duty cycle, the maximum repetition rate is limited to about 6 kHz.

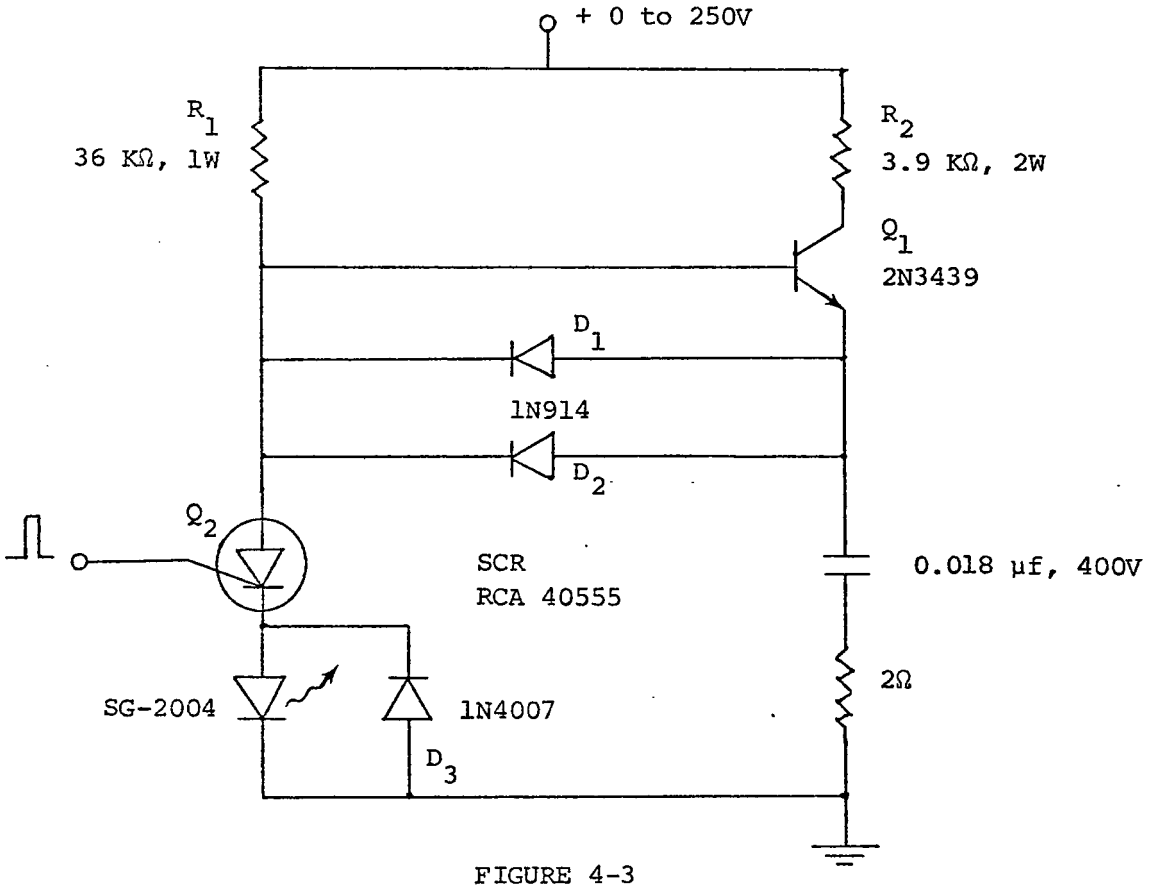

FIGURE 4-3

INJECTION LASER MODULATOR

In order to keep the charging time-constant small, the storage capacitor is charged to the supply voltage through a small resistance R_2. During the time the SCR is not conducting, diodes D_1 and D_2 are in the "off" state and the transistor is in saturation. With the onset of a trigger pulse at its gate, the impedance of the SCR drops rapidly and the capacitor discharges through the laser diode. During this period the transistor is reverse biased due to the voltage drop across the diodes D_1 and D_2, and hence it isolates the power supply from the SCR. The SCR turns off when the current drops below its holding

current, which determines the value of the 36 k resistor. D_3 is a clamping diode used to protect the laser against excessive undershoot. A small resistance is included in the discharge circuit to damp out the ringing.

4.2.2 Receiver design. Figure 4-4 is a schematic drawing of the receiver designed to process the received pulse and count the number of errors during transmission. The photodiode current is fed to the transimpedance amplifier which produces a voltage equal to $R_f I_s$ at its output, where R_f is the feedback resistance and I_s is the photocurrent. This configuration allows the use of a large value of a feedback resistance to obtain a large signal without sacrificing the speed. The signal is integrated and is compared with an adjustable threshold voltage. The timing and synchronization is obtained from the SCR gate trigger pulse which turns the laser on. The timing network formed by the interconnection of six monostable multivibrators provides signals to clear the integrator before and at the end of the pulse period. It also provides a sampling pulse to sample the integrator output at its peak. The timing diagram of Figure 4-5 explains the operation of the network. It can be seen that an error will be counted every time the received signal falls below the threshold or the threshold is exceeded by a spurious waveform.

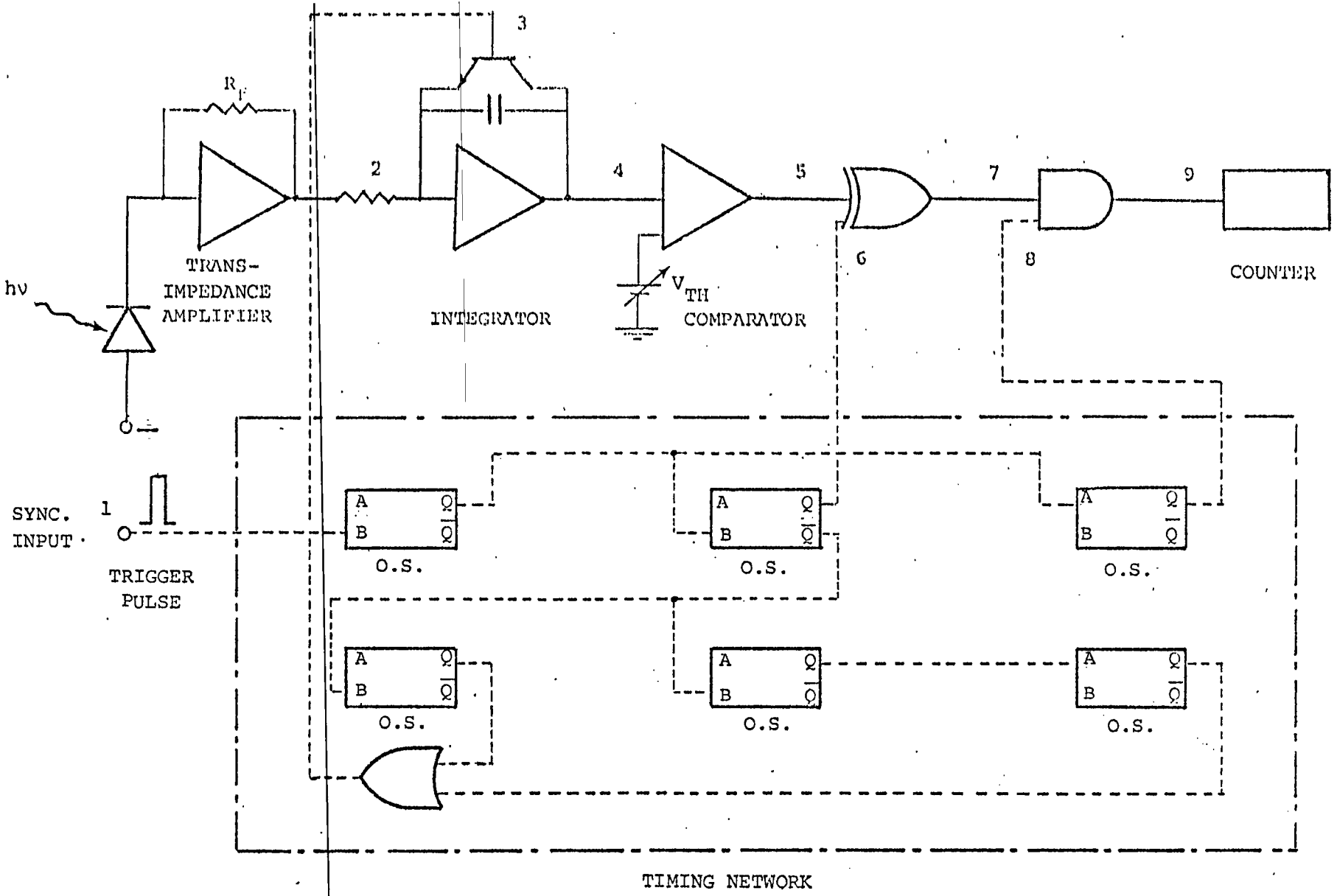

FIGURE 4-4

ERROR COUNTING RECEIVER

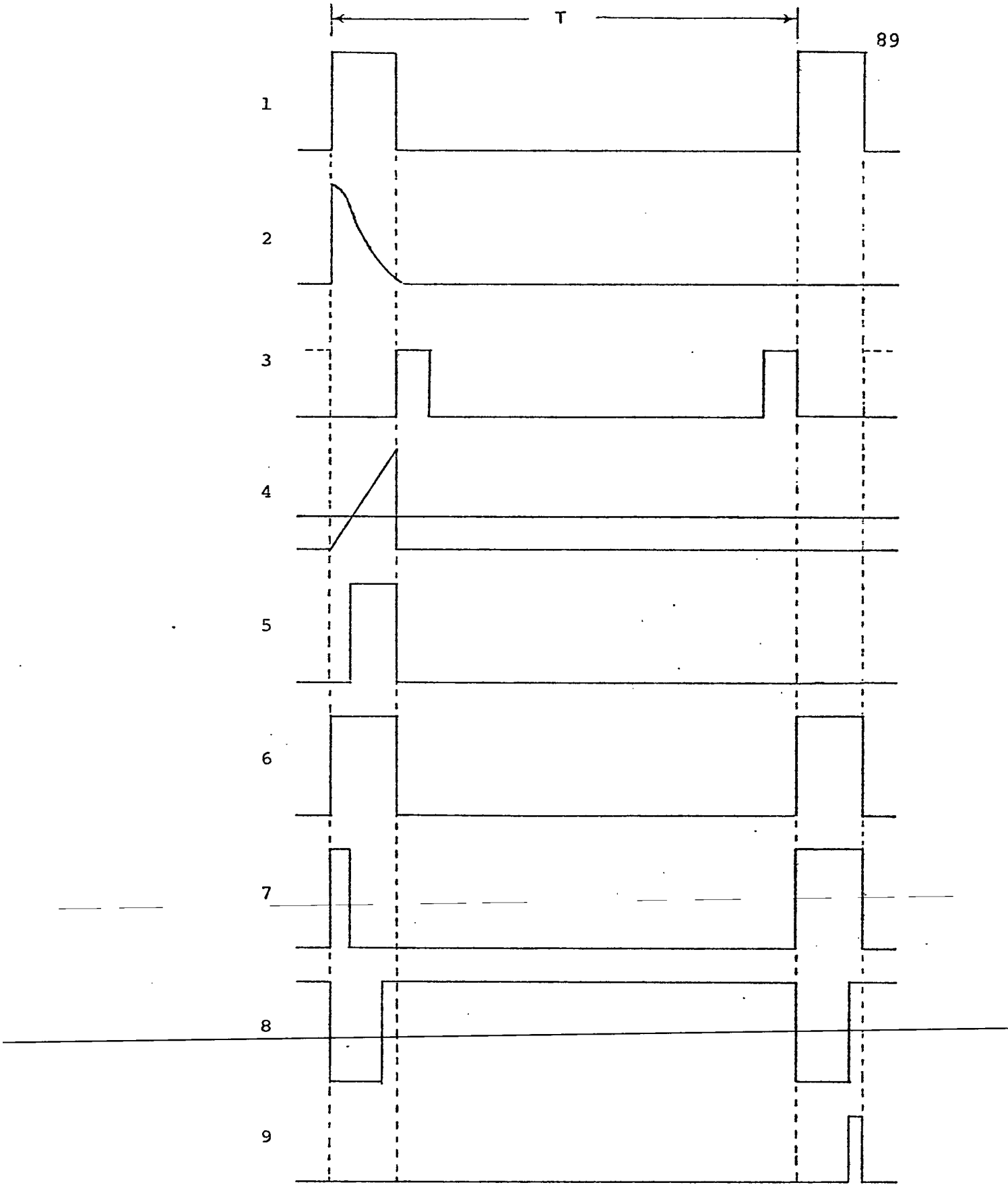

FIGURE 4-5

RECEIVER TIMING WAVEFORMS

4.3 System Performance

Some typical parameters of the system are calculated. Due to the several assumptions made in these calculations, the analysis, at best, is only approximate. However, this exercise serves well to give some idea of the performance of the system.

Sample Calculations

Assuming certain parameters, the performance of the system, in particular, the value of the received power and the signal-to-noise ratio for a known value of the transmitted power can be calculated. These calculations are shown here for clear weather conditions with a visibility of 15 km.

The known parameters are as follows;

Range of the link	$R = 780$ m
Transmitter optics diameter	$d_t = 2.4$ cm
Receiver optics diameter	$d_r = 20$ cm
Receiver optics focal length	$F = 38$ cm
Wavelength of radiation	$\lambda = 0.904$ μm
Detector effective load resistance	$R_L = 330$ kΩ
Detector responsivity	$R = 0.65$ A/W
Detector dark current	$I_D = 1 \times 10^{-8}$ amp
Detector area	$A = 0.8$ mm^2
Rise time of received pulse	$t_r = 0.3$ μs
Optical filter band pass	$B_{opt} = 128$ Å
Optical filter transmittance	$\tau_{opt} = 0.6$

Angular Beam Width of the Transmitter:

$$\theta_t = \frac{2.44\lambda}{d_t} \qquad (2\text{-}21)$$

$$= \frac{2.44 \times .904 \times 10^{-6}}{2.4 \times 10^{-2}}$$

$$= 0.1 \text{ mrad.}$$

This is the diffraction limited beam width. In practice the divergence will be somewhat higher. Therefore, a value of 0.5 mrad. will be assumed.

Receiver Field of View:

$$\theta_r = \frac{d_p - d_d}{F} \qquad (2\text{-}23)$$

The detector has a circular window of the sensitive area 0.8 mm^2, so that the detector diameter, d_p = 1 mm. The diameter of the focused beam spot is given by

$$d_d = \frac{2.44\lambda}{d_R} F. \qquad (2\text{-}24)$$

With the known values of λ, d_R and F; d_d can be calculated as 0.013 mm. Therefore,

$$\theta_r = \frac{1 - 0.013}{380} \simeq 2.5 \text{ mrad.}$$

A non-diffraction limited value of 10 mrad. will be assumed.

Receiver Bandwidth:

The electrical bandwidth of the receiver is

$$B = \frac{0.35}{t_r} \tag{2-20}$$

$$= \frac{0.35}{0.3 \times 10^{-6}} \simeq 1 \text{ MHz.}$$

Received Signal Power:

$$P_s = \frac{P_L A_r \tau_a \tau_o}{\theta_t^2 R^2} \tag{3-1}$$

Due to the strong received signals during the experiment, the laser was not pulsed to its full output capability of 5W. The transmitter power of 1W will be assumed for the calculations. For the clear weather conditions the attenuation coefficient σ, is found from Figure 3-3 as 0.2 km^{-1}. Assuming sea level altitude, the atmospheric transmittance τ_a, can be directly found from Figure 3-5 as,

$$\tau_a = e^{-\sigma R} = e^{-0.15} \simeq 0.9.$$

In the above equation, τ_o represents the overall transmittance of the optics. It consists of the transmittance of the transit and receiver lenses, transmittance of the window, transmittance of the optical filter and reflectance of the mirror. Readings were taken to approximately determine these quantities. It was found that the transit transmitted only about 60% of the power and the window transmitted

about 85% in a single passage. The following figures will be assumed in the calculations:

Transmittance of transmitter and receiver optics = 0.5

Transmittance of window = 0.7

Transmittance of optical filter = 0.5

Reflectance of the mirror = 0.98

Therefore, the overall transmittance of the optics becomes

$$\tau_o = 0.5 \times 0.7 \times 0.5 \times 0.98$$

$$= 0.17.$$

With all the known values, the received signal power can be calculated as

$$P_s = \frac{1 \times 0.031 \times 0.9 \times 0.17}{0.25 \times 10^{-6} \times 780^2}$$

$$\simeq 32 \text{ mW}$$

Background Power:

$$P_B = \frac{\tau_a \tau_r B_{opt} A_r \theta_r^2 \xi}{4} H_\lambda \qquad (3\text{-}8)$$

We will assume the value of solar irradiance to be $0.1 \text{ W/m}^2/\text{Å}$ [28]. The reflection coefficient of the background, ξ, is commonly assumed as 0.5 [26]. The combined transmittance due to the optical filter, the receiver optics and the window, τ_r, may be taken as 0.4. Then,

$$P_B = \frac{0.9 \times 0.4 \times 128 \times 0.031 \times 100 \times 10^{-6} \times 0.5 \times 0.1}{4}$$

$$\simeq 1.5\ \mu W$$

Signal-to-Noise Ratio:

$$\frac{S}{N} = \frac{R^2 P_s^2 R_L}{2\ qB(RP_s + RP_B + I_D)R_L + 2\ FkTB} \qquad (3\text{-}14)$$

The amplifier noise factor, F, will be assumed to be 2. Values of the physical constants are

$$q = 1.6 \times 10^{-19} \text{ coulombs}, \quad k = 1.38 \times 10^{-23} \text{ joules/°K}.$$

With all the quantities in equation 3-14 known, it can be found that

$$\frac{S}{N} \simeq 108 \text{ dB}.$$

It appears that at such high signal levels, the only significant noise is the signal shot noise itself. The effects of the atmospheric turbulence were not taken into account while calculating the signal-to-noise ratio. The actual value of the signal-to-noise ratio will, of course, be reduced by the loss factor as discussed in Section 3.7.4. It can be noted that the calculated value of the signal-to-noise ratio reasonably compares with the results found in the literature [40] as evidenced in Figure 4-6. The figure shows a plot of the signal-to-noise

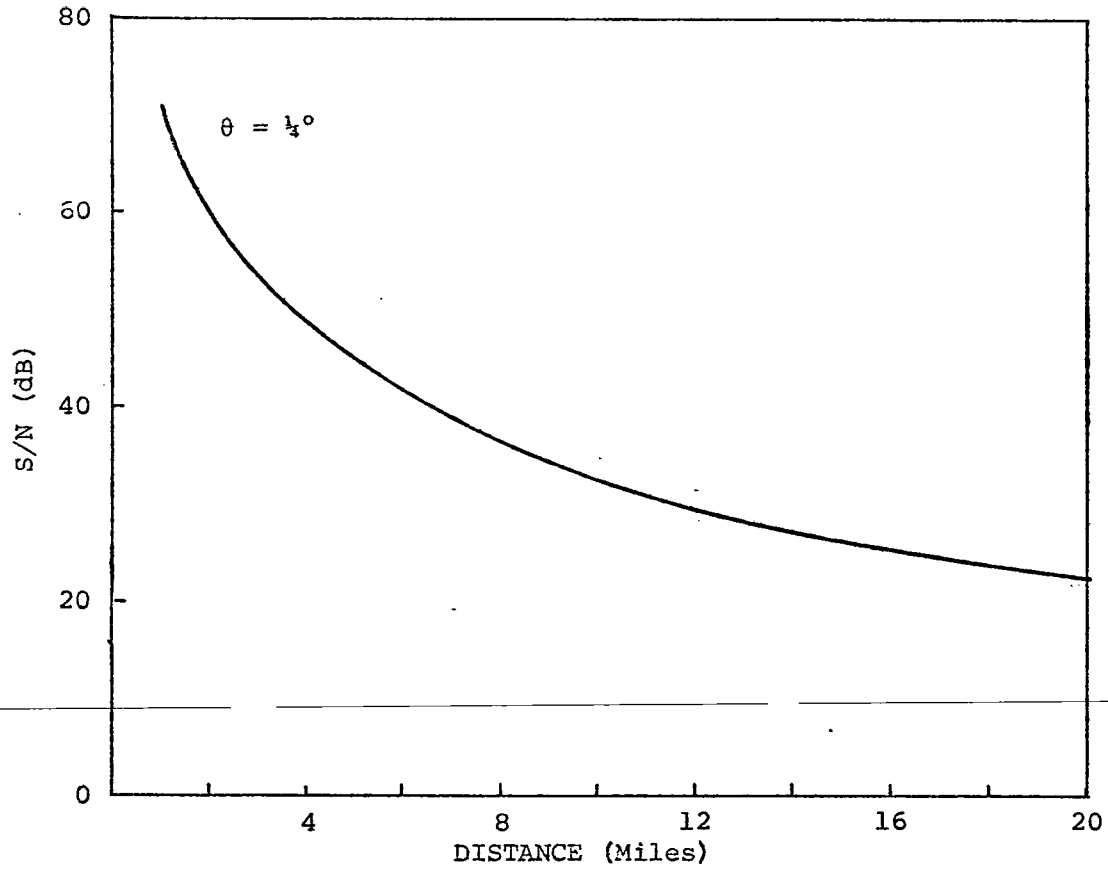

FIGURE 4-6

SIGNAL-TO-NOISE RATIO VERSUS DISTANCE

ratio versus distance for clear weather conditions with 100 mW transmitted power and ¼° beam width. A signal-to-noise ratio of about 75 dB was obtained over a one mile path.

Complete system parameters and performance are summarized in Table 4-1.

Description	Symbol	Value	Units
Wavelength	λ	0.904	μm
Range	R	980	m
Transmitted pulse width	τ	150	ns
Maximum repetition rate	PRF	6	kHz
Transmitter optics diameter	d_t	2.4	cm
Transmitted beam width	θ_t	0.5	mrad
Receiver optics diameter	d_r	20	cm
Receiver optics focal length	F	38	cm
Detector sensitive area	A	0.8	mm^2
Receiver field of view	θ_r	10	mrad
Detector responsivity	R	0.65	A/W
Detector effective load resistance	R_L	330	kΩ
Detector dark current	I_D	$1x10^{-8}$	A
Detector gain	G	1	-
Receiver bandwidth	B	1	MHz
Atmospheric attenuation coefficient	σ	0.2	km^{-1}
Atmospheric transmittance	τ_a	0.9	-
Transmittance of optics	τ_o	0.17	-
Bandwidth of optical filter	B_{opt}	128	Å
Solar irradiance	H_λ	0.1	$W/m^2/Å$
Background power	P_B	1.5	μW
Peak transmitted power	P_L	1	W
Peak received power	P_s	32	mW
Signal-to-noise ratio	S/N	108	dB

Table 4-1

System Parameters

4.4 Experimental Results

In order to evaluate the performance of the link it was necessary to plot the probability of error in receiving the bits against the transmitted power. Unfortunately, detailed characteristic curves of the injection laser source were not available. Therefore, before undertaking the investigation of the performance of the link itself, it was thought necessary to obtain some data on the operating characteristics of the laser. The relevent characteristics such as the pulser charging voltage versus laser pulse current, the pulse current versus laser power output and the output power variation with time were experimentally determined. This data was then used in determining the performance of the link.

4.4.1 Injection laser characteristics. Injection laser output depends upon the pulse current through the laser. The pulse current can be varied by varying the capacitor charging voltage in Figure 4-3. At any value of the charging voltage, the peak pulse current can be measured by observing the voltage pulse developed across the 2Ω resistor. The output characteristic of the laser was obtained by measuring the power output[1] at different values of the pulse current and is shown in Figure 4-7.

[1] All power measurements were carried out using Coherent Radiation Laboratories' power meter model No. 212. This power meter was calibrated for 0.633 μm. Therefore, the values shown on the graphs and data do not indicate the actual output power of the laser; rather they represent the normalized output power.

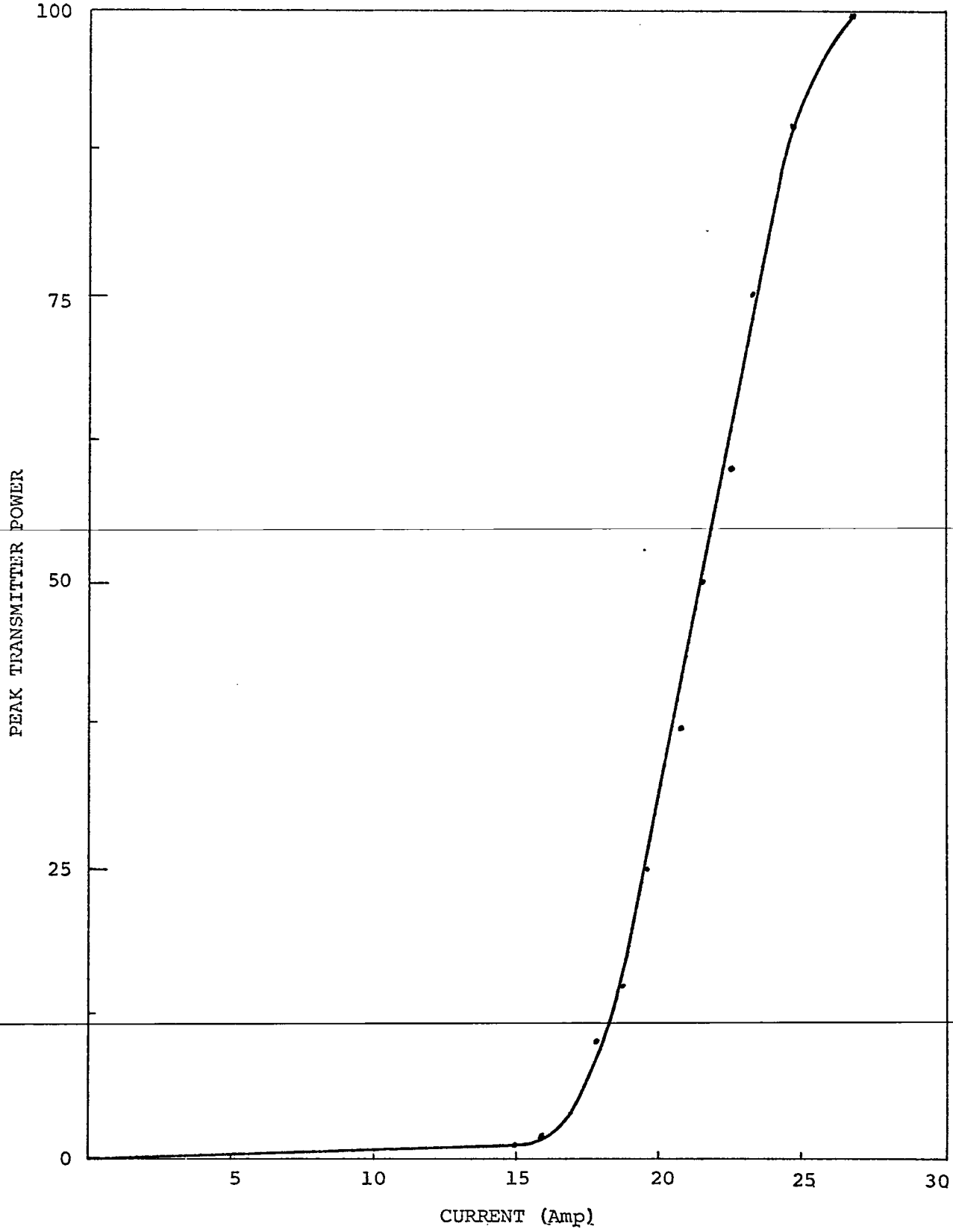

FIGURE 4-7

LASER OUTPUT VERSUS PULSE CURRENT

The figure clearly indicates a threshold current of about 15 amperes. It is also noticed that after the peak current of 25 amperes is reached, the laser output begins to saturate.

It was observed that the laser output dropped after some period of time. The drop was very noticable at higher pulse repetition rates. The power drop, no doubt, resulted from the heating of the laser. In order to determine the extent of the heating effect, the laser output was plotted against time at different pulse repetition rates. The results are shown in Figures 4-8 and 4-9. A very marked drop of power due to considerable heating is evident at a higher pulse repetion rate.

It was found more convenient to relate the charging voltage to the power output, since the voltage could be directly read from the power supply voltage indicator. Figure 4-10 is a plot of the charging voltage against the laser pulse current in the operating range. Figure 4-11 shows the maximum laser output versus charging voltage at different pulse repetition rates. The reduction in power at high repetition rates is evidently due to the failure of the storage capacitor to charge to the full supply voltage.

PRF = 2.5 kHz

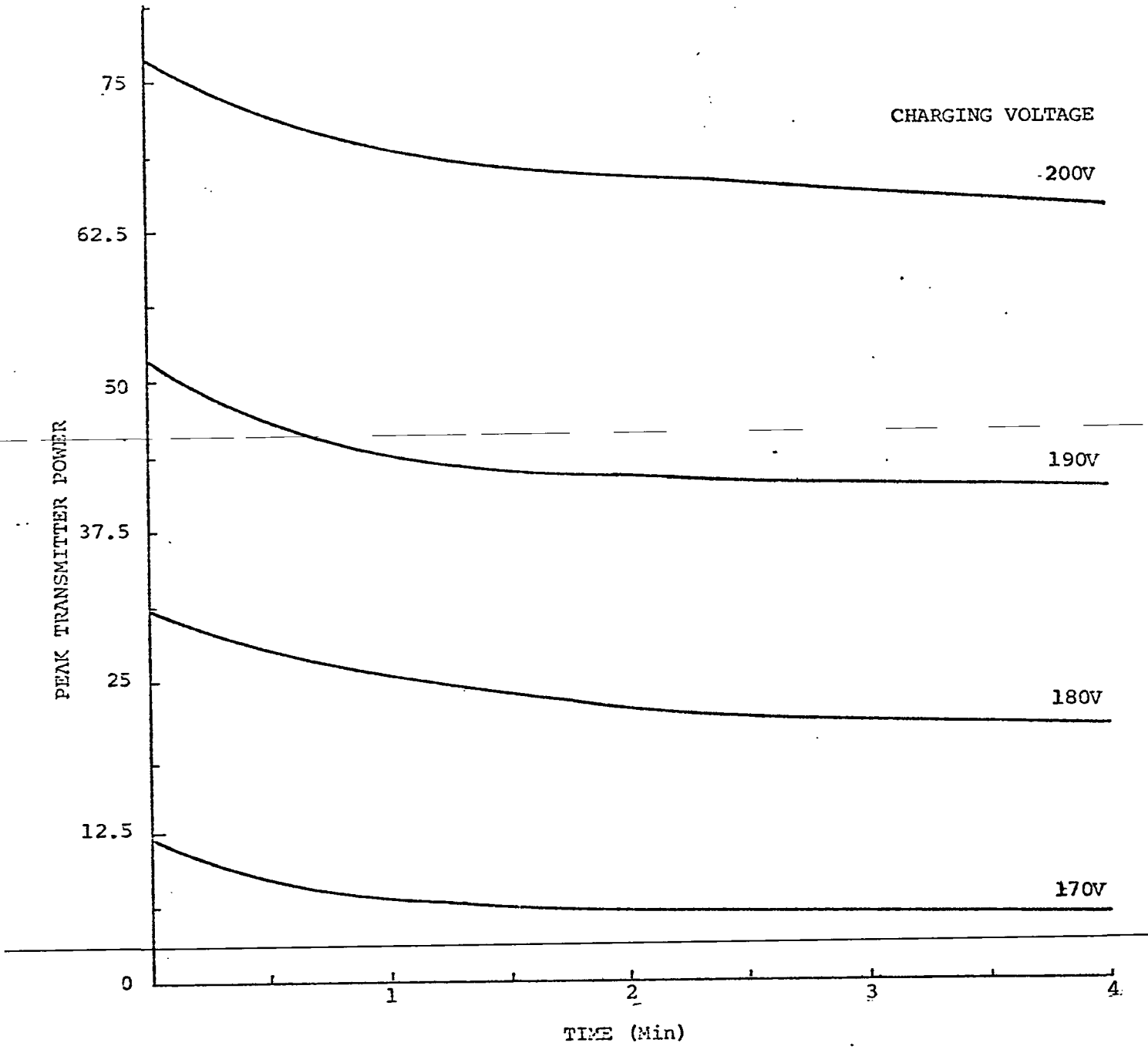

FIGURE 4-8

LASER HEATING EFFECT

PRF = 5 kHz

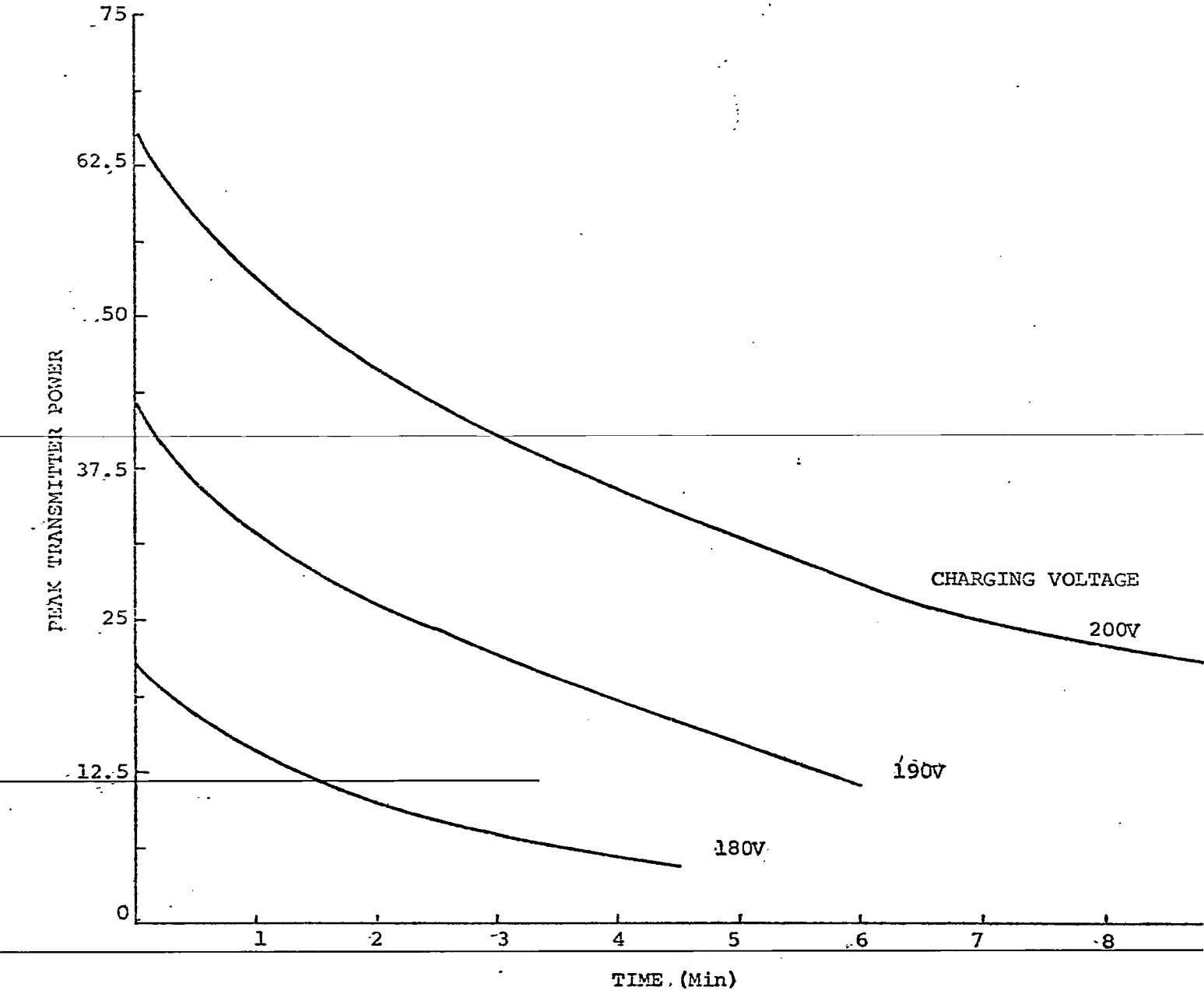

FIGURE 4-9

LASER HEATING EFFECT

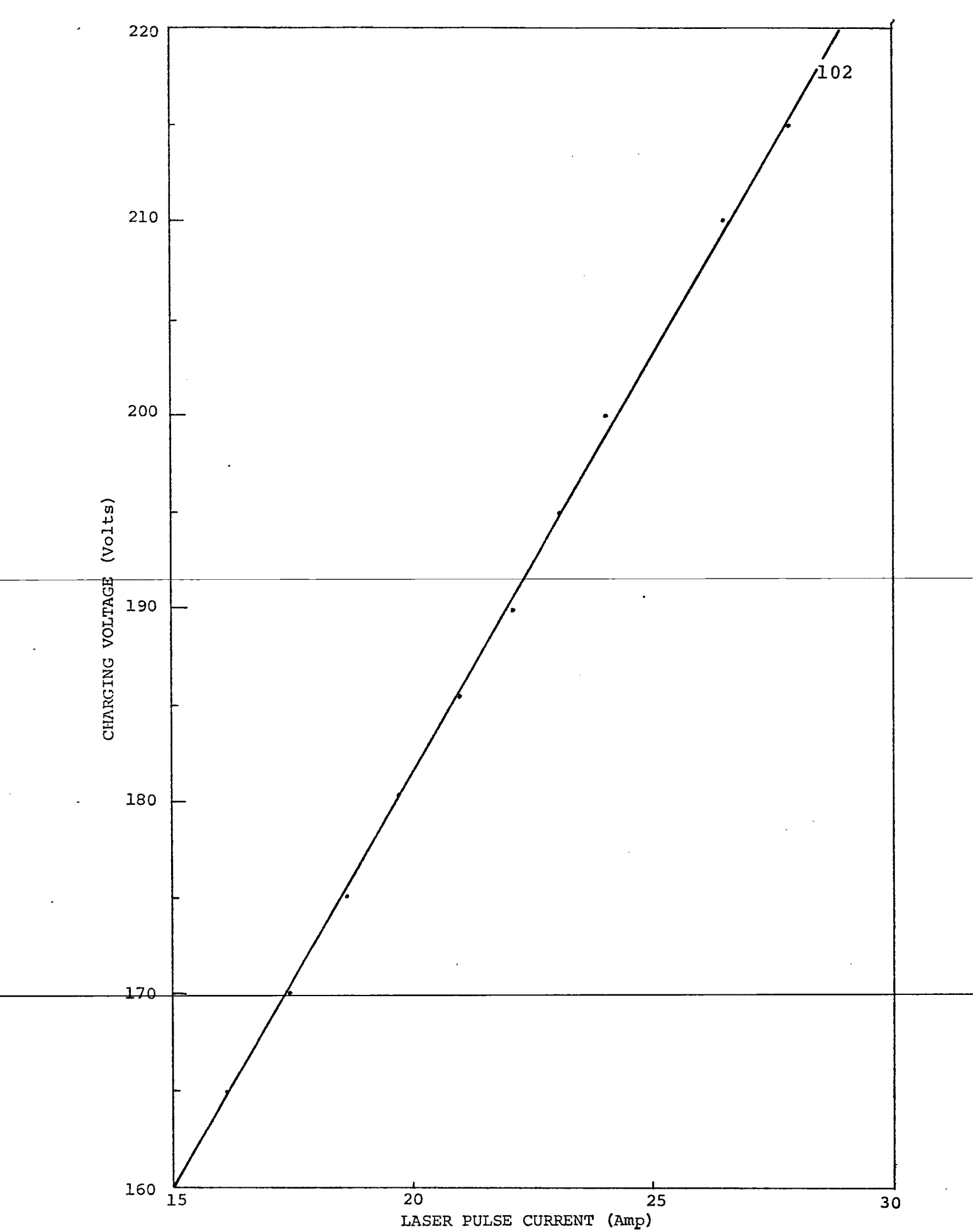

FIGURE 4-10

CHARGING VOLTAGE VERSUS LASER CURRENT

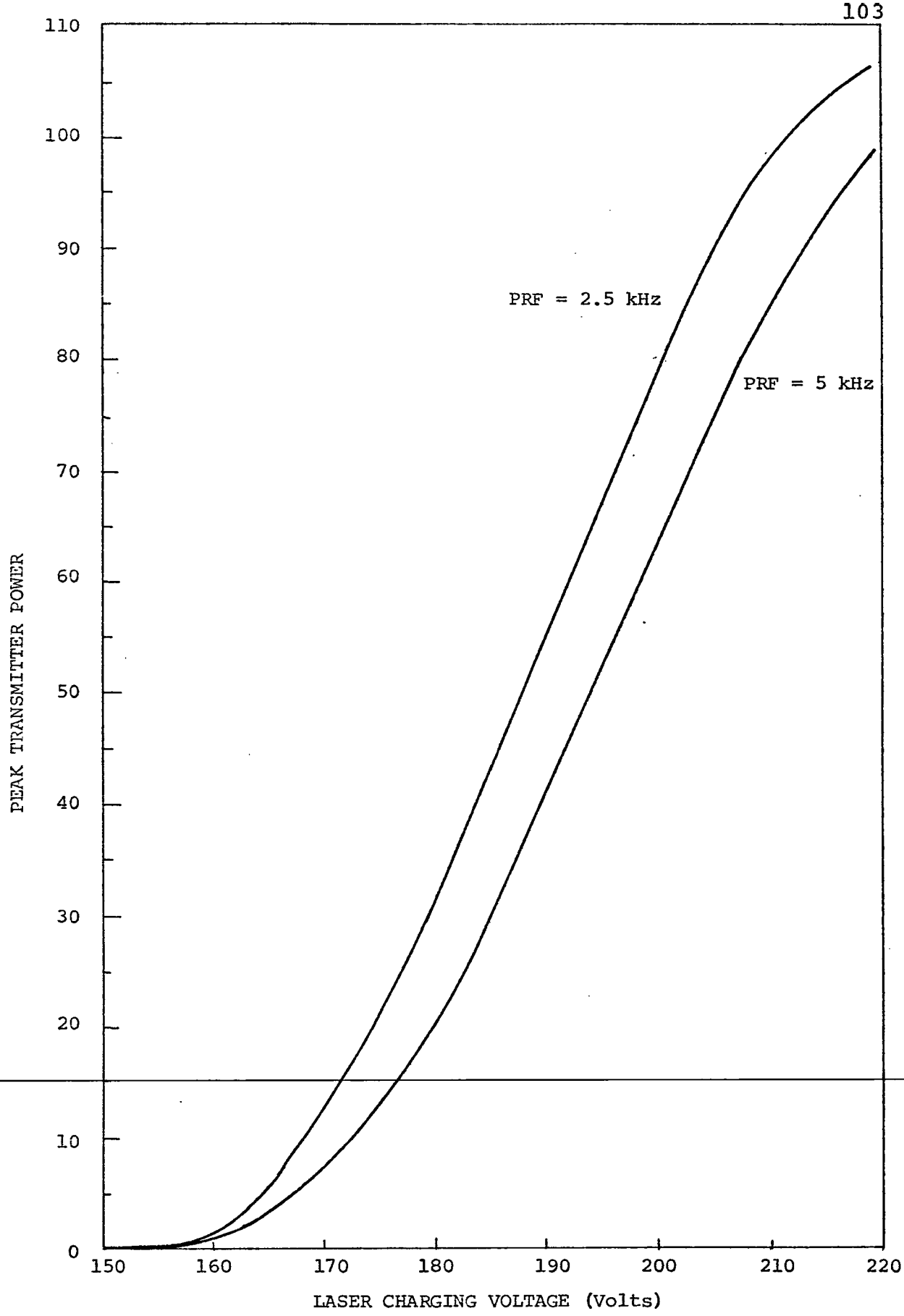

FIGURE 4-11

CHARGING VOLTAGE VERSUS TRANSIT POWER OUTPUT AT t = 0

4.4.2 Error rate performance. In order to determine the performance of the link, a signal was transmitted to the receiver at a known pulse rate and power. The transmission was continued until a sufficient number of errors were recorded to allow the statistical estimation of the error rate to be made. The error rate was determined by dividing the number of errors observed in a time period T, by the number of bits transmitted in that period. This procedure was carried out at different transmitted power levels and under different atmospheric conditions, and error rate performance curves were obtained. Table 4-2 shows a detailed record of a typical data run taken during night operation.

The atmospheric conditions were noted before the start of the run through the local weather information bureau. Since the laser output varied during the time for which the errors were recorded, it was necessary to use an average value of power for the purpose of plotting the error rate curves. This average value was deduced for each charging voltage with the help of Figures 4-11, 4-8 and 4-9. Figure 4-11 gave the maximum power output at the beginning of the counting period. Figures 4-8 and 4-9 gave the indication of the power drop for the length of the counting period. The average of the maximum and minimum powers thus estimated was recorded against the calculated error rate for that particular condition. The output at the integrator was recorded at the beginning and the

Set Number 11 Date: March 7, 1975 Time: 10-11 p.m.

ATMOSPHERIC CONDITIONS:

Temp: 62°F

Skies: Cloudy

Wind: N 15 mph

Humidity: 58%

Bit Rate: 5 kHz

COMMENTS:

1) Stable signal
2) Alignment satisfactory - beam was centered on the receiver lens
3) Optical filter was not used

Laser Supply Volts	Peak Transmitter Power with Heating Correction	Integrator Output Volts At Start	Integrator Output Volts At Finish	V_{Th}	Counting Period, T	No. of Bits Transmitted in Period T	No. of Errors Counted	Bit Error Rate Equal Errors/Bit Rate x T_{sec}
177	19	4.8	3.8	0.5V	18 min		20	3.5×10^{-6}
172	15	2.8	0.2	0.2	3 min		36	4.0×10^{-5}
171	13	2.1	1.5	0.2	2 min		32	5.33×10^{-5}
170	12	2.0	1.6	0.2	1 min		22	7.33×10^{-5}
169	11	1.7	1.6	0.2	30 sec		120	8.0×10^{-4}
168	9	1.5	1.5	0.15	30 sec		320	2.133×10^{-3}
167	7.5	1.4	1.4	0.1	30 sec		1177	7.84×10^{-3}
166	5	1.2	1.2	0.1	30 sec		2807	1.87×10^{-2}

Table 4-2

A Typical Data Set

end of the counting period. The drop in this output resulted mainly due to the power drop arising from heating. Recording the integrator output also helped in achieving the best alignment by comparing the signals obtained at that charging voltage level during different data runs. A typical data run took about 1½ hours. During the run, the alignment was periodically checked with the help of the fine controls available on the transit to insure that the maximum signal was received at each power level. Stable and satisfactory alignment could be easily obtained during night operations, but it was found that this alignment would be invariably disturbed during broad daylight. In fact, several attempts to obtain error rate data during bright sun light remained unsuccessful due to the complete loss of alignment.

In general during night operations and partially cloudy daylight operations for which alignment could be maintained, very strong signals were received, and it was necessary to limit the laser power output to keep the photodiode from saturating. To record errors with such strong signals, the receiver threshold was arbitrarily set at a very low voltage compared to the received signal. This is justified because of the high signal-to-noise ratios predicted by the sample calculations.

Several data sets were recorded at different atmospheric conditions during nights and afternoons. It was observed that during the operation under cloudy

skies, the signal remained strong and steady. The link needed little realignment during these data runs. With clear skies, however, large signal fluctuations were distinctly observed and frequent realignment was necessary. The error rate performance of the link during various atmospheric condition is presented in Figures 4-12 through 4-21.

Figures 4-12 through 4-14 show the error rate performance during cloudy nights. The turbulence is expected to be low under cloud covers. A visual confirmation of this fact was given by very stable signals under these operations. Transmitter power had to be substantially cut as the signals received were too strong. During clear nights the turbulence activity is expected to increase. Accordingly, marked signal fluctuations prevailed during these operations and to obtain the same error rates the signal power had to be increased. Figures 4-15 and 4-16 illustrate this fact. As the background noise did not significantly affect the performance of the system, it was not necessary to use the optical filter during night runs. Figures 4-17 and 4-18 show the performance during partly cloudy skies in the late afternoon. The turbulence activity should be mild. Small signal fluctuation existed. An optical filter was used during daytime runs. It reduced the received signal by about 40%. Figure 4-19 shows the operation during a bright and shiny afternoon. Severe signal fluctuations were noticed at this time. One data run was taken during early afternoon on an overcast day. The error rate curve showed more slope than the other

daytime curves, as can be seen in Figure 4-20. Figure 4-21 summarizes the performance during the different atmospheric conditions. It is apparent that the best performance of the link is obtained during night operations under cloudy skies.

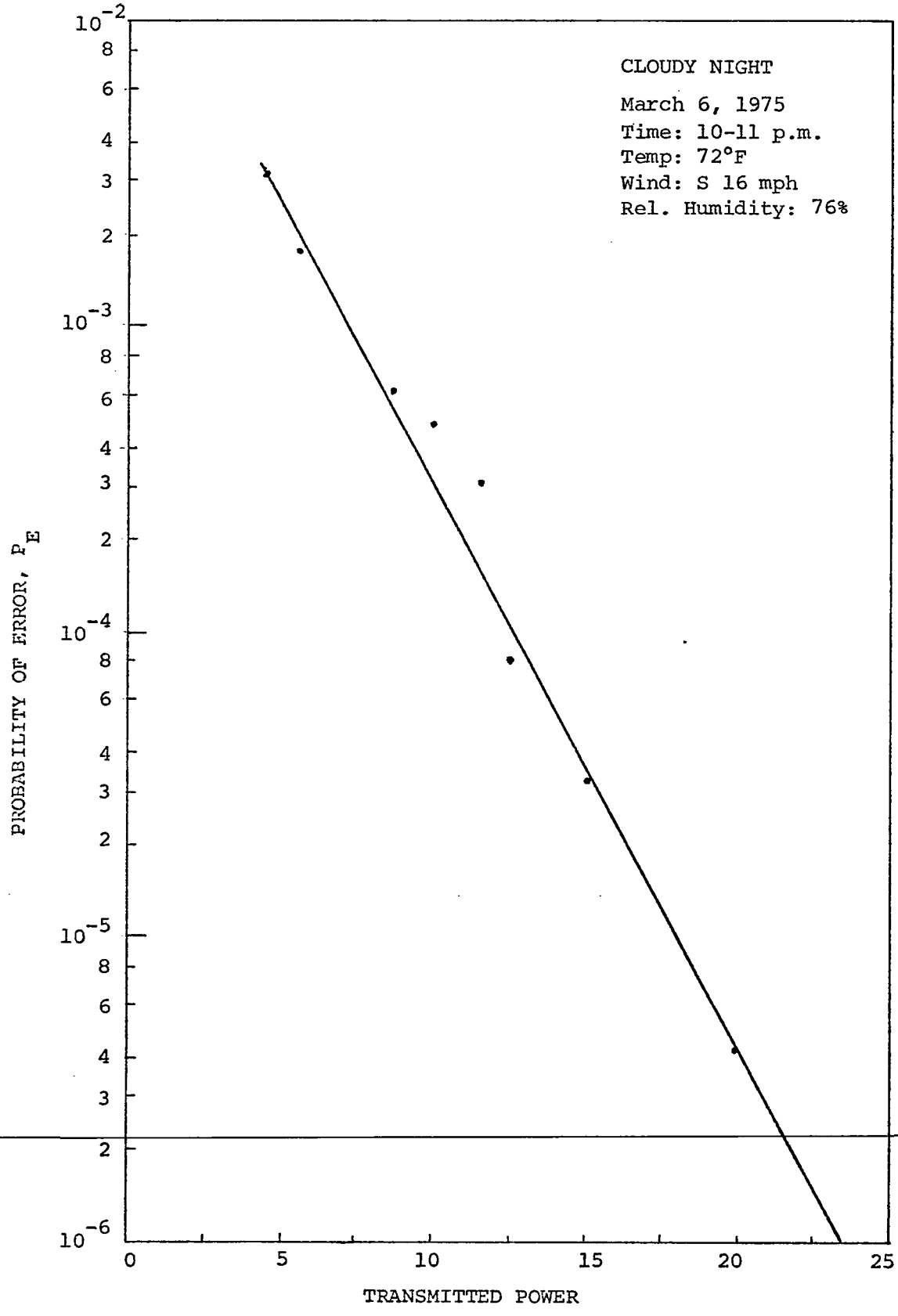

FIGURE 4-12

ERROR RATE VERSUS TRANSMITTED POWER

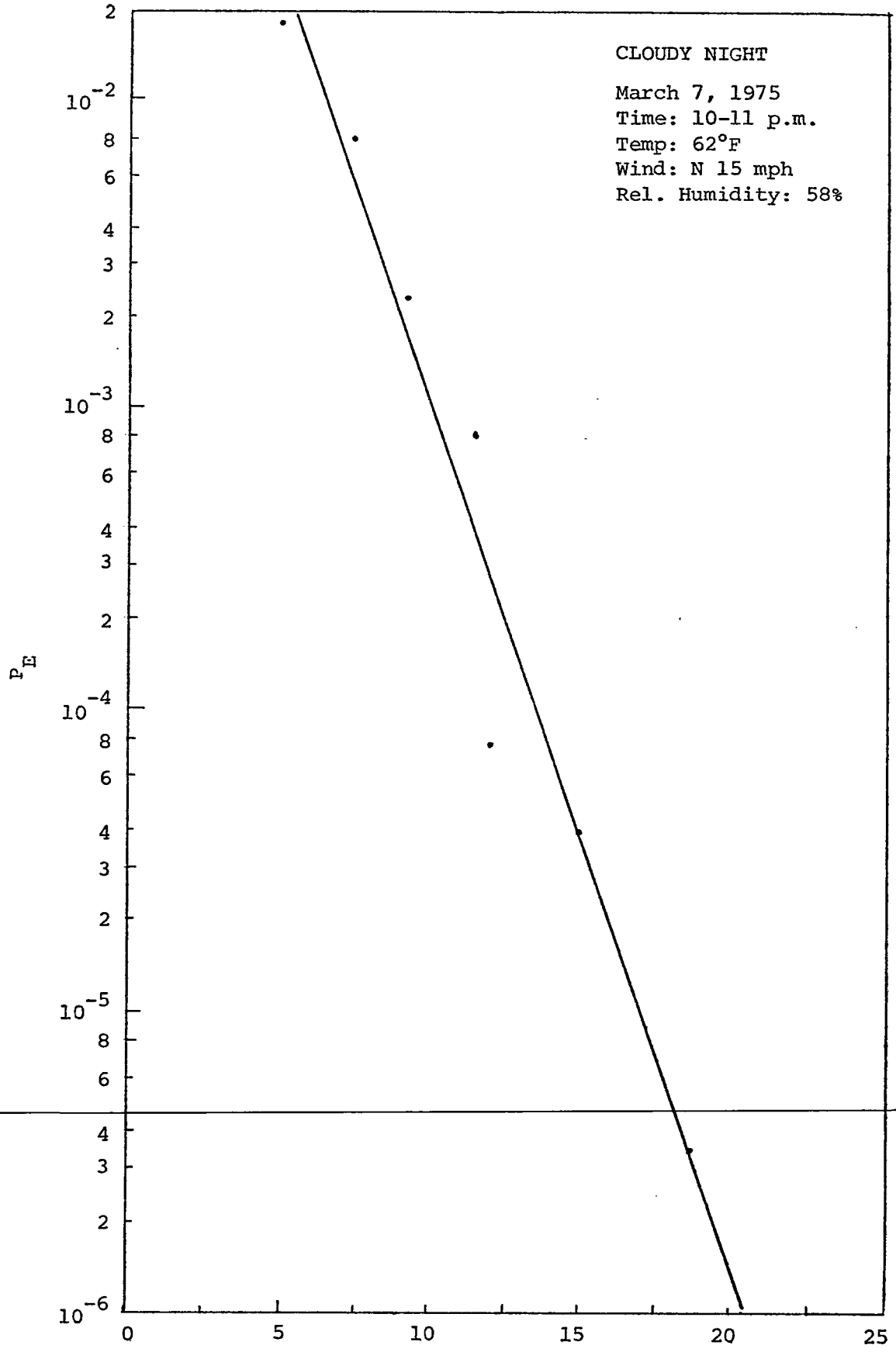
CLOUDY NIGHT
March 7, 1975
Time: 10-11 p.m.
Temp: 62°F
Wind: N 15 mph
Rel. Humidity: 58%
P_E
10^{-2}
10^{-3}
10^{-4}
10^{-5}
10^{-6}
0
5
10
15
20
25
TRANSMITTED POWER

FIGURE 4-13

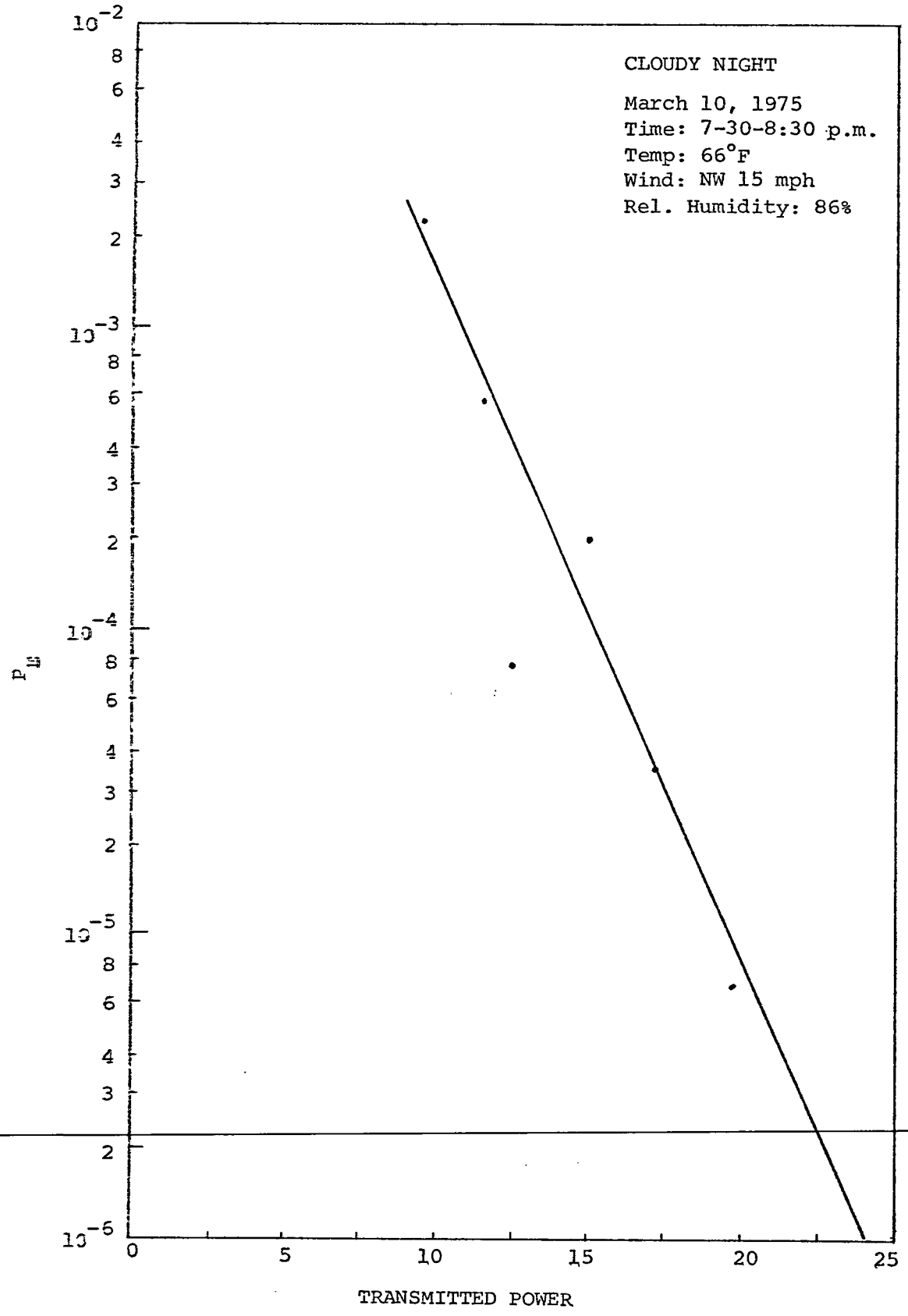
CLOUDY NIGHT
March 10, 1975
Time: 7-30-8:30 p.m.
Temp: 66°F
Wind: NW 15 mph
Rel. Humidity: 86%
10^{-2}
8
6
4
3
2
10^{-3}
8
6
4
3
2
10^{-4}
8
6
4
3
2
10^{-5}
8
6
4
3
2
10^{-6}
P_E
0
5
10
15
20
25
TRANSMITTED POWER

FIGURE 4-14

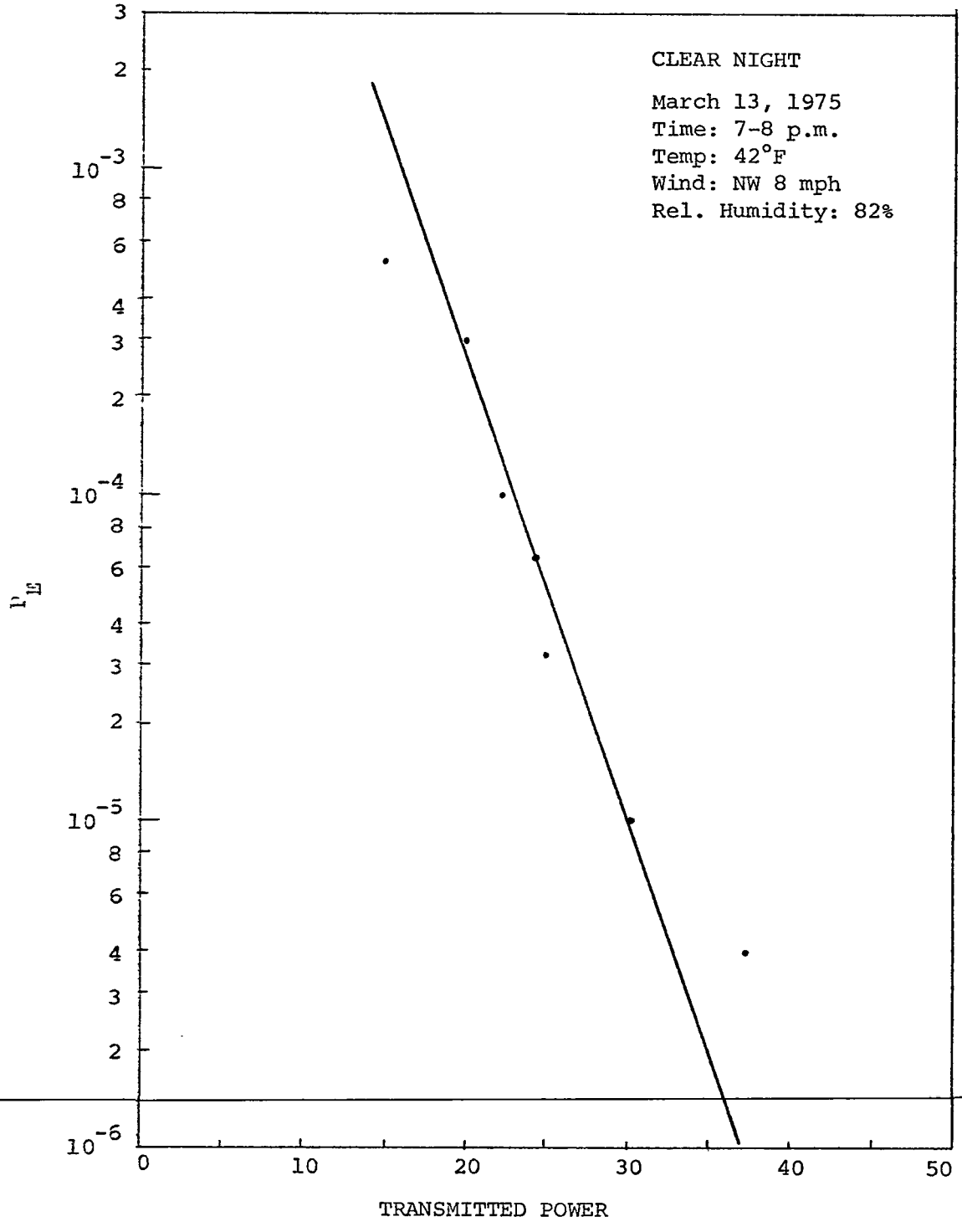
CLEAR NIGHT
March 13, 1975
Time: 7-8 p.m.
Temp: 42°F
Wind: NW 8 mph
Rel. Humidity: 82%
P_E
10^{-3}
10^{-4}
10^{-5}
10^{-6}
0
10
20
30
40
50
TRANSMITTED POWER

FIGURE 4-15

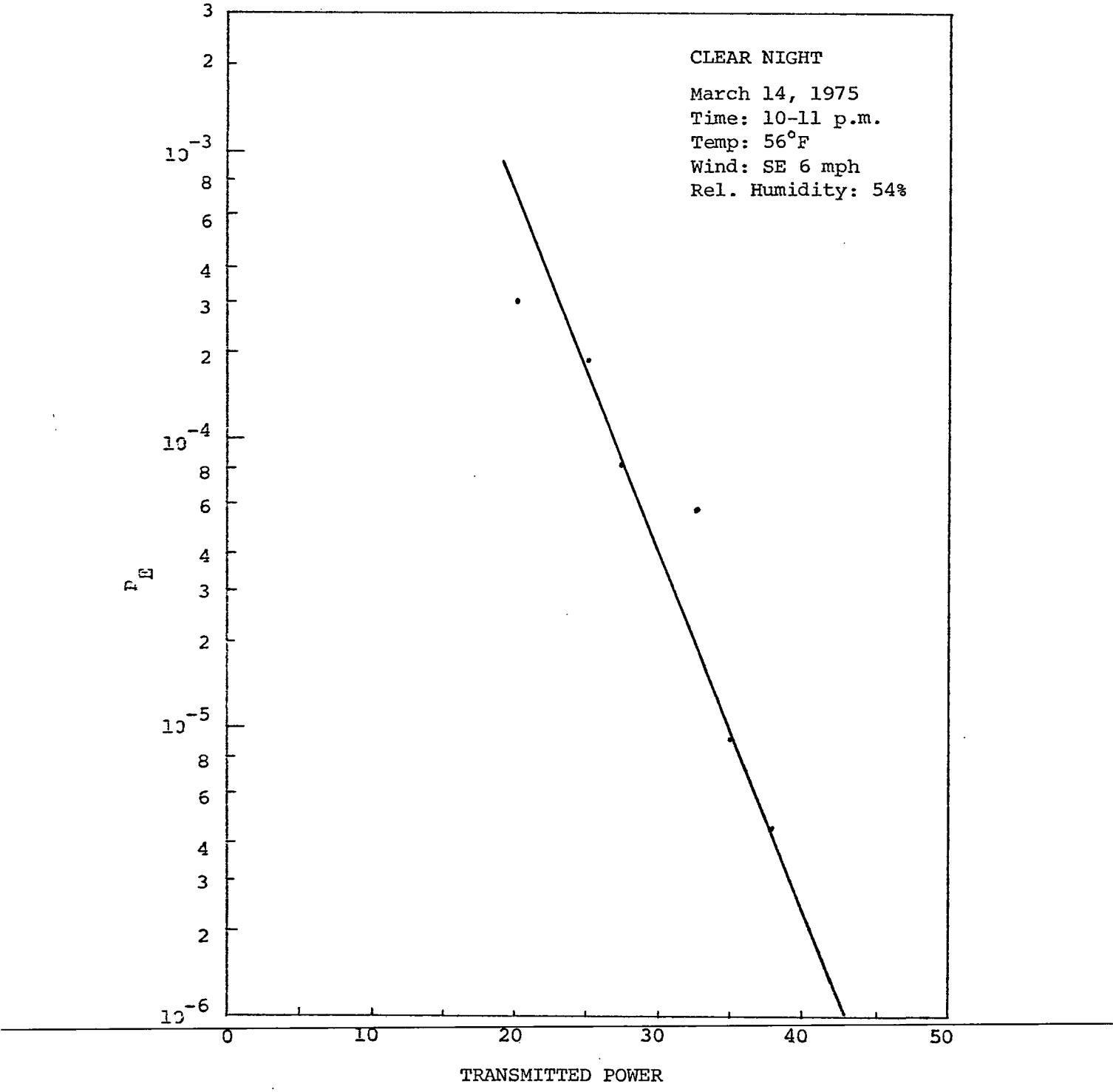
CLEAR NIGHT
March 14, 1975
Time: 10-11 p.m.
Temp: 56°F
Wind: SE 6 mph
Rel. Humidity: 54%
P_R
10^{-3}
10^{-4}
10^{-5}
10^{-6}
0
10
20
30
40
50
TRANSMITTED POWER

FIGURE 4-16

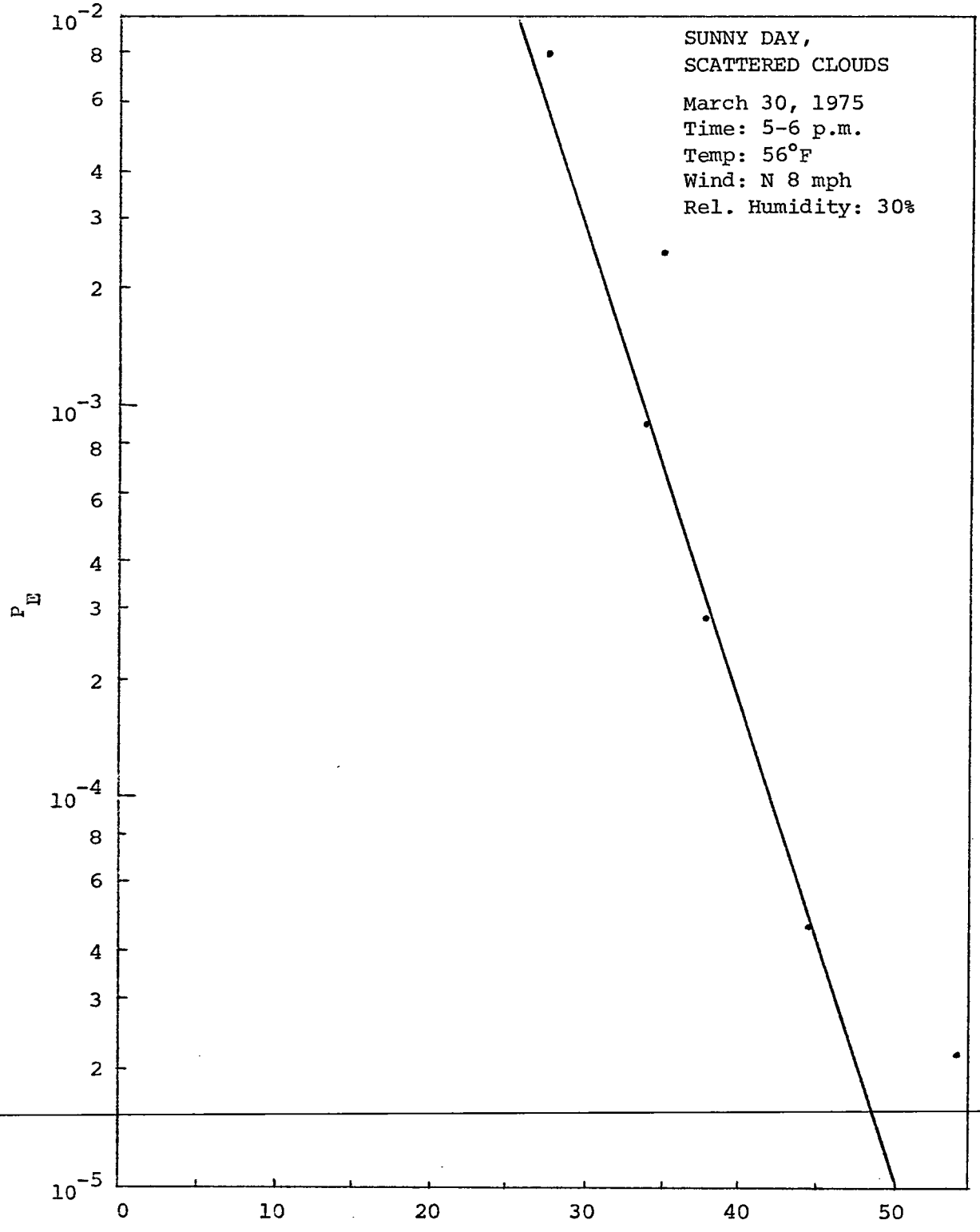
SUNNY DAY,
SCATTERED CLOUDS
March 30, 1975
Time: 5-6 p.m.
Temp: 56°F
Wind: N 8 mph
Rel. Humidity: 30%
P_E
10^{-2}
8
6
4
3
2
10^{-3}
8
6
4
3
2
10^{-4}
8
6
4
3
2
10^{-5}
0
10
20
30
40
50
TRANSMITTED POWER

FIGURE 4-17

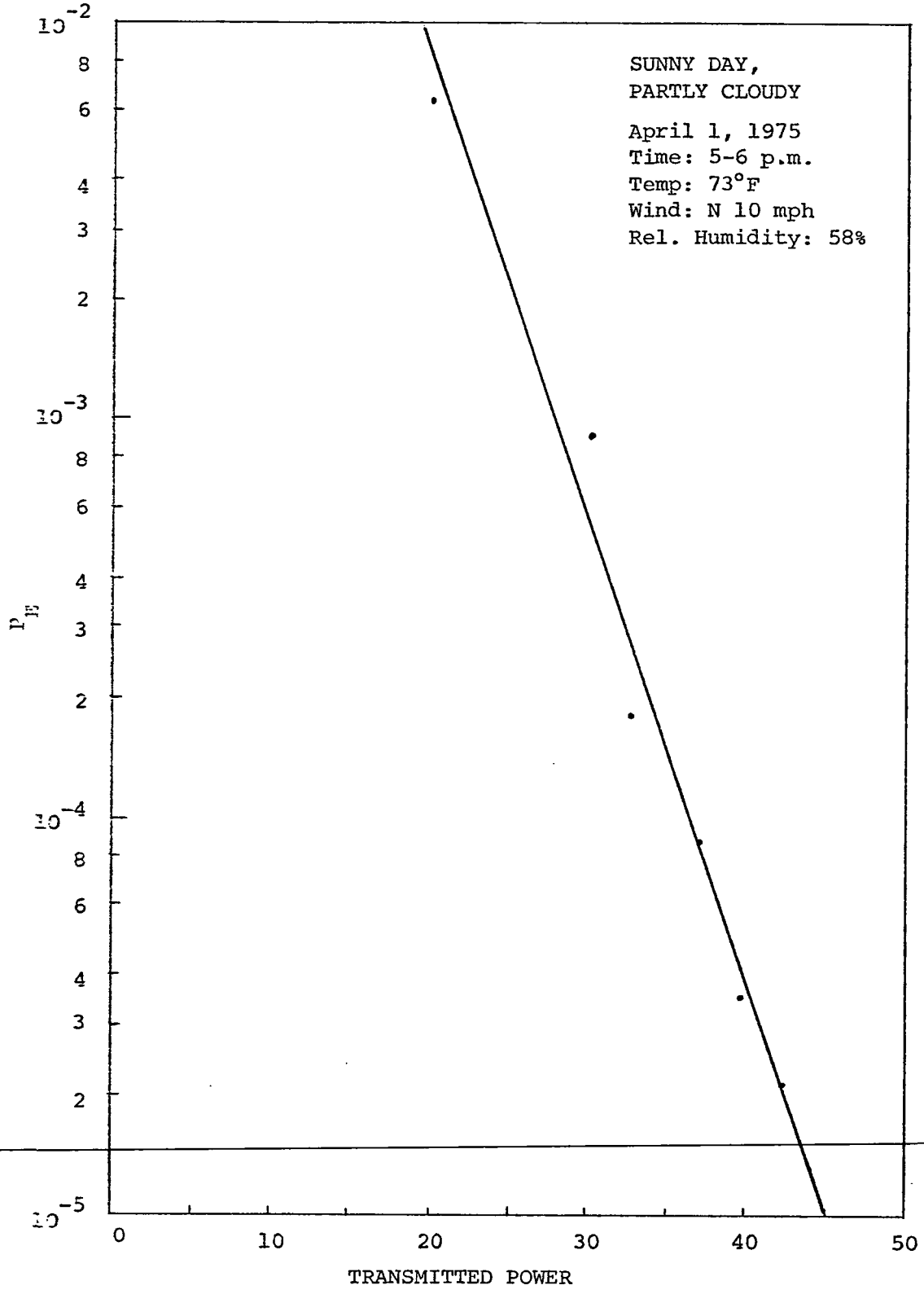
SUNNY DAY,
PARTLY CLOUDY
April 1, 1975
Time: 5-6 p.m.
Temp: 73°F
Wind: N 10 mph
Rel. Humidity: 58%
10^{-2}
8
6
4
3
2
10^{-3}
8
6
4
3
2
10^{-4}
8
6
4
3
2
10^{-5}
P_E
0
10
20
30
40
50
TRANSMITTED POWER

FIGURE 4-18

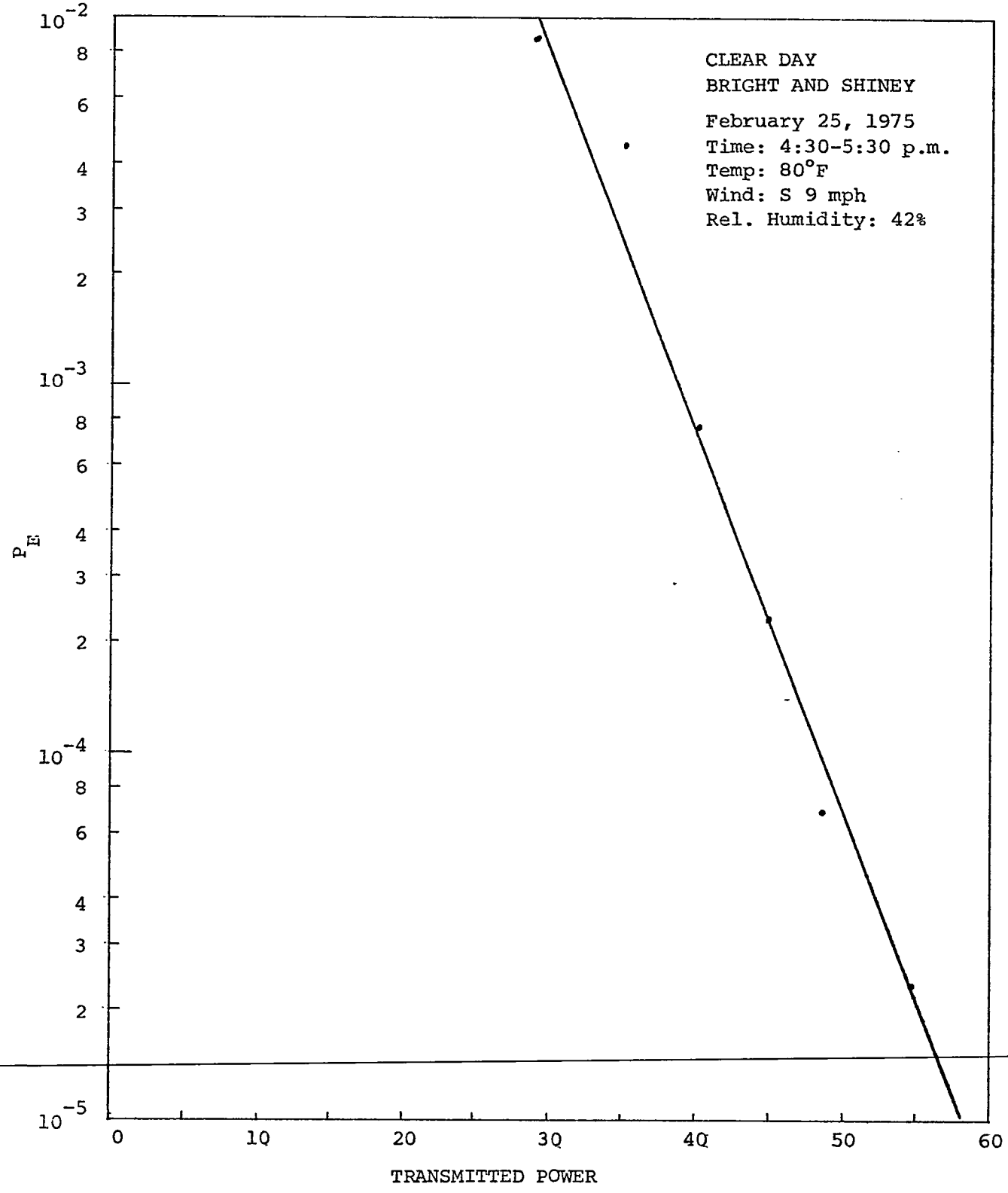
CLEAR DAY
BRIGHT AND SHINEY
February 25, 1975
Time: 4:30-5:30 p.m.
Temp: 80°F
Wind: S 9 mph
Rel. Humidity: 42%
10^{-2}
8
6
4
3
2
10^{-3}
8
6
4
3
2
10^{-4}
8
6
4
3
2
10^{-5}
P_E
0
10
20
30
40
50
60
TRANSMITTED POWER

FIGURE 4-19

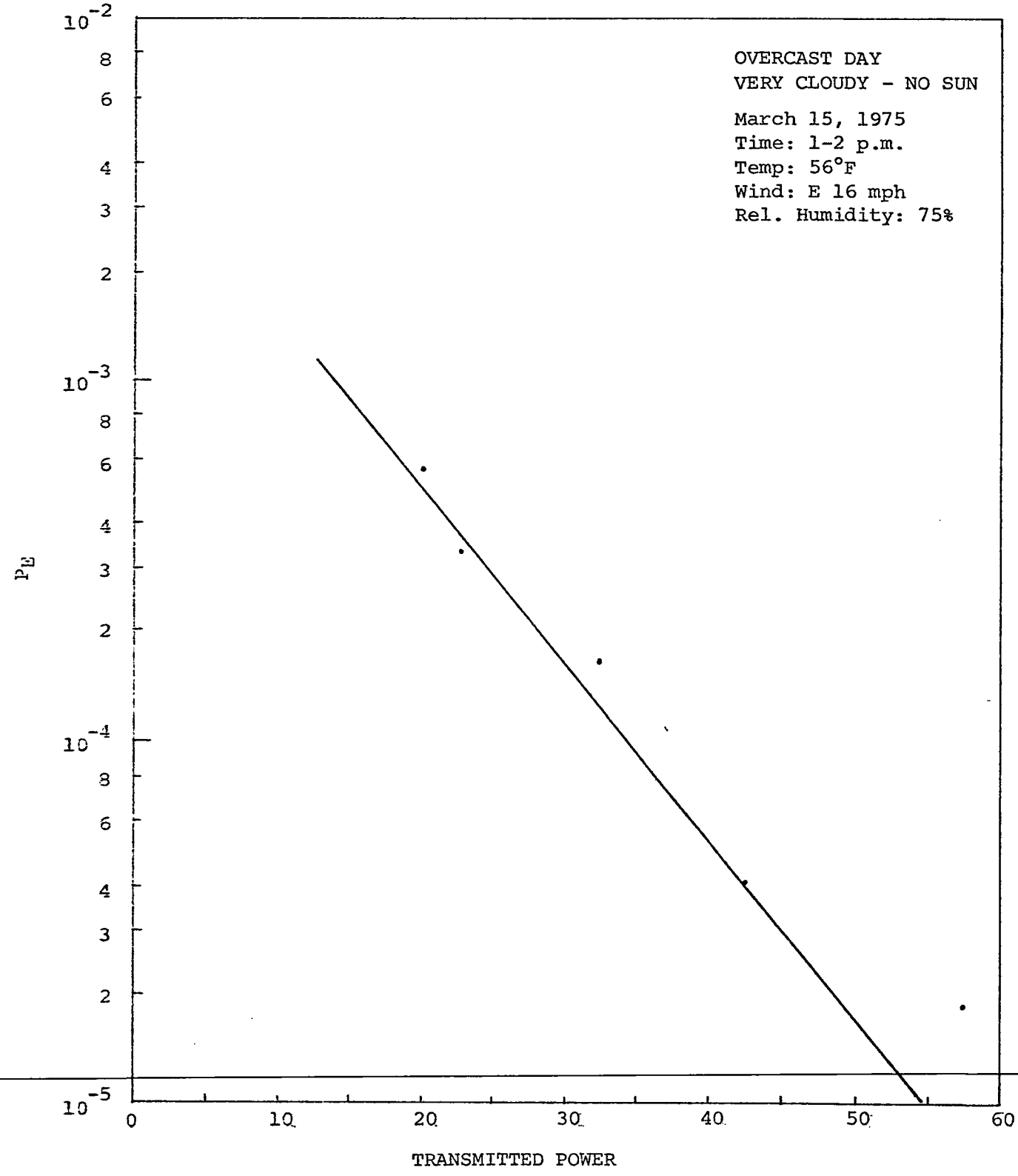
OVERCAST DAY
VERY CLOUDY - NO SUN
March 15, 1975
Time: 1-2 p.m.
Temp: 56°F
Wind: E 16 mph
Rel. Humidity: 75%
10^{-2}
8
6
4
3
2
10^{-3}
8
6
4
3
2
10^{-4}
8
6
4
3
2
10^{-5}
P_E
0
10
20
30
40
50
60
TRANSMITTED POWER

FIGURE 4-20

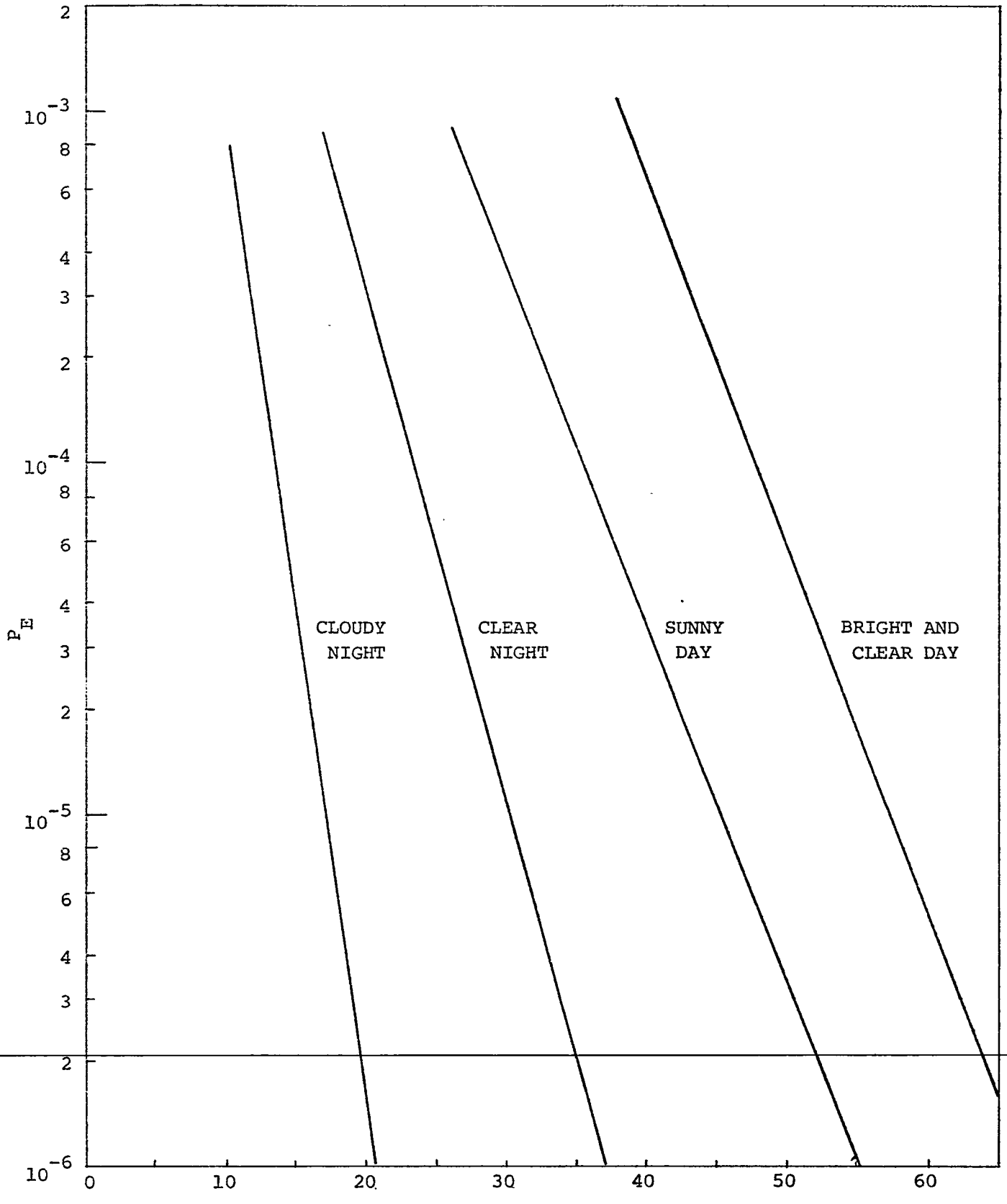

FIGURE 4-21

COMPARISON OF ERROR RATE PERFORMANCE FOR DIFFERENT ATMOSPHERIC CONDITIONS

Chapter 5

CONCLUSIONS

In general all the building blocks and the system as a whole worked well and gave a good feeling about the working of the hitherto unfamiliar infrared devices. In accordance with the high signal-to-noise ratio evinced by the sample calculations, very low error counts were observed at higher signal powers. Overall satisfactory performance was obtained during the operation at nights and afternoons. It was observed that error rates of the order of 10^{-6} or lower were obtainable during these operations. Full implications of the various atmospheric parameters and their influence on the performance of the system cannot be analysed at this stage. It forms a whole new topic for investigation and calls for more advanced work. However, the effect of the atmospheric turbulence was clearly observed and was found to be in conformation with the theory. Turbulent effects are predominent during windy and clear weather conditions (Chapter 3). This fact was confirmed by noticing higher signal fluctuations during such conditions. Figure 4-21 shows that much higher error rates were in fact obtained during the clear weather compared to the cloudy weather conditions.

The system could not be operated during the daytime in bright sun light. The primary reason for this

is believed to be the loss of alignment resulting from the excessive beam steering effect. The extent of this effect on the actual displacement of the beam could not be determined, however, the results of Figure 3-7 are revealing. Although the figure illustrates the beam wandering over a five kilometer path, it can be deduced that the beam displacement of several centimeters could take place with this experimental setup during the highly turbulent daylight hours. A couple of other points are worth mentioning in this respect. The alignment was complicated by the fact that only about two-thirds portion of the eight inch diameter mirror could be used to reflect the beam back to the receiver. This is because the beam entered the six feet long tube at an angle, as shown in Figure 5-1, before it could hit the mirror. This arrangement was very sensitive to beam steering as well as beam divergence effects.

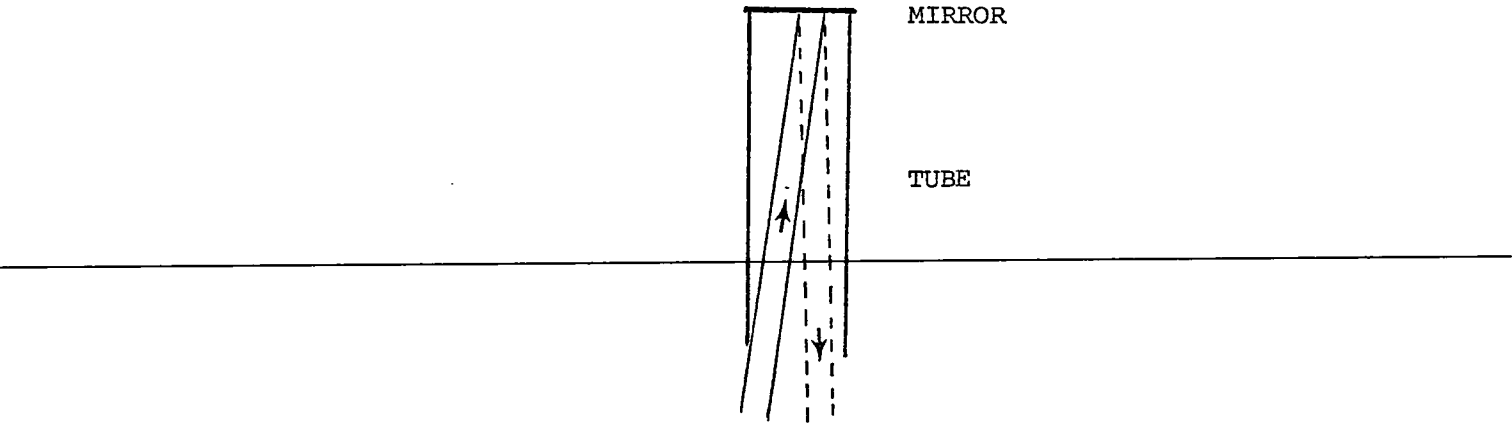

FIGURE 5-1

BEAM REFLECTING ARRANGEMENT

Another fact which probably contributed to the failure of the daytime operation is the very small detector area (0.8 mm^2) that was used to collect the reflected beam. In order to overcome the loss of signal which might result due to beam dancing in turbulent atmosphere, a detector having a large sensitive area must be used. Several photodiodes such as TIXL80 (5 mm^2area), C-30809 (50 mm^2 area) and C-30810 (100 mm^2 area) are available for this purpose. A large detector area will have a large capacitance and hence slower response to the signal. Similarly, a large detector area will mean a large receiver field of view which will introduce more background noise. However, these facts will not seriously affect the performance of the present system.

Appreciable laser heating and consequent output power reduction was noticed at repetition rates higher than five kilohertz. Although this did not significantly deteriorate the system performance because the power level was still quite high, this problem can be alleviated by using a faster switching device in the laser pulser to obtain current pulses much narrower than the presently available 150 ns pulses. This will also significantly increase the repetition rate, because for the same duty cycle limitation, PRF $\propto \frac{1}{\tau}$, where τ is the pulse width. Avalanche transistor 2N3507 or SCR GA201 will be very well suited for this application.

In conclusion, this project has shown that GaAs injection laser systems are a practical, feasible and reliable means of information transmission through atmospheric channels over short distances. Over all system cost is low and such links can favorably compete with their radio frequency or visible frequency counterparts.

Chapter 6

SUGGESTIONS FOR FURTHER STUDY

Some improvements in the present systems can be easily incorporated. The data rate available from the present system is very moderate, because the laser must be pulsed at a relatively low rate. The maximum operating PRF of six kilohertz of the present system is far below the state of the art rates of over one hundred kilohertz. An order of magnitude improvement is possible by using a faster switching device to switch the high current laser pulses. Avalanche transistors will be very desirable for this application. A design of an avalanche transistor pulser giving sixty nanosecond pulses at repetition rates up to one hundred kilohertz is described by Brown et. al. [40]. Another circuit giving pulse rise time of the order of one hundred picoseconds is described by H. V. Hattery [41].

With the experience and the encouraging results of this project, it will not be too optimistic to speculate on the possibility of setting up the link over a longer range. For example, a link between the university campus and downtown Houston may be considered. Hannan and co-workers [26] have plotted the required transmitter power versus range to obtain a signal-to-noise ratio of over fifteen decibels. It appears that even in a worse

case situation of twenty decibels fading margin, the present system with five watt peak power should give a satisfactory performance well over three miles.

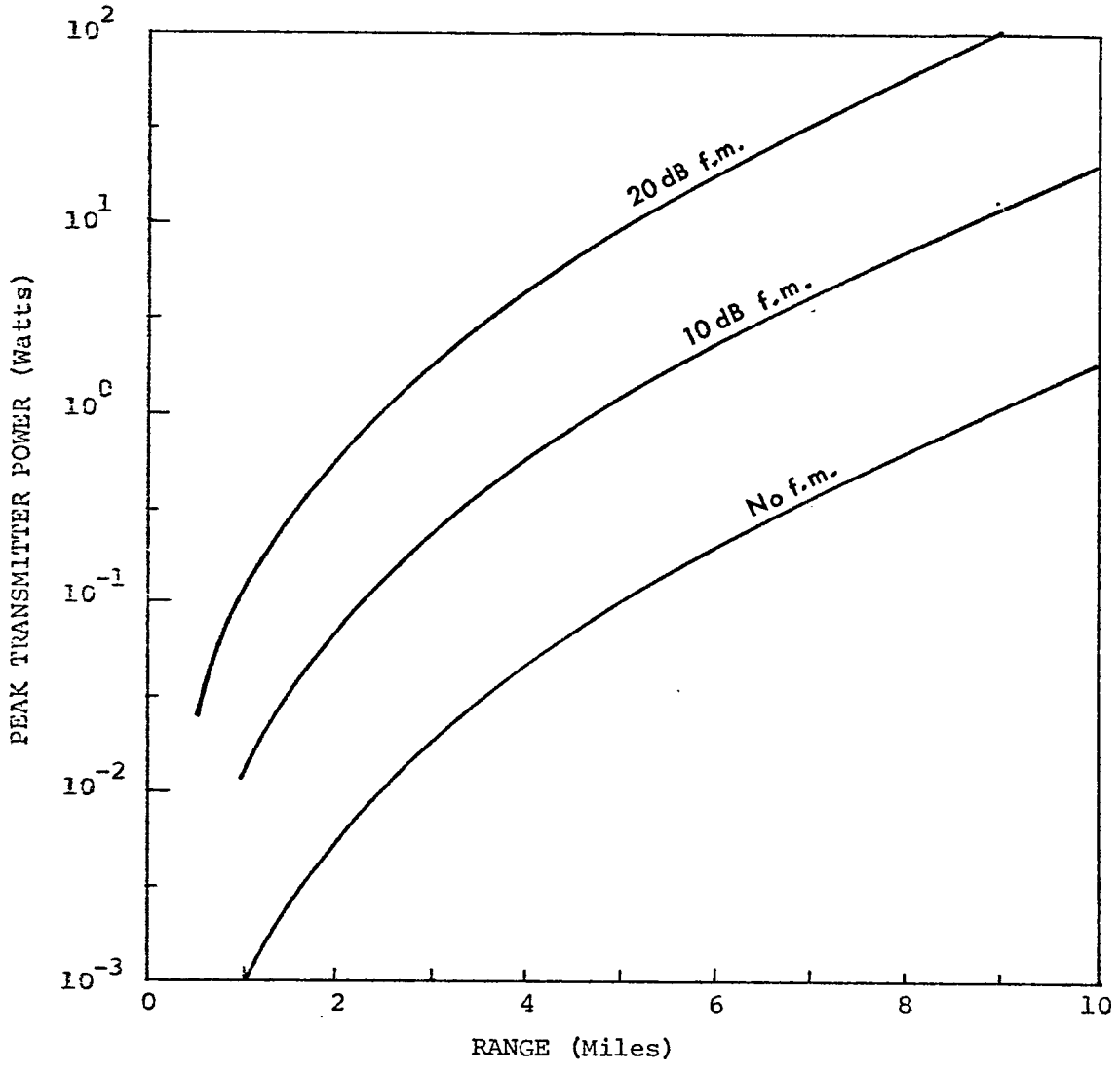

FIGURE 6-1

REQUIRED TRANSMITTER POWER VERSUS RANGE

An interesting research topic from the communication point of view would be to compare the performance of the link with different types of modulation formats. Pulse-position-modulation of injection lasers has been extensively studied [42, 43]. Because of the necessity of using a low duty cycle with injection lasers, Ross [44] has suggested a novel method of modulation called the pulse-interval-modulation. In this scheme each pulse transmits more than one bit and the coding mostly contains zeros, thus minimizing the heating of the laser. Another scheme especially suited for injection lasers exploits the delay between the application of a current pulse and onset of laser emission. The delay is strongly dependent upon the amplitude of the current pulse, and it decreases with increasing amplitude. Advantage could be taken of this dependence by amplitude modulating the driving pulses to produce pulse-width-modulation [45].

The present system could be modified to conduct some other experiments in optical communication and its related areas. TV and voice communication with injection laser beams has been tried successfully by several workers [1, 2, 7]. Figure 6-2 shows a block diagram of a typical injection laser voice communication system. The modulator driver could be a delay line whose charging time can be controlled to pulse frequency modulate the laser. The frequency discriminator may be a single-shot multivibrator to standardize the received pulses.

Injection laser applications in short distance ranging have been studied and the laser diodes are found to be very attractive due to their high peak output powers at narrow pulse widths. In this respect they can provide a method of supplying range information for airborne surveillance systems or landing aids for an aircraft. An experimental system described by Koechner [46] measures the range within 5% accuracy. An injection laser radar operates by receiving the laser light reflected off a target as shown in Figure 6-3. The presence or absence of the target can be determined by the presence or absence of this reflected beam. An experimental injection laser radar designed by Goldstein and Dalrymple [47] observed individual objects like trees over a distance of 235 meters during night time operation.

It is obvious that this initial attempt in injection laser communication opens exciting possibilities for a whole new area of experimental research.

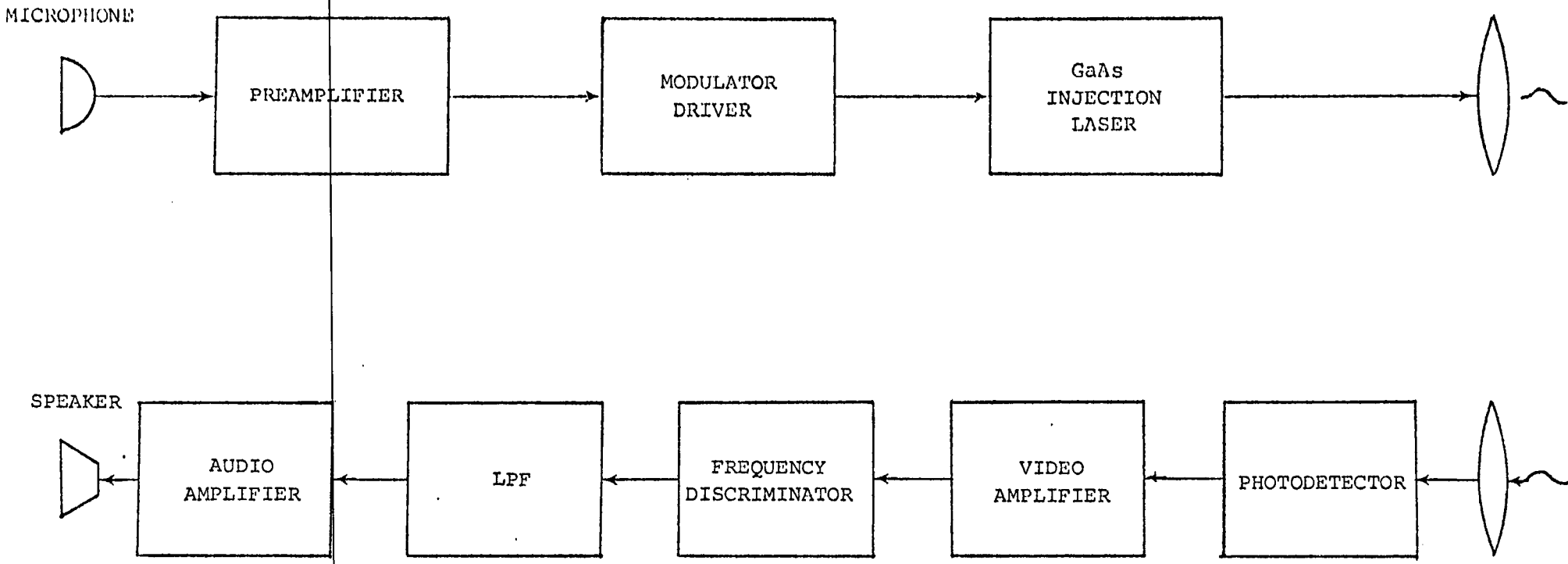

FIGURE 6-2

INJECTION LASER VOICE COMMUNICATION LINK

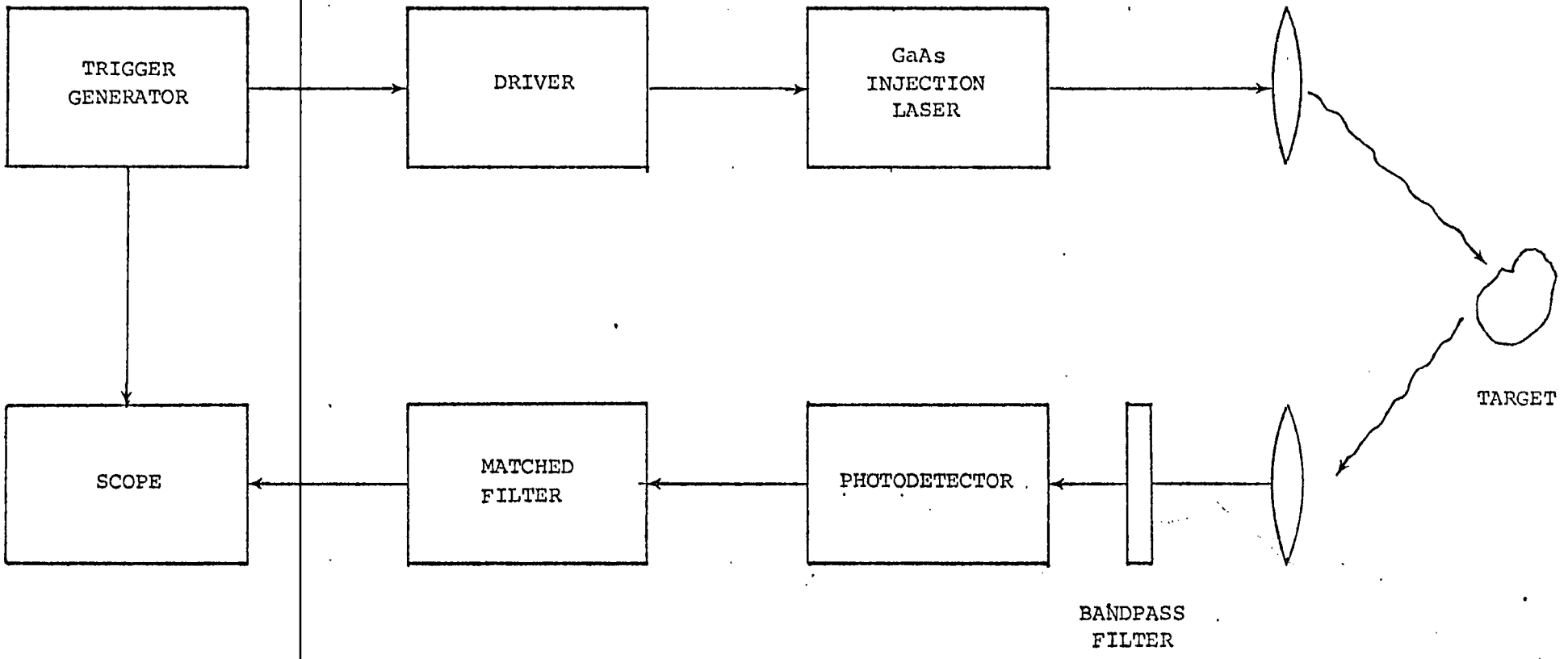

FIGURE 6-3

INJECTION LASER RADAR

LIST OF REFERENCES

1. Rediker, R. H., et al. "GaAs Sends TV by Infrared Beam," Electronics, October 5, 1962, pp. 44-45.

2. Keyes, R. W. et al. "Modulated Infrared Diode Spans 30 Miles," Electronics, April 5, 1963, pp. 38-39.

3. Goodwin, F. E. "A Review of Operational Laser Communication Systems," Proceedings of the IEEE, October, 1970, pp. 1746-1752.

4. Ross, M. Laser Receivers. John Wiley and Sons, 1966.

5. Keyes, R. W. "Injection Lasers," Industrial Research, October, 1974, pp.46-55.

6. Kressel, K., H. Lockwood and M. Ettenberg. "Progress in Laser Diodes," IEEE Spectrum, May, 1973, pp. 59-64.

7. Karlson, D., N. Reno and W. Hannan. "Room Temperature GaAs Voice Communication Systems," Proceedings of the IEEE, November, 1964.

8. Schiel, E., et al. "Pulse Modulation of an Electron Injection Laser Transmission System," Eighth IEEE International Conference on Military Electronics, 1964.

9. Dworkin, L., M. Lipton and L. Coryell. "Tactical Laser Ground Communication," Proceedings of the IEEE, Fall Electronics Conference, 1971.

10. Electronics, March 16, 1970.

11. Lilly, D. S. "Optical Communications Experiments on Gemini VII," Proceedings of the Space Optical Technology Conference, April, 1966, pp. 81-90.

12. Gammarino, Schiel and Aras. "Design and Performance of an Injection Laser Link for 10 MHz Data Rate Transmission," Proceedings of the First Electro-Optical Systems Design Conference, New York, September, 1969.

13. Hall, R. N., et al. "Coherent Light Emission from GaAs Junctions," Physical Review Letters, November, 1962, pp. 366-368.

Keyes, R. W. and T. M. Quist. "Recombination Radiation Emitted by Gallium Arsenide," Proceedings of the IRE, August, 1962, p. 1822.

Nathan, M. I. and G. Burns. "Recombination Radiation in GaAs by Optical and Electiical Injection," Applied Physics Letters, December 1, 1962, pp. 89-90.

14. Gooch, C. H. Gallium Arsenide Lasers. Wiley-Interscience, 1969.

15. Burns, G., F. H. Dill and M. I. Nathan. "The Effect of Temperature on the Properties of GaAs Lasers," Proceedings of the IEEE, June 1963, pp. 947-948.

16. Sturge, M. D. "Optical Absorption of Gallium Arsenide Between 0.6 and 2.75 eV," Physical Review, August 1, 1962, pp. 768-773.

17. Medved, D. B. and K. M. Kunz. "Matching a Sensor to a Diode Source," Laser Focus, May, 1972, pp. 34-36.

18. Clifton, M and P. P. Debye. "On the Parameters Which Affect the C. W. Output of GaAs Lasers," Applied Physics Letters, March 15, 1965, pp. 120-121.

19. DeLange, O. E. "Optical Heterodyne Detection," IEEE Spectrum, October, 1968, pp. 77-85.

20. Siegman, A. E. "The Antenna Properties of Optical Heterodyne Receivers," Proceedings of the IEEE, October, 1966, pp. 1350-1356.

21. Melchior, H., M. B. Fisher and F. Arams. "Photodetectors for Optical Communication Systems," Proceedings of the IEEE, October, 1970, pp. 1466-1486.

22. Biard, J. and W. Shaunfield. "A Model of Avalanche Photodiodes," IEEE Transactions of Electron Devices, May, 1967, pp. 233-238.

23. UDT Silicon Photodetector Design Manual, 1973.

24. Pratt, W. K. Laser Communication Systems. John Wiley and Sons, 1969.

25. Born and Wolf. Principles of Optics. Pergamon Press, 1964.

26. Hannan, W. G., J. Bordogna and D. Karlson. "Practical Aspects of Injection Laser Communication Systems," RCA Review, December, 1967, pp. 609-619.

27. Battelle, R. B., P. R. Gillete and R. C. Honey, "An Analysis of the Feasibility of Laser Systems for Naval Applications," Defense Documentation Center Report AD-350353, Noverber, 1963.

28. RCA Electrooptics Handbook, 1968.

29. Lawrence, R. S. and J. W. Strohbehn. "A Survey of Clear-Air Propagation Effects Relevant to Optical Communications," Proceedings of the IEEE, October, 1970, pp. 1523-1545.

30. Davis, J. I. "Consideration of Atmospheric Turbulence in Laser Systems Design," Applied Optics, January, 1966, pp. 139-146.

31. Tatarski, V. I. Wave Propagation in a Turbulent Medium. McGraw-Hill, 1961.

32. Ochs, G. R. "Measurements of Laser-Beam Scintillation in Strong Atmospheric Turbulence," ESSA Technical Reports ERL 154-WPL10, 1970.

33. Whatley and Smith. "Atmospheric Effects on Digitally Modulated Laser Transmission," Research and Development Technical Reports AD 676814.

34. Fried, D. L. "Aperture Averaging of Scintillation," Journal of the Optical Society of America, February, 1967, pp. 169-174.

35. Kerr, J. R., et al. "Atmospheric Optical Communications Systems," Proceedings of the IEEE, October, 1970, pp. 1961-1709.

36. Fried, D. L. and J. B. Seidman. "Laser-Beam Scintillation in the Atmosphere," Journal of the Optical Society of America, February, 1967, pp. 181-185.

37. Curran, T. F. and M. Ross. "Optimum Detection Thresholds in Optical Communications," Proceedings of the IEEE, November, 1965, pp. 1770-1771.

38. Fried, D. L. and R. A. Schmeltzer. "The Effect of Atmospheric Scintillation on an Optical Data Channel," Applied Optics, October, 1967, pp. 1729-1737.

39. Wozencraft, J. M. and I. M. Jacobs. Principles of Communication Engineering. John Wiley and Sons, 1965.

40. Brown, H. E., R. A. Bond and J. C. Bloomquist. "Avalanche Transistors Drive Laser Diodes Hard and Fast," Electronics, November, 1966, pp. 137-139.

41. Hattery, H. W., et al. "Subnanosecond Rise-time Pulses from Injection Lasers," IEEE Journal of Quantum Electronics, July, 1974, pp. 570-572.

42. Ripper, J. E. and T. L. Paoli. "Frequency Pulling and Pulse Position Modulation of GaAs Injection Lasers," Applied Physics Letters, October, 1969.

43. Karp, S. and R. M. Gagliardi. "The Design of a Pulse-Position Modulated Optical Communication System," IEEE Transactions on Communication Technology, December, 1969, pp. 670-673.

44. Ross, M. "Pulse Interval Modulation Laser Communications," IEEE Transactions on Aerospace and Electronic Systems, November, 1967.

45. Paoli, T. L. and J. E. Ripper. "Direct Modulation of Semiconductor Lasers," Proceedings of the IEEE, October, 1970, pp. 1457-1465.

46. Koechner, W. "Optical Ranging System Employing a High Power Injection Laser Diode," IEEE Transactions on Aerospace and Electronic Systems, January, 1968, pp. 81-91.

47. Goldstein and Dalrymple. "GaAs Injection Laser Radar," Proceedings of the IEEE, February, 1967, pp. 181-188.